# Critical Review—The Versatile Plane Parallel Electrode Geometry: An Illustrated Review

*Journal of The Electrochemical Society*, 2020 **167** 023504

# Critical Review—The Versatile Plane Parallel Electrode Geometry: An Illustrated Review

**L. F. Arenas,[*] C. Ponce de León, and F. C. Walsh[z]**

*Electrochemical Engineering Laboratory, Energy Technology Group, Faculty of Engineering and Physical Sciences, University of Southampton, Southampton SO17 1BJ, United Kingdom*

The features of the plane parallel geometry are reviewed since this cell geometry occupies a prominent position, both in the laboratory and in industry. The simple parallel plate can be enhanced by inclusion of porous, 3D electrodes, structured surfaces and bipolar electrical connections, with adequate attention to the reaction environment. Unit cells are often arranged in a modular, filter-press format. Scale-up is achieved by increasing the size of each electrode, the number of electrodes in a stack or the number of stacks in a system. The use of turbulence promoters in the flow channel, textured (including nanostructured) and porous electrodes as well as cell division by an ion exchange membrane can considerably widen the scope of the plane parallel geometry. Features of plane parallel cell designs are illustrated by selected examples from our laboratories and industry, including a fuel cell, an electrosynthesis cell and hybrid redox flow cells for energy storage. Recent trends include the development of microflow cells for electrosynthesis, 3D printing of fast prototype cells and a range of computational models to simulate reaction environment and rationalise performance. Future research needs are highlighted.

 [DOI: 10.1149/1945-7111/ab64ba]

Manuscript submitted July 16, 2019; revised manuscript received October 28, 2019. Published January 31, 2020. *This paper is a Critical Review in Electrochemical and Solid State Science and Technology (CRES[3]T). This article was reviewed by Fikile Brushett (brushett@mit.edu).*

## List of symbols

| | |
|---|---|
| $A$ | Geometrical electrode area, $cm^2$ |
| $A_e$ | Volumetric electrode area, $cm^{-1}$ |
| $B$ | Breadth of flow channel, cm |
| $c$ | Reactant concentration, mol $dm^{-3}$ |
| $c_{in(0)}$ | Reactant concentration at the inlet of a plug flow reactor at time 0, mol $dm^{-3}$ |
| $c_{in(t)}$ | Reactant concentration at the inlet of a plug flow reactor at time $t$, mol $dm^{-3}$ |
| $d_e$ | Equivalent diameter of a rectangular flow channel, cm |
| $D$ | Diffusion coefficient of a species, $m^2\ s^{-1}$ |
| $E$ | Electrode potential vs a reference electrode, V |
| $E^\theta$ | Standard electrode potential, V |
| $U$ | Cell potential difference, V |
| $U_e$ | Equilibrium cell potential difference, V |
| $F$ | Faraday constant, C $mol^{-1}$ |
| $I$ | Current, A |
| $I_L$ | Limiting current, A |
| $J_{(x,t)}$ | Diffusive flux of a species at location $x$ and time $t$, mol $cm^{-2}\ s^{-1}$ |
| $j$ | Current density, A $m^{-2}$ |
| $k$ | Apparent first order rate constant, $s^{-1}$ |
| $k_m$ | Mass transfer coefficient, cm $s^{-1}$ |
| $L$ | Electrode length, cm |
| $p$ | Pressure, Pa |
| $Q$ | Volumetric flow rate of electrolyte, $cm^3\ s^{-1}$ |
| $R$ | Electrical resistance, ohm |
| $S$ | Separation between electrode surface and membrane in a divided cell or electrode and counter electrode in a divided flow channel, cm |
| $t$ | Time, s |
| $v$ | Mean linear flow velocity past the electrode surface, cm $s^{-1}$ |
| $V_R$ | Volume of electrolyte in the reactor, $cm^3$ |
| $V_T$ | Volume of electrolyte in the tank, $cm^3$ |
| $x$ | Velocity exponent, Dimensionless |
| $X_A$ | Fractional conversion of reactant in a single pass, Dimensionless |
| $X_{A,t}$ | Fractional conversion of reactant at time $t$, Dimensionless |
| $z$ | Electron stoichiometry, Dimensionless |

### Greek

| | |
|---|---|
| $\delta_N$ | Thickness of the Nernst diffusion layer, $\mu$m |
| $\varepsilon$ | Volumetric porosity, Dimensionless |
| $\eta$ | Overpotential, V |
| $\phi$ | Current efficiency, Dimensionless |
| $\rho$ | Electrical resistivity, ohm cm |
| $\tau_T$ | Mean residence time in the tank, s |

This review summarises the features and benefits of plane parallel cells for electrochemical processing and electrochemical energy storage together with their established uses in order to provide an introduction to the field and encourage future developments. Recent progress, the continued need to improve efficiency and the need for a general overview demand a reconsideration of the most useful and widespread electrode configuration of electrochemical reactors. In order to provide a perspective of the applications, scale and characterisation of electrochemical cells, selected examples are drawn from the literature and the authors' experience.

Amongst many possible electrode configurations and cell designs, the vertical, plane parallel configuration continues to be the most common choice of electrode geometry in applied electrochemistry and electrochemical engineering.[1–13] This is easily appreciated since plane parallel electrodes enjoy key advantages:

a) The ready availability of varied electrode forms,
b) The diversity of possible electrode materials,
c) Relatively uniform potential and current distributions,
d) Easy scalability, ranging from laboratory through pilot scale to industrial scale,
e) Flexibility of cell architecture, e.g., undivided or membrane divided cells,
f) Well defined fluid flow and mass transfer in a rectangular flow channel,

*Electrochemical Society Member.
[z]E-mail: f.c.walsh@soton.ac.uk

g) Process scale-up is possible by increasing the electrode area or number of electrodes.

The versatility offered by the above features, plus facile assembly and electrical connections makes the plane parallel geometry, in an agitated beaker, a stirred tank or a channel flow cell, the preferred choice for many applications. Some relevant examples are the chlor-alkali industry,[14] organic electrosynthesis,[15–17] inorganic electrosynthesis,[5,18], redox flow batteries,[19] fuel cells,[20] metal air batteries,[21] electroplating of static components,[22] electroplating of moving sheets,[23] electroforming,[24] electrowinning,[5] electrodialysis,[25] and environmental treatment.[26,27] In fact, this cell configuration has been applied in industry for at least 130 years. Plane parallel bipolar electrodes in reactors were introduced as early as 1880,[28] followed by filter-press fuel cell stacks in 1888,[29] porous electrode bipolar cells in 1893,[30] and filter-press flow reactors in 1899.[28] These cell designs face new challenges in view of modern demands, while future developments can be envisaged, such as new electrode materials, optimization using numerical simulation, advanced manufacture and imaging techniques, synergy with green technologies and a reconsideration of traditional electrochemical processes.

The following sections elaborate on these topics. Types of Cell Design and the Parallel Plate introduces the characteristics of planar electrodes in agitated beakers and tanks as well as in electrochemical flow cells. Given their importance, Features of the Plane Parallel Flow Cell highlights the features and benefits of rectangular channel electrochemical flow reactors. Types of Electrodes focuses on the properties of different forms of electrodes together with their manufacture and construction. Selected Examples of Cell Designs and their Performance emphasises the diversity of electrochemical operations possible in parallel plane cells, from the laboratory to pilot plant scale. A summary is provided, indicating trends; this is followed by suggested needs for further R & D.

## Types of Cell Design and the Parallel Plate

***Vertical plates in an agitated beaker.***—This is a very common option in the laboratory (Fig. 1) having the benefits of:

a) dry, secure electrical connections,
b) ease of electrolyte additions and sample withdrawal,
c) ease of electrode insertion and removal, possibly without draining the container,
d) convenient mixing and stirring plus heating using a magnetic stirrer/hotplate and
e) the facility to probe the electrode potential and its distribution, by carefully adjusting the position of a reference electrode probe.

For example, simple 250 $cm^3$ beakers, sharing a common flange to accept a cation exchange membrane are shown in Fig. 1. This arrangement has been useful for the demonstration of electrochemical batch kinetics of the reduction of 0.1 mol $dm^{-3}$ Ce(IV) to Ce (III) ions in 1 mol $dm^{-3}$ $H_2SO_4$ for educational purposes.[31] The reaction is carried out at constant current in a constant volume decay experiment in order to estimate the averaged mass transfer coefficient to the planar cathode surface at a fixed stirring rate provided by a magnetic stirrer. The concentration decay, determined by volumetric analysis, yields overall first order kinetics. The inverse batch reaction, Ce(III) oxidation to Ce(IV), has also been carried out in beakers in 2 mol $dm^{-3}$ methanesulfonic acid in the laboratory,[32] studying the effect of current density and temperature on the concentration profiles. The yield and purity of anthraquinone, naphthaquinone and benzoquinone produced via Ce(IV)-mediated oxidation of polycyclic aromatics was later evaluated in a stirred, divided cell using a planar Pt/Ti anode.[33] Similar procedures carried out in laboratory batch cells are useful in screening studies of reaction yield, electrode material suitability, proof of concept of redox flow battery chemistries and in the preparation or purification of small quantities of reagents.

Despite their convenience, the limitations of such agitated beaker cells need to be realised:

a) the fluid flow and mass transfer are poorly defined and difficult to reproduce, being dependent on the shape and position of the stirrer follower as well as its rotation speed; complex, rotational flow effects are normally present and can be complex,
b) the mass transfer coefficient in such cells is very limited compared to flow cells,
c) care should be taken to avoid interface and edge effects on potential, current and flow distributions,
d) the precise definition of electrode area by adhesive tapes, stop-off lacquer or polymer masks should be considered,
e) it is important to include reference electrodes to facilitate measurement of electrode potentials, enabling performance to be related to steady state voltammetry and controlled potential or current coulometry.
f) as explained below, scale-up efforts must be initiated, instead, in larger cells with controlled reaction environment.

***Vertical plates in a stirred tank.***—In this type of cell design, shown in Fig. 2, parallel electrodes are immersed in tanks containing the electrolyte. Stirring can be performed by pump flow, gas-injection or paddles.[34] This design provides simplicity and versatility for industrial processing, mainly in electrometallurgical operations. While the undivided cell configuration, Fig. 2a), is common, it is possible to incorporate a microporous polymer or ion exchange membranes into an "anode box" or "cathode box", as seen in Fig. 2b), and to modify the anode box as a basket to receive pieces of scrap metal wire, plate or particles as shown in Fig. 2c). Such cells typically contain electrolyte volumes between tens of $dm^3$ and several $m^3$. Robust, monopolar electrode connections are common.

Industrially, the plate-in-tank geometry is often used to synthesise metal salts or metal oxides by anodic dissolution of (possibly scrap) metal in a suitable solvent. Examples of the production and recycling of electroplating baths include:

1) Dissolution of tin pellets in alkaline, e.g. KOH solutions:

$$Sn + 4OH^- - 2e^- \rightleftarrows Sn(OH)_4^{2-} \quad [1]$$

followed by air oxidation of the stannite to stannate ions in the anolyte:

$$Sn(OH)_4^{2-} + H_2O + 0.5O_2 \rightleftarrows Sn(OH)_6^{2-} \quad [2]$$

or anodic dissolution of tin foil, powder or pellets in acid sulfate baths:

$$Sn - 2e^- \rightleftarrows Sn^{2+} \quad E^\theta = -0.137 \text{ vs SHE} \quad [3]$$

These alkaline and acidic tin electroplating baths can be used in many coatings in microelectronics and printed circuit board manufacture as well as in engineering and decorative surfaces.[35]

2) Preparation of indium electroplating solutions by dissolution of foil or wire in acid sulphate or methanesulphonate solutions:[36]

$$In - 3e^- \rightleftarrows In^{3+} \quad E^\theta = -0.338 \text{ vs SHE} \quad [4]$$

The resulting baths can be employed to realise deposits of lead alloys for wear resistant bearings[22] and in semiconductors (following an electrorefining process).[37]

3) Recycling of spent chromic acid electroplating and etching solutions in the metal finishing industry by combining anodic Cr (III) oxidation with cathodic removal of contaminant metals such as copper, iron and zinc in a membrane divided cell to exploit cathodic metal deposition and electrodialysis.[27] During use, hexavalent chromium anions can be degraded to $Cr^{3+}$ cations. At the platinised titanium mesh anode, regeneration of

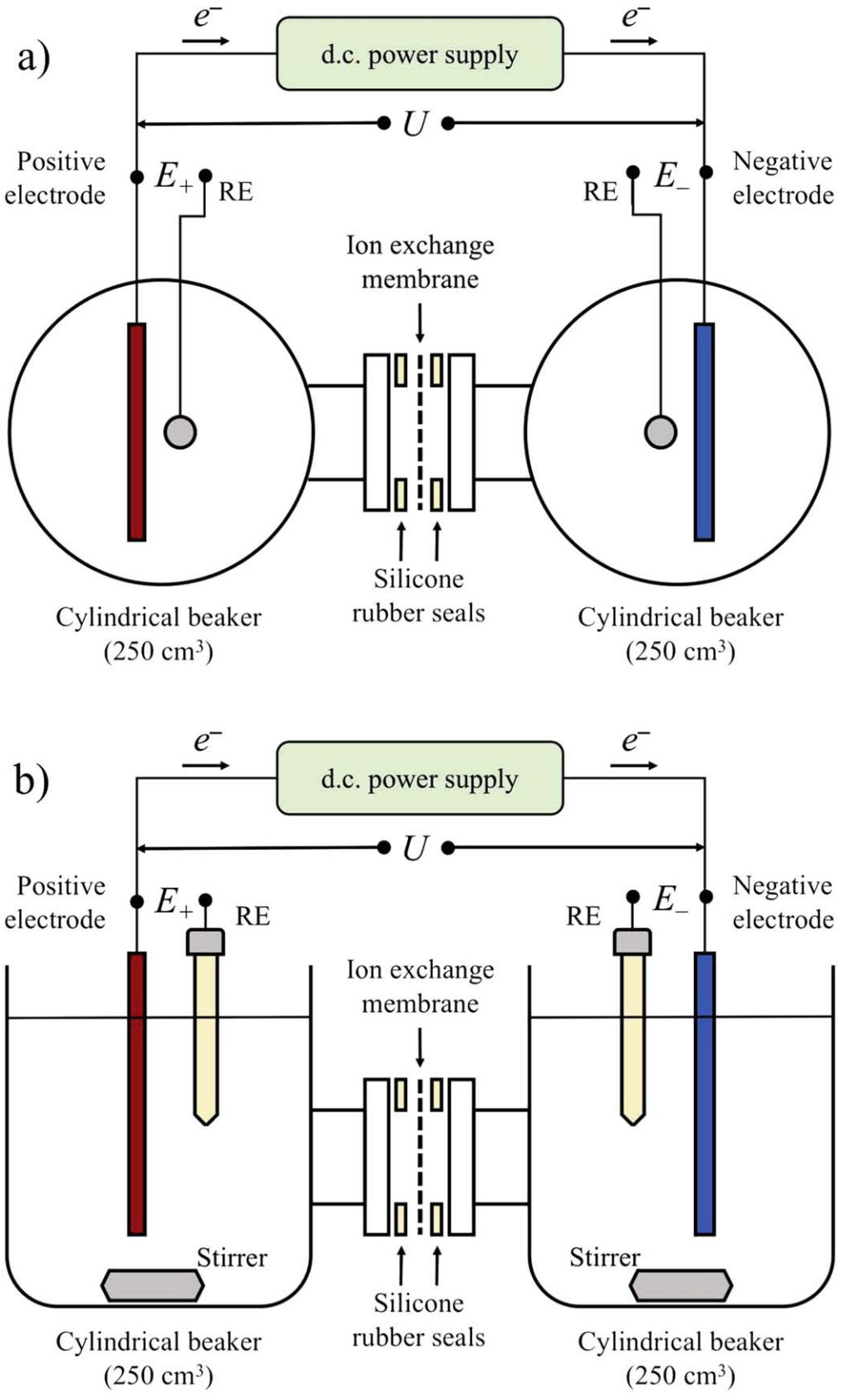


**Figure 1.** A divided laboratory electrolysis cell using planar electrodes using magnetically stirred, 250 $cm^3$ cylindrical beakers joined by a flange containing a cation ion exchange membrane. (a) plan view and (b) sectional view. A smooth, direct current power supply is connected between the cathode and anode, the cell potential between these electrodes being $U$. The potentials of the negative and positive electrodes, $E_-$ and $E_+$ are monitored vs a reference electrode in each compartment.

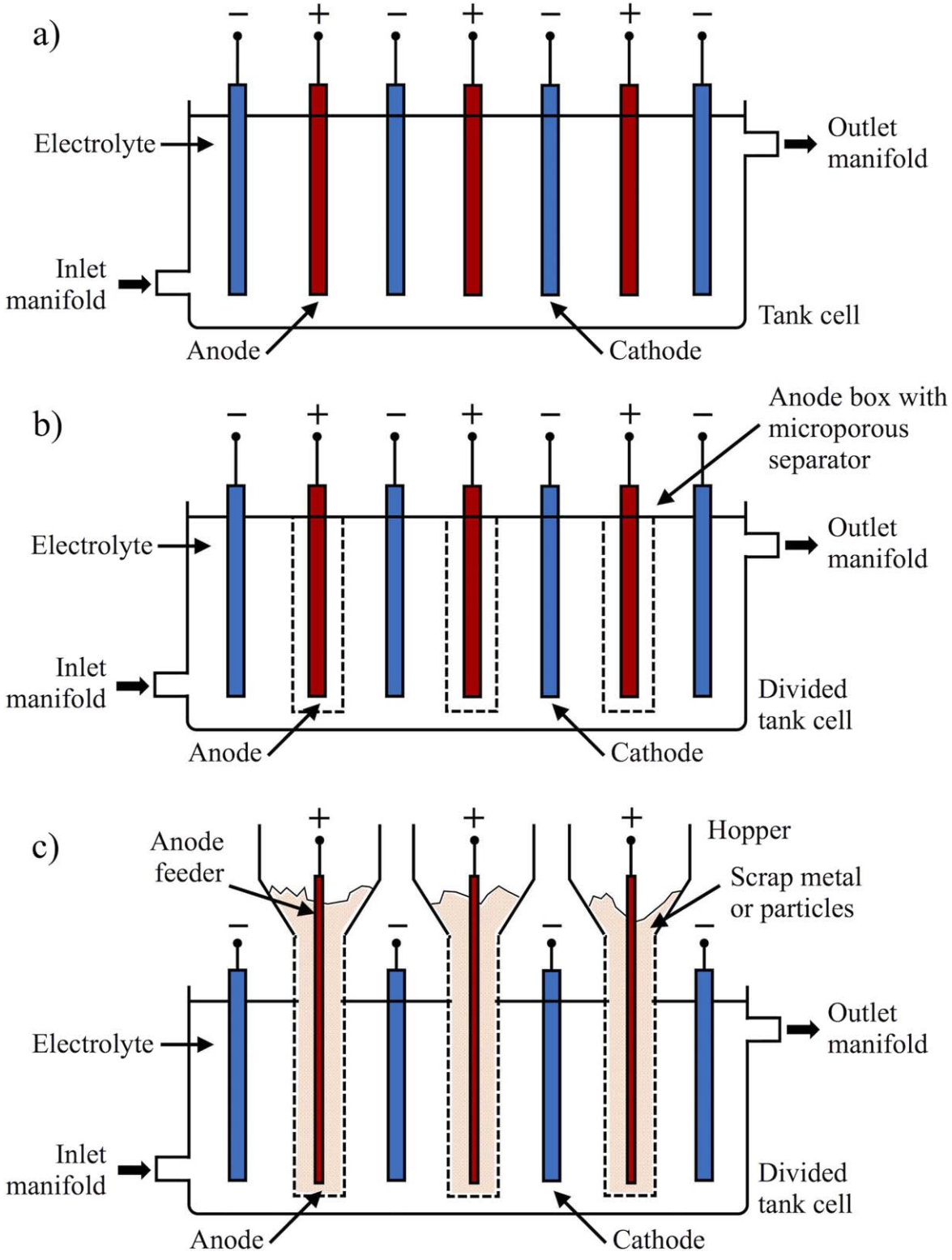


**Figure 2.** A common industrial cell employing vertical plates in a stirred tank. (a) an undivided cell configuration, (b) a divided cell incorporating a microporous polymer or ion exchange membrane into an "anode box" or "cathode box" and (c) modification of the anode box with a hopper to receive pieces of scrap metal wire, plate or particles.

Cr(VI) ions takes place:

$$Cr^{3+} + 4H_2O - 3e^- \rightleftarrows HCrO_4^- + 7H^+ \quad E^\theta = +1.350 \text{ vs SHE} \quad [5]$$

is combined with migration of divalent metal ion contaminants, e.g. $Cu^{2+}$, $Fe^{2+}$ and $Zn^{2+}$, through the cation membrane, followed by their reduction to metal at an inert, e.g. stainless steel, cathode:

$$Cu^{2+} + 2e^- \rightleftarrows Cu \quad E^o = +0.342 \text{ vs SHE} \qquad [6]$$

Recent studies have shown the advantages of a titanium or graphite anode in realising good current efficiency over a wide range of dissolved chromium concentration, at a stable, non-passivating surface.[38]

4) Cuprous oxide can be synthesised in monopolar, undivided cells in *ca.* 3 mol $dm^{-3}$ sodium chloride solution at 45°C–60°C. In simple cases, copper anodes and cathodes, cast from melted scrap, are suspended in open tanks with an interelectrode gap of 2–4 cm. Typically, a $Cu_2O$ slurry containing 3–5 $\mu$m diameter particles is produced at the anode surface using a current density of 30 mA $cm^{-2}$:

$$2Cu + 2OH^- - 2e^- \rightleftarrows Cu_2O + H_2O \qquad [7]$$

while hydrogen evolution occurs at the cathode, generating hydroxyl ions:

$$2H_2O + 2e^- \rightleftarrows H_2 + 2OH^- \qquad [8]$$

To utilise both anode and cathode, the cell polarity can be reversed at 30–45 min intervals, as indicated on page 291 of Ref. 5. By suitable control of the electrolyte and electrolytic process conditions, the particle size can be kept low and catalytic activity maintained, making the $Cu_2O$ product suitable for simple solar cells.[39,40]

5) Synthesis of diverse electrodeposition baths in methanesulfonic acid (MSA).[5] MSA has low vapour pressure and toxicity, mild corrosivity (compared to other strong acids) and supports a high concentration of many metals.[41] MSA and other sulfonic acids have been successfully used in industry to produce noble metal solutions (e.g., for electroplating) and to cathodically recover metals from electronic scrap.

Another use of the plate-in-tank geometry consists on the inverse process to electrode dissolution, i.e., electrowinning and selective metal recovery. Such electrometallurgical operations are relevant to the mining and recycling industries. The main examples are copper,[42,43] nickel,[44] zinc,[45] and cobalt[46] electrowinning from acidic sulfate or chloride baths. Figure 3 shows a pilot industrial facility for copper electrowinning at parallel plate electrodes. Zinc is recovered at aluminium cathodes from an acidic sulfate liquor following the extraction of impurities in an organic phase[45,47] and silver electrorefining is performed from impure silver, cast planar anodes placed in vertical or horizontal boxes in tanks immersed in silver nitrate acid solutions[5]; a recent example is found in Claessens et al.[48] Planar cathodes are used so that the reclaimed metal can be scraped off after achieving an optimal thickness. Expanded metal mesh anodes (counter-electrodes) can be employed, e.g., platinized titanium, but lead anodes are more traditional.[47]

An application of increasing importance is the separation and recovery of precious and high value metals from electronic scrap. Copper and silver can be recovered from acidic sulfate liquors at planar electrodes with high efficiency, allowing the separation of gold and palladium after their dissolution in acidic chloride solutions.[49] Alternatively, copper is dissolved in a mixture of bleach and HCl.[50] Its recovery is coupled with gold enrichment from solutions containing lead, antimony or tin has also been demonstrated.[43,51] Industrial developments have made such operations in tanks routine,[49] encouraged by the urgent need to preserve critical resources. Such recycling operations are rarely reported in the literature and offer opportunities for research of sustainable electrochemical technologies.

***The rectangular channel flow cell.***—The rectangular channel flow cell is the most appropriate design for continuous electrochemical operations where ability to scale-up the process is essential. Successful scale-up implies delivering controlled electrolyte flow (reactant supply, product removal) at a reasonable pressure drop to a number of larger electrodes. In contrast to stirred batch beakers, the reaction environment in a flow cell can be accurately and quantitatively described. As pointed out by Pletcher et al.,[17] flow cells provide a faster reactant conversion than beaker cells due to their superior mass transfer coefficient and their high surface area to volume ratio. Indeed, for the same mass transfer coefficient and electrode area, the reactant conversion is faster in flow cells than in stirred tank cells.[52] Furthermore, filter-press cells with monopolar or bipolar connections are a robust and proven technology.[53] These cells are found in a wide range of electrode sizes, from a few $cm^2$ in the laboratory up to 6 $m^2$ in brine electrolysis plants, with operating currents ranging from the mA to the MA scale.

Rectangular channel flow cells have a number of benefits:

a) they can be scaled-up by increasing electrode size or by constructing stacks of multiple cells,

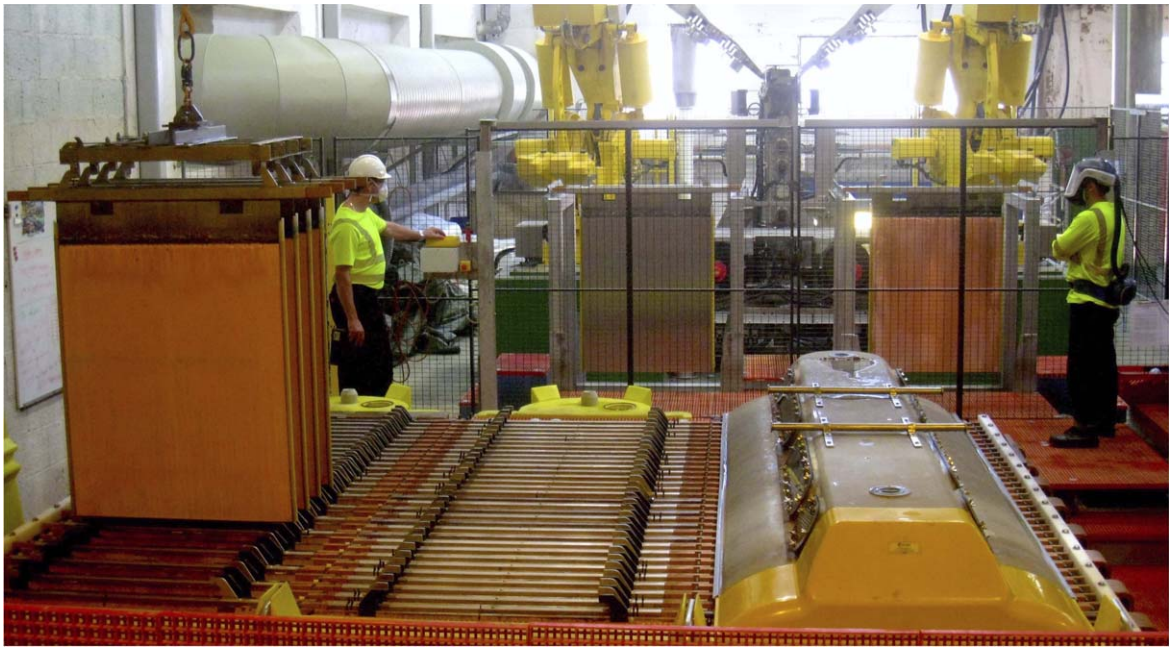

**Figure 3.** A copper electrowinning pilot plant employing full scale monopolar parallel plate electrodes in a tank cell. The plate on which the metal is deposited measures 1.0 m × 1.2 m. Courtesy of Glencore Nikkelverk AS, Norway.

b) mass transfer is controlled by the electrolyte flow rate (laminar, transitional or turbulent),
c) they can operate in batch recirculation or cascade mode, greatly increasing conversion rates,
d) there is the possibility of using a diversity of electrode materials and electrode structures,
e) their components are suitable for mass production,
f) the electrode geometry helps to maintain uniform potential and current distribution,
g) they have the ability to exploit large surface area, porous electrodes.

A general rectangular flow channel cell is shown in Fig. 4, illustrating the wide range of choice in selecting the electrode material and structure, membrane/separator type and the approach used to fabricate the cell body material. As shown in Fig. 5a), electrochemical flow reactors can accommodate numerous unit cells, with their electrodes typically connected in bipolar configuration and separated by ion permeable membranes or microporous materials.[53] In addition to the power supply or load, flow cells are accompanied by a hydraulic system that circulate the electrolytes between their reservoirs and the stack at a controlled rate. Figure 5b) shows an example for a single divided cell in the laboratory with magnetically coupled centrifugal pumps. Several variants are possible depending on the scale and application requirements, e.g., undivided systems connected to an individual reservoir, gravity flow from constant head tanks, use of peristaltic pumps, non-recirculating flow (from holding tank to receiving tank), etc. Walsh et al. have outlined the decisions needed to choose an appropriate plane parallel cell design elsewhere,[5,27] including an updated decision tree approach to cell type, filter press cell configuration and electrode material.[54] An example of an extensively used laboratory flow cell, the FM01-LC electrolyser, has recently been reviewed from the perspectives of general characteristics/applications[55] and reaction engineering.[56]

The rectangular channel flow cell with plane parallel electrodes has found many uses.[15,53,57] The most significant is in the chlor-alkali industry, where a flowing sodium chlorine brine undergoes electrolysis to produce chlorine and sodium hydroxide, with hydrogen as a by-product. Examples of bipolar and monopolar chlor-alkali cell rooms are shown in Fig. 6. The worldwide installed chlorine production capacity in 2012 was 76.8 Mtonne,[58] of which 41% can be attributed to China and 19% to North America. In Europe, the installed capacity is 9.6 Mtonne chlorine,[59] of which 80% is produced using membrane or diaphragm cells. The reaction at the $IrO_x$ and $RuO_x$-coated titanium anodes is:[60]

$$2Cl^- \rightarrow Cl_2 + 2e^- \quad E^\theta = +1.358 \text{ vs SHE} \qquad [9]$$

while the combined reaction at the steel- or nickel-based cathodes in diaphragm- and membrane-divided cells is:

$$2Na^+ + 2e^- + 2H_2O \rightarrow 2NaOH + H_2 \qquad [10]$$

The parallel electrodes in large plants can have a projected area of up to 3 $m^2$. Chlorine is employed in numerous industries,[58] mainly in the production of PVC, isocyanates and oxygenates, disinfectants and water treatment. Caustic soda is used in the paper industry, production of many organic and inorganic compounds, food industries bleach, etc. Recent developments in industry include the implementation of oxygen depolarised cathodes (ODC) in combination with updated cell designs, which can reduce energy consumption by up to 30% in membrane cells.[61] A woven metal mesh gas diffusion electrode GDE, similar to those found in fuel cells, is employed to avoid hydrogen evolution and higher cell potentials when this reaction takes place. The cathodic reaction becomes oxygen reduction:

$$O_2 + 2H_2O + 4e^- \rightarrow 4OH^- \quad E^\theta = +0.401 \text{ vs SHE} \qquad [11]$$

allowing the thermodynamic cell potential to be decreased by 1.23 V, with associated energy savings. The use of GDEs in large chlor-alkali cells requires careful redesign of the cathodic compartment to ensure

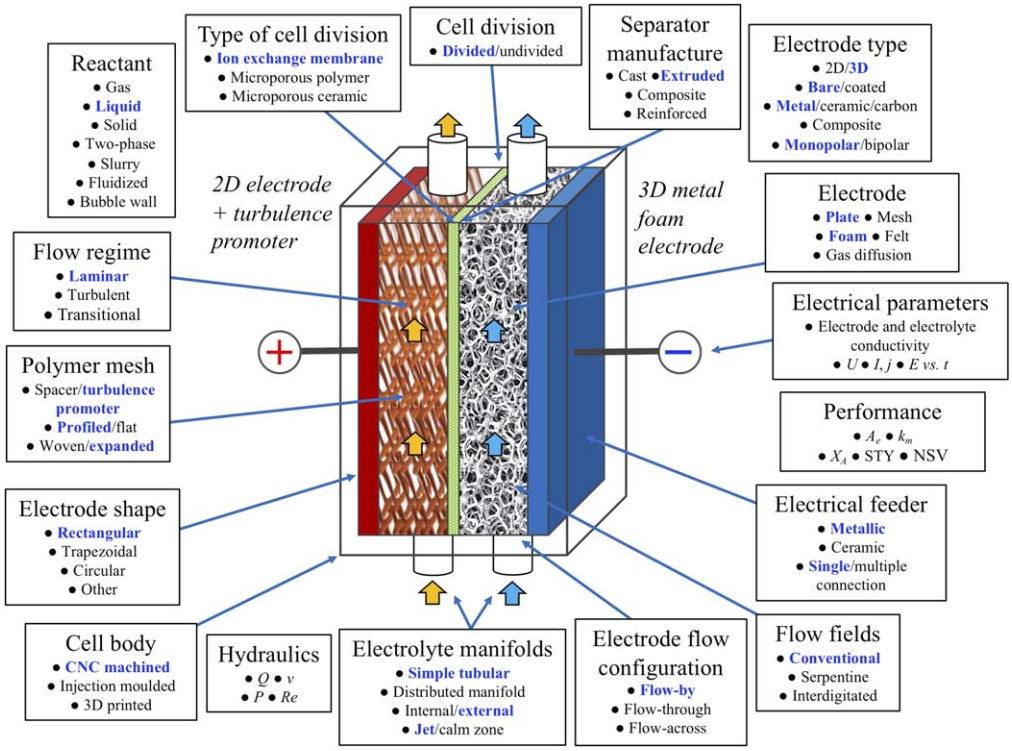


**Figure 4.** A conceptual rectangular channel flow cell, indicating the available choice of cell components, including electrodes, separator, cell divider and turbulence promoter as well as the approach to cell body fabrication and manifold design. Performance indicators include: volumetric mass transfer coefficient, $k_m A_e$, fractional conversion of reactant, $X_A$, the space time yield (STY) of an electrosynthesis cell and the normalised space velocity (NSV) of an environmental treatment cell.

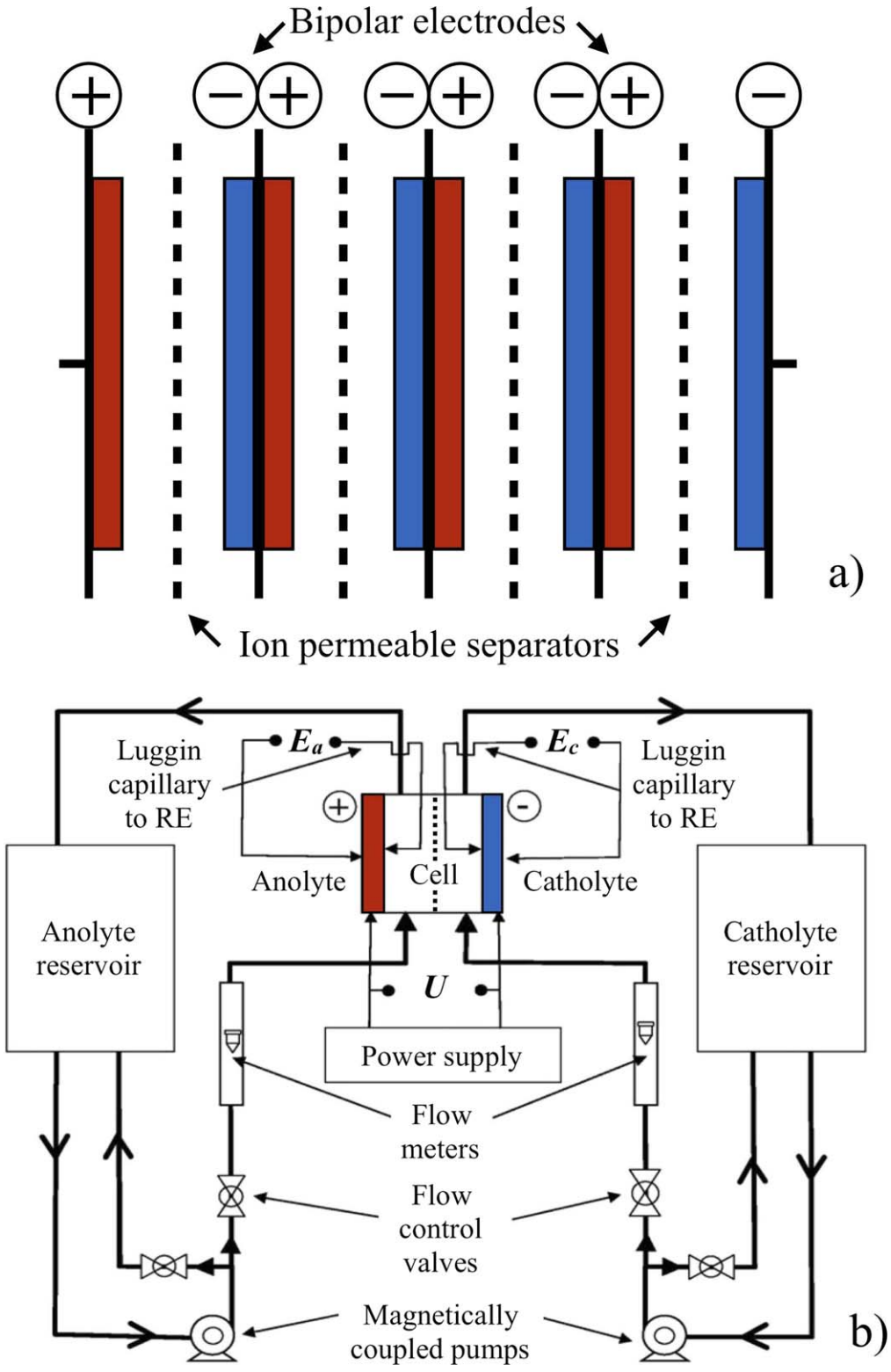


**Figure 5.** Typical divided electrochemical flow reactor. (a) An array of bipolar plane parallel electrodes separated by ion exchange membranes. (b) Experimental arrangement of a divided plane parallel flow cell in electrolytic mode, showing hydraulic circuits for anodic and cathodic compartments as well as electrical instrumentation.

controlled diffusion of oxygen and removal of the caustic product. A physical porous divider enables simultaneous downstream and upstream flow of the NaOH and oxygenated solutions, respectively.[62]

The production of sodium chlorate is similar to chlor-alkali processing, although the cells are undivided.[63] Chlorine ions form hypochlorous acid and hypochlorite ions before chlorate in a solution with a pH between 6 and 7. The overall reaction is:

$$NaCl + 3H_2O \rightarrow NaClO_3 + 3H_2 \quad [12]$$

Direct and mediated electrosynthesis of many organics is also performed in flow cells.[5,16,64] An example relevant for its scale is the

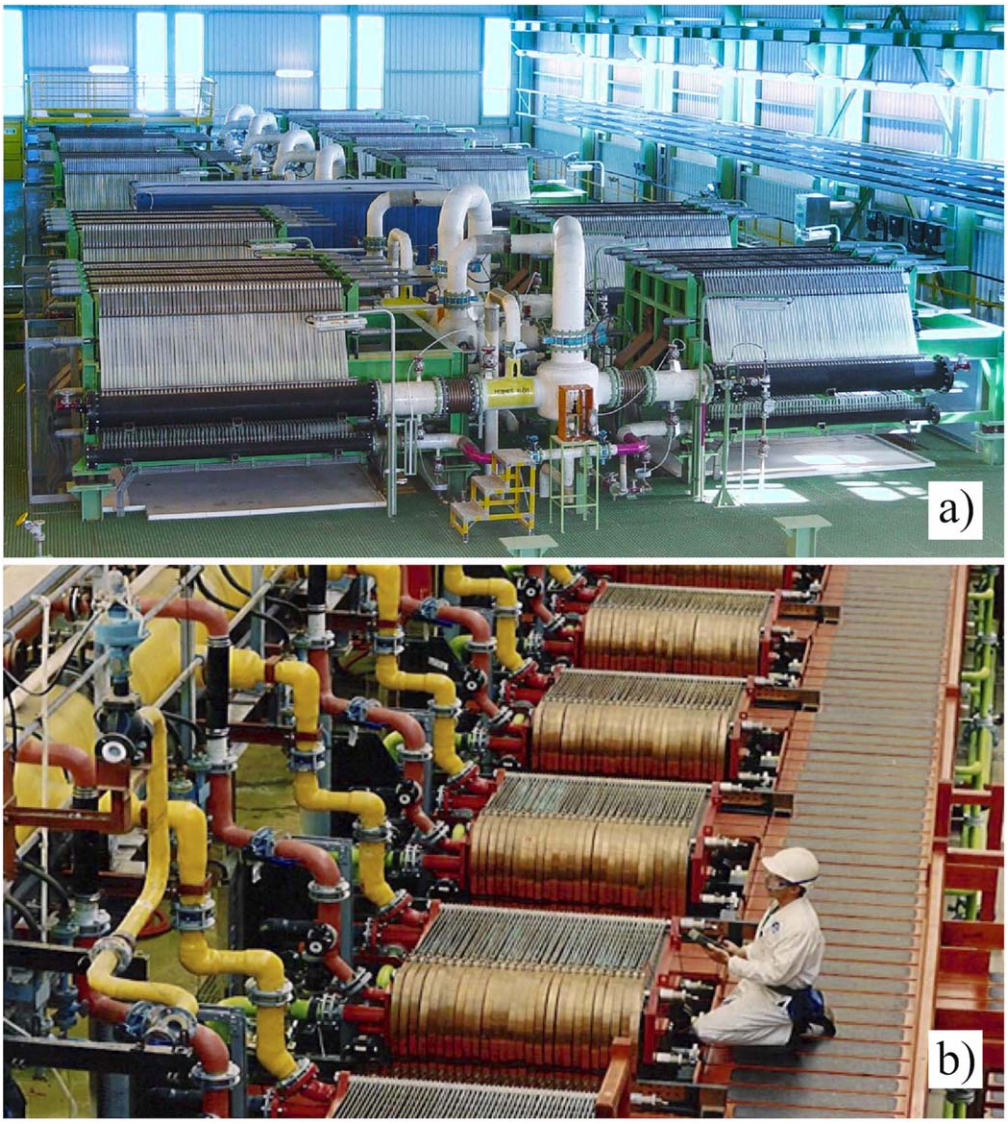


**Figure 6.** Examples of industrial filter-press cells. (a) A cell room with membrane divided bipolar cell stacks for chlorine and caustic soda (chlor-alkali) electrosynthesis. Courtesy of ThyssenKrupp Uhde Chlorine Engineers, ThyssenKrupp Industrial Solutions and De Nora. (b) Monopolar stacks of the FM21-SP electrolyser for chlor-alkali processing. Courtesy of ICI Chemicals and Polymers Ltd (now INOVYN ChlorVinyls Ltd).

hydromerisation of acrylonitrile to adiponitrile, an intermediate in the production of Nylon 6,6:[65]

$$2CH_2 = CHCN + 2e^- + 2H_2O \rightarrow (CH_2)_4(CN)_2 + 2OH^- \quad [13]$$

Among non-mediated reactions, the electrochemical conversion of lignosulfonates to vanillin has been intensively studied.[66] Selective mediated electrosynthesis is also performed, for instance, in the production of tetrahydroquinone via oxidation by Ce(IV) ions at a rate of 400 tonnes per year,[67] as well as the production of vitamin $K_3$.[68] Interest continues in developing novel organic electrosyntheses, as highlighted in recent reviews.[17]

Other common uses of rectangular channel flow cells are found in water technology, particularly in the removal of metal ions from wastewater,[69] decontamination of waste streams through degradation of organics,[70,71] or the production of hypochlorite solutions for diluted brine for water treatment and disinfection.[72,73] Electrodialysis cells employ an arrangement of plane parallel electrodes for water desalination[25] and food processing,[74] although electrochemical reactions are avoided, apart from the production of hydroxyl and hydronium ions. Water electrolysers are another example of plane parallel cells, usually in the bipolar configuration.[75] High purity $H_2$ and $O_2$ are generated in alkaline media for applications where $H_2$ from the chlor-alkali or the reformate process is not suitable. The prospect of exploiting low cost renewable energy sources to drive a hydrogen economy has maintained interest in this technology.[75]

Electrochemical power sources based on flowing reagents have exploited the optimal solution presented by plane parallel electrodes in order to maximise their efficiency. Fuel cells consist of stacks of such electrodes.[76] In this case, the reagents are present in the gaseous phase and flow through machined flow fields within bipolar plates, feeding GDEs impregnated with a catalyst, e.g., platinum on carbon powder. There are several types of fuel cells: proton exchange membrane (PEMFC), phosphoric acid (PAFC), alkaline (AFC), direct methanol (DMFC) and solid oxide (SOFC). In a PEMFC with acid electrolytes, the electrode reactions at the anode and cathode are:

$$2H_2 \rightarrow 4H^+ + 4e^- \quad E^\theta = 0.00 \text{ vs SHE} \quad [14]$$

$$O_2 + 4e^- + 4H^+ \rightarrow 2H_2O \quad E^\theta = +1.229 \text{ vs SHE} \quad [15]$$

Redox flow batteries (RFBs) are a promising energy storage technology which receives increasing attention due to the urgent

demand for large-scale energy storage.[77] Normally, electrochemical filter press reactors containing stacks of planar or interdigitated bipolar electrodes are used.[19] During charge, the cells drive the non-spontaneous conversion of two redox couples dissolved in flowing liquid electrolytes, with reverse, electricity-generating reactions occurring during discharge. At present, the market is dominated by the all-vanadium RFB,[78] which is based on the following reactions at the negative and positive carbon felt electrodes, respectively:

$$V^{3+} + e^- \underset{Discharge}{\overset{Charge}{\leftrightarrows}} V^{2+} \quad E^\theta = -0.255 \text{ vs SHE} \qquad [16]$$

$$VO^{2+} + H_2O \underset{Discharge}{\overset{Charge}{\leftrightarrows}} VO_2^+ + 2H^+ + e^- \quad E^\theta = +0.991 \text{ vs SHE} \qquad [17]$$

The zinc-bromine battery is another type of commercial hybrid RFB.[79] It involves the deposition and redissolution of zinc at the negative electrode and reversible redox of Br complexes at the positive electrode. A large number of alternative chemistries are currently under development.[80] Particular attention is being paid to potentially cost-effective organic redox couples.[81]

Laboratory flow cells used during the first development stages of electrochemical process technology are quite common. Many examples can be found of cells involving electrode areas of 1 $cm^2$ to 100 $cm^2$ for many applications. Such cells permit the evaluation of electrode materials, current efficiency, cell potential, effect of operational conditions, study of mass transfer, reaction yield, rate of conversion, residence time and pressure drop among other parameters. Cell design, uniformity and dispersion of fluid flow have an important effect in their efficiency. For instance, it is known that manifold flow can dominate in small cells, especially if there is appropriate attention to design.[82] In principle, it is also possible to use these flow cells to study the effect of mass transfer on the electrodeposition of metals.[83] Plane parallel electrodes have also received some attention in electrochemical microfluidics and sensors, e.g., in a micro 3-electrode cell for direct analysis of ferrocenemethanol and dopamine.[84] Unusual variations are also possible, such as baffled bipolar gravity-fed open cells.[85] The examples presented here, ranging from industrial chlor-alkali cells to microflow devices, demonstrate the exceptional versatility of plane parallel electrodes in rectangular channel flow cells.

## Features of the Plane Parallel Flow Cell

***General considerations.***—The classical plane parallel electrode geometry has been extensively incorporated in modular filter-press type electrochemical reactors due to many practical advantages. The reaction environment in these cells has been described both experimentally and theoretically, especially in relation to fluid flow, fluid dispersion, mass transfer, potential distribution and concentration change.[86] A wide variety of cells have been documented in diverse application fields such as water electrolysis,[87,88] organic electrosynthesis,[16,17,89] electrodialysis,[25] treatment of water effluents,[90,91] and redox flow batteries.[80,92] Flow cells are versatile, they can be employed throughout the initial evaluation of an electrochemical process, pilot tests and plant scale operation.[82,93] The cell bodies and electrode frames of filter-press electrochemical flow cells can be manufactured in a simple manner by traditional or CNC (computer numerical control) machining of non-conductive, chemically stable polymers such as PVC.[94] When mass production is a necessity, the components can also be produced by extrusion moulding.[95] Glass reinforced polymer composites have also been used for rigidity and chemical resistance.[96,97] These repetitive components are hydraulically sealed with gaskets and held together by compression between two strong, rigid plates.

Adequate characterization and control of the reaction environment are necessary to optimize reactor performance. Important aspects include:

a) the global, local and time-dependent reaction kinetics, hence the electrode reaction rate,
b) mass transfer of all reactive species as a function of flow rate, electrode type and turbulence promoter (if used),
c) concentration, potential and current distribution across and along the electrodes,
d) hydrodynamics, hence electrode geometry and roughness, flow regime, pressure drop and flow dispersion and
e) shunt currents through electrolyte manifolds.

The reaction environment is characterised by the fluid flow regime, mean linear flow velocity past the electrode surface, mass transfer coefficient, flow dispersion, current distribution and pressure drop across the channel. These interrelated parameters determine the performance of the electrochemical reactor. While it is difficult to prioritize them, those related to the electrode process, such as reaction kinetics and mass transfer, should be considered predominant. Various types of experimental studies can be carried out in flow cells to measure them. Some representative examples include: mass transfer characterisation of planar and porous electrodes using the limiting current method[98,99] or reactant conversion method,[100,101] the effect of turbulence promoters,[102–106] effect of manifold flow,[82,107] flow dispersion by conductivity[101,108–110] and dye flow visualisation,[111–115] bubble or particle image velocimetry,[116,117] local potential distribution by probes,[118–120] local current distribution by segmented electrodes,[113,121,122] determination of polarisation curves,[98,123] plus the the importance of operational conditions.[124–126]

A myriad of applications has been explored and commercialised over several decades, making an impact in several fields. In addition to the chlor-alkali industry, water electrolysis and fuel cells, laboratory studies can give an idea of the widespread scope of filter-press flow cells. For instance, such cells have been used as a convenient testbed for organic electrosynthesis,[127] production of pharmaceutical drugs,[128] destruction of toxic halogenated phenols,[129] purification or concentration of acids,[130] production of colloids[131] and nanopowders,[132] palladium recovery from automotive catalysts,[69] removal of heavy metals from water,[133] ozone generation,[134] electrolysis of ammonia,[135] electrodeposition of platinum,[136,137] degradation of organic dyes via an electro-Fenton approach,[138] redox flow batteries,[98] remediation of ground water[139] and treatment of nuclear wastes.[68,140,141]

Another possible use for flow cells is in paired electrosynthesis,[142] where both anodic and cathodic reactions generate products of interest, which can even further combine into a third product. This strategy can increase the energy efficiency of the system, substituting the wasteful gas evolution that often takes place at the counterelectrode. Relevant industrial examples include the electrolysis of 4-tert-butylbenzaldehyde dimethylacetal and phthalide,[142] the convergent electrosynthesis of glyoxylic acid,[143] and the series (anode and cathode) production of $N_2O_5$ (see section Anodic synthesis of $N_2O_5$ in anhydrous nitric acid (in a divided flow cell). Paired electrosynthesis has also been considered in microflow cells.[144]

***Flow velocity and pressure drop.***—Fluid flow in rectangular flow channels is usually described in terms of flow rate and dimensionless correlations. The mean linear flow velocity, $v$ (cm $s^{-1}$) is essential in describing electrolyte flow across the electrode surface. It can be easily calculated for unrestricted rectangular channels or those occupied by a porous electrode or turbulence promoter (TP). Its relationship to the volumetric flow rate, $Q$, ($cm^3$ $s^{-1}$) for a porous electrode is given by:[98,145]

$$v = \frac{Q}{A_x \varepsilon} \qquad [18]$$

where $\varepsilon$ and $A_x$ are the volumetric porosity and cross-sectional area of the homogeneous electrode channel, respectively. An unrestricted

channel has an $\varepsilon$ value of 1. In contrast to the volumetric flow rate, the mean linear flow velocity describes the flow regime past the electrode surface and provides a normalised figure that enables comparing the reaction environment around different electrodes in various cells. Current, current efficiency and cell potential should be reported as a function of $v$. The volumetric flow rate is relevant but refers to a particular cell design and size. The case of $v$ in interdigitated channels containing porous electrodes is more complex since its value changes at different positions in the electrode according to their distance from the inlet and outlet channels (see the section on electrolyte flow configurations at electrode structures). An estimation of $v$ can be obtained from the cross section of the electrode between such channels, although CFD simulations are needed to describe the gradient of flow velocity.[146]

Regardless of electrode geometry, fluid flow though electrochemical cells involves frictional losses that result in increasing pressure drop as a function of flow rate, particularly when porous electrodes with small pore sizes are present. Pressure drop is directly related to pumping energy and the overall energy efficiency of the process. Furthermore, pressure differences between the compartments in divided cells can promote osmotic flow though the membranes and, in extreme cases, their rupture. As a result, the prediction and experimental measurement of the pressure drop in flow channels are important for establishing design requirements, such as channel thickness, sealing, pump size as well as capital and running costs. If cell design considers the minimization of pressure loses, pumping energy demand can be less than 5% of the total energy of the system.[19] Strategies to reduce pressure drop include: short fluid paths through porous materials (e.g., by using an interdigitated flow field configuration, which is also beneficial to the electrochemical performance[147]), minimization of turbulence and changes in the direction of the fluid, sufficient cross-sectional area in manifolds and the flow channel, avoidance of roughness or changes of cross-sectional area in tubbing and connectors and elimination of constricted points in the flow system.

The measurement of pressure drop across flow channels and (internal and external) stack manifolds is usually performed with the aid of differential, gauge or digital manometers. Examples can be found for different types of polymer turbulence promoters in the laboratory,[103,104,148,149] the ElectroSynCell,[95] and a utility scale bromine-polysulfide flow battery.[100,101] The geometry and pore size of porous electrodes determines the pressure drop and has been studied in the FM01-LC reactor with expanded metal, mesh and grid electrodes,[150] the ElectroSynCell with nickel foam,[151] and carbon felt electrodes.[152,153] Recently, pressure drop measurements have been reported in an electrochemical reactor having a thin interelectrode gap[154] and fitted with diverse platinised titanium electrode structures.[155] There is an opportunity to present experimental pressure drop data in large industrial reactors; such data is scarce in the open literature.

Normalised factors allowing the hydraulic characteristics of electrodes and cells can be applied to pressure drop measurements. For example, permeability and friction factor can be presented as a function of the channel Reynolds number and the pressure drop fitting to the Ergun equation for materials having small pore sizes.[156] The mass transfer and area of electrodes has also been related to pressure drop,[150] showing that, in general, higher mass transfer involves an increment in frictional losses. Meanwhile, CFD and numerical simulations increasingly applied to predict the pressure drop at electrochemical cells, e.g., in rectangular channels[157] and in interdigitated or serpentine flow fields.[158–160] Surface roughness and Cassie-Baxter effects on the wettability of felt electrodes have not been considered in such features. Modelling can also be used to estimate the pumping energy demand, e.g., for vanadium RFBs.[161,162] The importance of validating such simulations against experimental data has often been overlooked.

The significance of inlet and outlet manifold design and its relation to the pressure drop at cell stacks has been undervalued in the academic literature despite noteworthy studies on the effect of manifold size and shape on fluid flow and mass transfer by Frias-Ferrer et al. [82] and commercial CFD software by Vazquez et al.,[163] as mentioned in section Current density and potential distributions. For this reason, several cell designs have implemented "calm zones" to develop a laminar flow pattern before solution contacts the electrodes.[133] Deviations from ideal flow in large stacks also contribute to pressure loss. As shown in pilot-scale RFBs,[19] real pressure losses can be higher than those predicted, while manifold losses can have a significant contribution. In cell stacks incorporating gas evolving electrodes, fluid flow can differ considerably from that observed in single-channel cells due to the accumulation of small bubbles.[164,165] Pressure drop has also been predicted for electrochemical reactors involving two phase fluids.[166,167] The flow velocity within porous electrodes can be considered by implementing a modified version of the Brinkman equation.[168] This approach has recently been used in the modelling of flow batteries incorporating carbon felt electrodes.[169–171]

***Mass transfer characterisation and enhancement.***—In practice, the need to realise useful reaction rates at relatively high current densities, particularly with limited reactant concentrations, often means that the electrode reaction rate becomes mass transfer controlled in the cells, e.g., in electrosynthesis studies by Hitchman et al.[172] The main methods for increasing the rate of mass transfer to, or away from, an electrode are:

a) a higher flow rate through the channel,
b) greater flow turbulence due to better electrolyte agitation,
c) improved local turbulence using a roughened electrode surface (see section 2D and 3D, porous electrodes) or
d) improved local turbulence using profiled polymer meshes (see the section on Polymeric inert turbulence promoter meshes).

Planar and mesh electrodes tend to operate at higher current densities, where the effect of mean linear flow velocity is more important. On the other hand, provided sufficient mass transfer, its effects on porous electrodes with large surface area are less pronounced. Sufficient mass transfer rates are necessary to prevent mass transfer overpotentials and secondary reactions. At gas evolving electrodes, the flow rate should be high enough to remove bubbles from the electrode and to avoid shielding of the electrode surface.[173] Most reported electrochemical flow cells for electrosynthesis, flow batteries and environmental remediation operate at mean linear velocities $< 10$ cm $s^{-1}$. An exception is the electrodialytic concentration of aqueous nitric acid, which can involve linear velocities of 66 cm $s^{-1}$.[130] Electrolyte mean linear velocities over 100 cm $s^{-1}$ and up to 1,500 cm $s^{-1}$ in a turbulent flow regime have been utilised during electroforming in plane parallel cells with the purpose of controlling surface morphology.[24,174] One of the highest velocities studied is due to Landolt et al.,[175] who obtained electrochemical mass transfer correlations at a flow velocitity up to 2,000 cm $s^{-1}$ in a specially designed apparatus. The possibility of using drag-reducing additives[176] in electrolytes and the study of their effects on electrochemical reactions are areas of opportunity.

Under full convective-diffusion control, the reactant conversion rate is of first order and the mass transfer characteristics of the cell can be described by an empirical dimensionless group correlation of the form:[1,9,177]

$$Sh = aRe^{b}Sc^{d}Le^{e} \qquad [19]$$

In order to characterise reaction environment, a model reaction in a flow cell can be driven into mass transfer control to determine the mass transfer coefficient, $k_m$ experienced at 2D electrodes or the volumetric mass transfer coefficient, $k_mA_{e.}$ at 3D electrodes. This can be achieved by a) following the reactant conversion in to a plug flow reactor (PFR),[52,178,179] or b) by measuring the limiting current at the electrode.[116] These techniques have been employed to study mass transfer characteristics at many electrode geometries and in several configurations.

The first method can be performed with most electrode reactions and electrolytes. It is common to study applications such as degradation of pollutants, metal recovery and electrosynthesis. See section 3.6. A recent example of a mass transfer controlled process determined from the first order reaction rate is the electrochemical oxidation of gallic acid (3,4,5-trihydroxybenzoic acid) to $CO_2$ on a circular 50 $cm^2$ BDD planar anode with an interelectrode gap of 1 cm from a 50 $cm^2$ area stainless steel flat circular cathode.[180] The electrolyte was stored in a 0.3 $dm^3$ reservoir at 25 °C. Both direct and mediated electrochemical processes were involved in the oxidation and the degradation of gallic acid. The degradation rate was favoured by high flow rates of electrolyte. While the authors stated that the volumetric flow rate varied between 100 and 300 $dm^3\ h^{-1}$, the mean linear flow velocity is unknown.

Limiting current measurements are usually performed in steady state, using electrolytes containing low concentrations of the electroactive species, at planar or mesh electrodes. Thick porous electrodes usually produce deviations due and reactant conversion across its length,[181,182] requiring also ohmic drop correction.[183] Numerous correlations have been reported in the literature since the 1970 s,[184] mainly for the reduction of millimolar $K_3Fe(CN)_6$ in alkaline solutions. The limiting current can also be measured, when convenient, for a practical reaction. For instance, Coria et al. have measured the limiting current for oxygen reduction to hydrogen peroxide at BDD, graphite felt and RVC.[185] Another example is the reduction of Ce(IV) ions at platinised titanium electrodes.[98] Since the mass transfer for $K_3Fe(CN)_6$ reduction depends on the viscosity of the solution, electrolyte thickeners can be added in order to achieve viscosities similar to those of technical electrolytes.

The limiting current technique has often been restricted to planar electrodes or highly conductive or thin porous electrodes with low tortuosity. Assumptions of steady state are also not valid for large electrodes with a high conversion per-pass or those in which the current density and reactant concentration are not uniform along/across their geometry,[186] or when parasitic reactions takes place. The experimental determination of mass transfer in most porous electrodes is more complex. Considerable work has been reported on current/potential distribution models. As pointed out by Masliy et al.,[187,188] early models neglecting the electric field within the pores,[189–192] were later developed into two-dimensional models considering both current and reagent distribution.[190–194] Recently, the current distribution along the current feeder has also been considered.[187,188]

***Current density and potential distributions.—***The relatively large electrodes employed in industrial practice always show a non-uniform current density across their surface. As explained below, this is a consequence of electrode and electrolyte resistivity, flow channel and electrode geometry, reaction kinetics and mass transfer environment. Design and sizing of electrochemical flow cells is based around potential and current distribution, in addition to controlled fluid flow. Neglect of current distribution can result in low coulombic efficiency, corrosion of electrodes, predomination of parasitic reactions, under-utilisation of electrode surface area, potential losses and uneven reaction rates. In view of its importance, current and potential distributions should be studied experimentally and by computational modelling.

The current distribution at an electrode involves electrical resistivity, electrode kinetics and mass transfer but simplified models can be applied to rationalise the parametric effects or achieve useful approximations with modest efforts in computation. Three types of current distribution can be considered, namely primary, secondary and tertiary. Detailed descriptions of the mathematical principles have been given in the early literature, e.g., by Newman et al.[195] However, it is worth considering their main qualitative characteristics and implications, which were summarised by Ibl:[196]

a) *primary current distribution* is experienced at open-circuit, neglecting activation and mass transfer ovepotentials. It depends mainly on the geometry of the electrolyte cross-section between the electrodes and the conductivity of the electrolyte. Under these conditions, the current density tends to infinity at the edges of electrodes which are at an angle of 180 deg or more to an insulator plane but diminishes when this angle is less than 90 deg.
b) *secondary current distribution* considers the electrode kinetics, i.e., the activation overpotential. The potential differences at the electrode are less acute than in the case of the primary current distribution, as electrode regions with high current density also result in larger activation overpotentials. A convenient way to characterize secondary current distribution is by calculating the dimensionless Wagner number,[196,197] which is the ratio of polarization (kinetic) resistance at the electrode to the (ohmic) resistance of the electrolyte. Larger values represent uniform current distribution, while values close to zero are essentially equal to the primary current distribution. For mathematical models, linear, Butler-Volmer and Tafel kinetics can be implemented,[195] the last often being convenient in practical scenarios. In general, the current distribution is more homogeneous with highly conductive electrolytes, steeper slopes of activation overpotential and smaller electrode dimensions. Simplified approaches, where the resistivity of the electrodes is considered infinite, are common. If the resistance of the electrode materials is significant, the model is more complex. The secondary current distribution is a more complex problem in porous electrodes, since the conductivity and potential at the electrode structure and across the permeating electrolyte is a function of the distance from the current collector/feeder.[198]
c) *tertiary current distribution*, is due to a combination of the charge transfer and mass transfer control over the electrode reaction rate. The mass transfer overpotential is determined by electrolyte fluid flow and electrode geometry/roughness. Fluid flow and reaction kinetics vary as a function of electrode length and thickness (the latter in porous electrodes). In view of such complex interactions, numerical methods are an indispensable tool in the study of tertiary current distributions together with experimental measurements of local electrode potential. Conditions outside full mass transfer control, i.e., mixed control, require the assumption of a power series for the surface concentration.[199]

The experimental study of current and potential distribution is not only needed to achieve reliability and efficiency in industrial developments but is also essential to validate mathematical models. Pletcher and Walsh have noted that the *actual* current distribution is often further complicated by gas evolution, multiphase flow, surface films and changes in surface texture.[5] Experimental studies give immediate insights into the reaction environment when modelling becomes too complex. For example, an array of 32 circuit board-printed planar segmented electrodes has permitted the determination of local limiting current density for ferricyanide ion reduction in the laboratory FM01-LC electrolyser, showing that the incorporation of turbulence promoters results in a higher averaged mass transfer and a more uniform current distribution,[121] compared to the non-uniformity near the inlet at unrestricted channels.[113] Similar circuit board-printed arrays were later implemented in fuel cells.[200] Individually connected stacked meshes[201] and segmented porous electrodes[202] have also been considered, as well as indirect current measurements with magnetic loop arrays.[203] In complex arrangements involving new cell designs and/or gas evolution, the segmented electrode approach can be especially useful. For instance, during hypochlorite production in the presence of gas evolution[204] or in dished electrode cells for potassium bromide production.[205] Current distribution at large gas evolving electrodes has also been studied, e.g., for silver ion deposition as an alternative to ferricyanide ion reduction.[206]

Bisang et al. have systematically employed segmented electrodes to reveal the current distribution at different types of reactors studied from the perspective of dimensional analysis, often validating

models coupled to CFD. Early studies were carried out for a gas evolving planar electrode made up by 192 segments.[207,208] Later, the performance of a multipurpose electrochemical reactor having 10 inclined segmented electrodes was considered;[209] fluid dispersion, secondary current distribution and localised mass transfer were determined. The fluid flow inside the reactor could be represented by a dispersed PFR model. The mass transfer at plane parallel electrodes under laminar flow conditions, also used ferricyanide ion and segmented electrodes to provide a comparison between localised experimental and literature mass transfer rates.[210] The reactor construction is well described; the cathode was made of 25 nickel segments, 100 mm wide, 9.5 mm high and 1 mm thick, mutually insulated by strands of epoxy resin. This was followed by mass transfer studies reduction in an electrochemical reactor having a small interelectrode gap of 1.0 or 2.2 mm. Reynolds numbers ranged from 370 to 3,700 and two types of turbulence promoters, based on an expanded or woven structure, were evaluated.[154] The axial current distribution at trapezoidal plane parallel cells with 25 nickel segments and convergent flow was also studied and modelled,[211,212] showing that this configuration, while increasing mass transfer, still maintains a nonuniform current distribution. It was also demonstrated that CFD simulations can predict typical dimensionless groups correlations in such reactors.[213]

The potential distribution can be measured directly against a reference electrode by scanning the electrode surface or the inter-electrode gap with a Luggin probe.[118] This technique has also proved of utility in packed bed electrodes.[214] Multiple probes can measure potential at different points on the electrode.[119] The potential porous different electrodes bipolar electrodes has also been established by placing dynamic hydrogen electrodes within unit-cell compartments, for instance in a flow battery.[120]

One of the fundamental aims of computational modelling of electrochemical systems is the accurate description of current and potential distribution at plane parallel electrodes. Simulations normally involve 1-, 2- and 3-dimensional, static or dynamic as well as "multi-physics" models. Although numerous publications on modelling are available, representative examples focused on current density distribution are discussed here. Current distribution models have been available for over 60 years. For example, Wagner provided a model for parallel plate cells,[215] which was validated against zinc electrodeposition in a electroplating test cell. In addition to the primary current distribution, Parrish and Newman,[216] later calculated analytical secondary distributions for parallel plate flow cells (both anodes and cathodes) using Tafel kinetics. Similar approaches then considered the effect of local current density[217] and axial migration[218] on conversion per pass and current efficiency. Advances in computers eventually allowed to achieve numerical solutions of the Laplace equation and resistor networks representing electrolysers by the finite difference method, considering Butler-Volmer kinetics.[219] Models solved by the finite difference method were later formulated for electrolytes containing several ions,[220] showing that turbulent flow has little effect on the current distribution.[221] Over the last 30 years, modelling of plane parallel flow cells has become more accessible and has been implemented on personal computers for many possible geometries, e.g., to study the effect of elevations at the electrode resulting from dendritic growth.[222]

More recently, "multi-physics" software has been employed to resolve models numerically. For example, Pérez et al. have modelled various current distributions at several flow cells, including the FM01-LC reactor[223] and a multi-purpose laboratory cell.[224] Other examples include studies of tertiary current distribution by Rivero et al.[225] and the related local current efficiency,[226] e.g., for chlorine production, in improved versions of the same reactor having a more uniform flow. Current distribution models relevant to redox flow batteries have also been considered by Nandanwar et al.[227] In the next few years, it can be expected that improvements in computational power will enable real-time, interactive calculation and visualisation of the current distribution in electrochemical flow cells, either in steady state, simulated batch recirculation or other modes of operation. The ease of use in commercial software packages integrated with CAD models will approach modelling to the non-specialist. However, experimental results remain vital to an appreciation of fundamental reaction environment and are needed to validate models.

***Reactant conversion over time.***—Electrochemical flow reactors fitted with plane parallel electrodes should provide an efficient conversion of reactants into products. This implies the prediction (by cell design) and monitoring of reactant or product present in the electrolyte over time in a batch system or over the reactor inlet and outlet in a continuous flow reactor. A common strategy consists on describing the change of concentration in flow cells by PFR models,[178] under mass transfer control. Cells having a higher Peclet number show smaller deviations from the PFR model.[228] The simplest expression is the single pass fractional conversion of reactant, $X_A$, at an electrode in a flow cell:

$$X_A = 1 - \exp\left(-\frac{k_m A}{Q}\right) \qquad [20]$$

where, $k_m$ is the mass transfer coefficient, Q is the volumetric flow rate and $A$ is the electrode area. The product of the latter two terms, $k_m A$, is a characteristic performance factor for the electrode/cell combination.[1,8,178]

The single pass expression is the basis for more elaborated PFR equations that account for the conversion rate in flow cells hydraulically connected to electrolyte tanks holding constantly recirculating solutions (batch recirculation[52]) and flow cells hydraulically connected in series (cascade of reactors[179]). These modes of operation are usually more convenient, as single pass conversion is more often limited at electrodes of practical length and because they permit to process larger volumes of reactant. Improved accuracy in models for plane parallel flow cells can be obtained by considering the inevitable deviations from laminar flow and plug flow in real cells.[229] The critical time for the transition between charge transfer and mass transfer reaction control under constant current operation can be easily calculated,[230] together with the fractional conversion over time for applied current densities below the limiting current density value by using PFR expressions in a dimensionless form.

The fractional conversion of reactants can be followed using various techniques. Some examples in the recent literature on plane parallel flow include volumetric analysis,[131,231] ion selective electrodes,[135] UV visible spectroscopy,[71,232] open circuit potential in monitoring flow cells,[233] gas chromatography (GC) and high-performance liquid chromatography (HPLC).[234]

## Types of Electrodes

An increasing diversity of electrode form, composition and structure is possible; both coated and uncoated materials are used, including modern composites, alloys and hybrid structures.[235] This section illustrates examples and their features.

***General properties and possible electrode materials.***—Many electrode materials and forms are available or can be easily manufactured using classical or additive manufacturing routes. Metal, ceramic and carbon-based materials can be found in many forms, ranging from uncoated plates and foils to more complex structures such as catalyst-coated metal meshes, composites, conductive textiles and porous paper or felt GDEs. Practical aspects, such as cost, availability, lifetime and maintenance requirements can dominate the choice of electrode material.[236] The main properties of electrode materials include area, porosity, conductivity and activity towards redox reactions. Electrochemical applications usually demand chemical stability, wettability, high electrocatalytic activity and selectivity. Mechanical properties and density can also be important factors, especially in large cell stacks. In some cases,

the electrodes are deliberately dissolved, as discussed in the section on Vertical plates in a stirred tank. Typical electrode materials are described below in order to indicate their diversity.

Perhaps the most common *insoluble* electrodes are metal sheets, meshes or foams coated with a catalytic metal or metal oxides.[237] Platinised titanium electrodes[238] and dimensionally stable anodes (DSA®)[239] are well-known examples. Other, more specialised, electrodes comprise variations of the platinum group oxides deposited on refractory metals, such as tantalum.[240] Non-precious metals and alloys are also relevant, such as nickel or nickel-coated stainless steel is employed in chlor-alkali cells.[58] Other example are aluminium cathodes, which are used in zinc electrowinning.[47] Manufacturing methods must also be considered. Simple sheets and meshes are usually produced by cutting and machining, while carbon-polymer composites are often extruded or moulded. Titanium fibres are manufactured using plasma melt overflow and melt spinning.[241] Metal foams can be made in various ways, including pressure infiltration of molten metal into a wax or polymer foam mould.[242] Recently, specialised small-scale reactors have been produced by fast prototyping techniques, particularly 3D printing, e.g.[243,244]

Lead dioxide coatings provide a traditional example of ceramic electrodes,[245] which have been extensively applied to the manufacture of various chemicals. Magnéli phase titanium oxides display a conductivity comparable to graphite and a corrosion resistance superior to titanium.[246,247] More recently, boron doped diamond (BDD) coatings have received much attention for anodic oxidation in view of their stability and large overpotential for oxygen and hydrogen evolution, which is useful for the selective oxidation of organic pollutants contained in wastewater and electrosynthesis.[248] An important aspect is the application of the catalyst, which can be achieved by electrodeposition, electroless coating, or "dip and bake" methods as well as physical or chemical vapor deposition.[249,250] An important trend is the development of micro- and nanostructured materials to provide new substrates and catalysts.[251,252]

Carbon-based materials are important in many electrochemical applications, since they offer a low cost, electrically conductive material of acceptable chemical stability. Types include graphite, glassy, pyrolytic and impervious carbon.[240] The ability to process carbon means that these materials can be found in multiple forms, such as solid plates, foams, cloths, felts, textiles, paper and powders. Carbon materials have been used extensively as bipolar plates and GDLs in fuel cells. Composite carbon-polymer bipolar plates and carbon felt electrodes are also common in redox flow batteries.[253] Carbon fibres can be melt-spun to produce carbon felt, paper and textiles.[254] Carbon foams are produced by heat treatment of polyurethane precursor foams.[255]

All of these electrode materials can be reunited and compared in terms of their broad range of electrical resistivity, $\rho$, as shown in Fig. 7. This property is important in cell design and sizing due to its effect on current and potential distribution as well as on ohmic and heat losses. In order to increase efficiency, components supporting high currents, such as busbars, are manufactured with conducive materials such as copper or, if corrosion resistance is a concern, titanium clad copper. Active electrodes are chosen more in terms of catalytic activity and selectivity but it should be kept in mind that their resistivity is linked to cell potential. Porous materials display the highest resistivity, which imposes some limitations on their application.

***2D and 3D, porous electrodes.—***Electrodes can be classified as 2D materials, consisting of smooth or profiled plates, foils or sheets, or in 3D materials, such as meshes, foams, fibres or cloths. 2D and 3D electrodes differ in their available surface area, hydrodynamic interaction with the flowing electrolyte and intensity of current distribution. A diverse range of both types of materials is available in bulk or coated form. Figure 8 illustrates the diverse form and surface morphology of electrode materials in the case of a) appearance of planar surfaces, b) pore sizes (and shapes) in porous carbon electrodes, c) diverse 3D porous metal structures. Due to their 2D surface area limitations, improvements have long been considered aiming to increase productivity of flow cells. Early attempts to extend the surface area involved serrated and knurled surfaces.[196] A cost-effective approach to increase mass transfer is the placement of polymer turbulence promoters next to a planar surface.[102,104] Other types of surface extensions and mixing devices involve inserting baffles,[265,266] fences or steps[267] into the channels.

Tailored 3D porous electrodes can extend the active surface area many times compared to planar electrodes, increasing the mean linear velocity of the electrolyte, Reynolds number and mass transfer coefficient. These effects can rise the volumetric mass transfer coefficient by several orders of magnitude over 2D electrodes.[98] Some of the first porous electrodes in plane parallel flow reactors consisted on carbon particle packed-beds[268] and metal wool.[8] However, stacks of woven or expanded metal mesh provide several advantages over packed beds and offer a robust solution still in wide use.[269,270] Regarding cost-effective carbon materials, graphite felt,[271] graphite cloth,[272] and reticulated vitreous carbon[255,273] offer a good combination of surface area and permeability. Analogous materials in metal can be titanium felt[136] and mesh,[137] metal foams such as nickel,[259] copper,[274] and titanium.[275] Embroidered wire electrodes have also been considered.[276] The development of porous, 3D electrode architectures and nanostructured surfaces has been one of the major reforms making plane parallel cells more versatile and useful. Examples of classical porous, 3D electrodes are considered in more detail in Pletcher and Walsh,[145] while recent developments, including "nanofelts" and "nanomeshes" are discussed by Arenas et al.[277] A wide variety of commercial materials are readily available.

Additional diversity can be found in the overall shape of the electrode. The rectangular channel with parallel plate rectangular or parallelepiped electrodes is well known, but dished,[278] circular,[34,279] serpentine or spiral,[34,280] and trapezoidal[211,212] geometries are also possible. A well-known disadvantage of long labyrinthine and spiral channels in flow cells is their tendency to accumulate evolved (or trapped) gas, which decreases the electrode active area and changes current distribution, efficiency and selectivity.

Recent advances in the study of 3D electrodes can be found in the use of micro x-ray computed tomography to characterize their structure and determine their surface area, for instance, in the case of reticulated vitreous carbon.[273] Parameters such as volumetric porosity, pore size distribution and tortuosity can be obtained digitally, as demonstrated for nickel foam electrodes.[281] The distribution of metal deposits on 3D electrodes has also been analysed, for instance, iridium on titanium felt.[282] The digital representation of porous structures has been used to simulate hydrodynamics and pressure drop in flow cells,[283] having being applied to the study of diffusion and mass transfer in carbon felts for vanadium RFBs.[284,285] Challenges to this approach involve the definition of voxel resolution, boundary thresholding and limited sample sizes.

***Electrolyte flow configurations at electrode structures.—***The main flow modes in divided rectangular channel cells, according to modern definitions (see also Savinell et al.[286]), are shown in Fig. 9. The flow-by and flow-through modes, which involve orthogonal arrangement of current and electrolyte flow are the most common, since they facilitate a uniform current density distribution and are easy to manufacture. In the first case, shown in Fig. 9a), the electrode channels can contain inert polymer meshes known as turbulence promoters that help maintaining a constant electrode-membrane distance in divided cells and increase mass transfer, e.g. by Bengoa et al.[111] The flow-through mode in Fig. 9b) is used with porous electrodes, being restricted to relatively thin electrodes to avoid non-uniform current distribution, but is a compromise to prevent a high pressure drop, e.g. in Rivera et al.[55] The flow-across mode in Fig. 9c) can be used to decrease the effective thickness of a porous electrode, hence reducing the pressure drop, or to encourage dislodgement of evolving gas. This configuration is common in

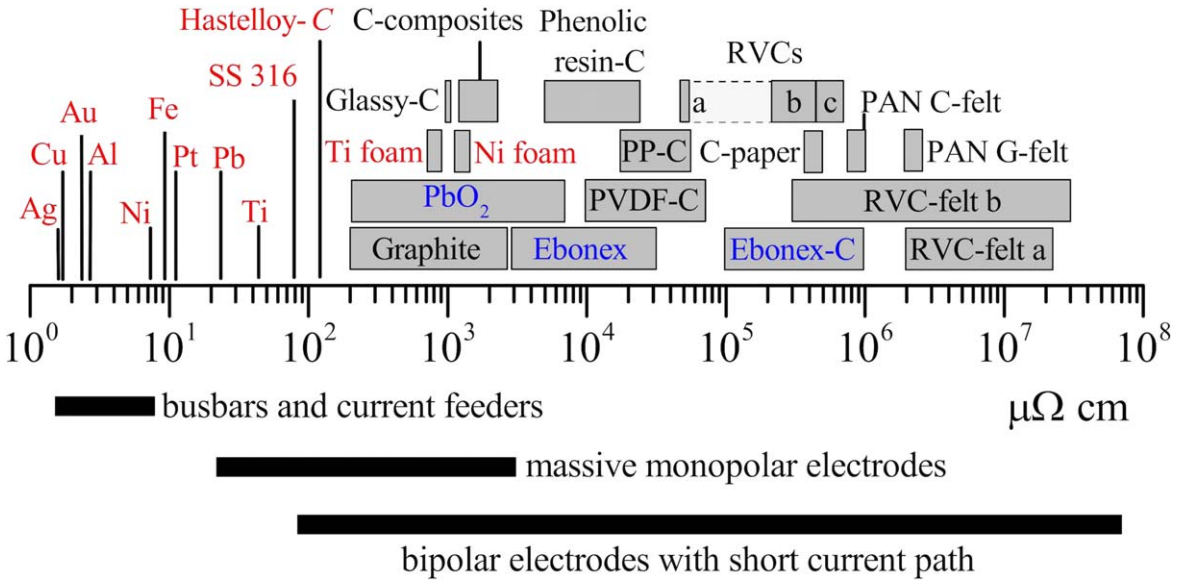


**Figure 7.** The electrical resistivity of common electrode materials and its application in electrochemical engineering. Various metals;[256] stainless steel (AISI 316);[257] Hastelloy-C;[256] Ebonex and Ebonex-carbon composite (C);[240] glassy carbon;[258] nickel foam 100 ppi;[259] carbon composite bipolar plates;[260] other phenolic resin, PVDF and PP composite bipolar plates;[261] 100 ppi RVC;[258,262]; 26 ppi to 78 ppi RVC;[263] carbon paper;[254] PAN carbon (C) and graphite (G) felt;[264] carbon felt;[152] and RVC felts (a), (b).[156] Metals are indicated in red, carbon-based materials in black and ceramics in blue.

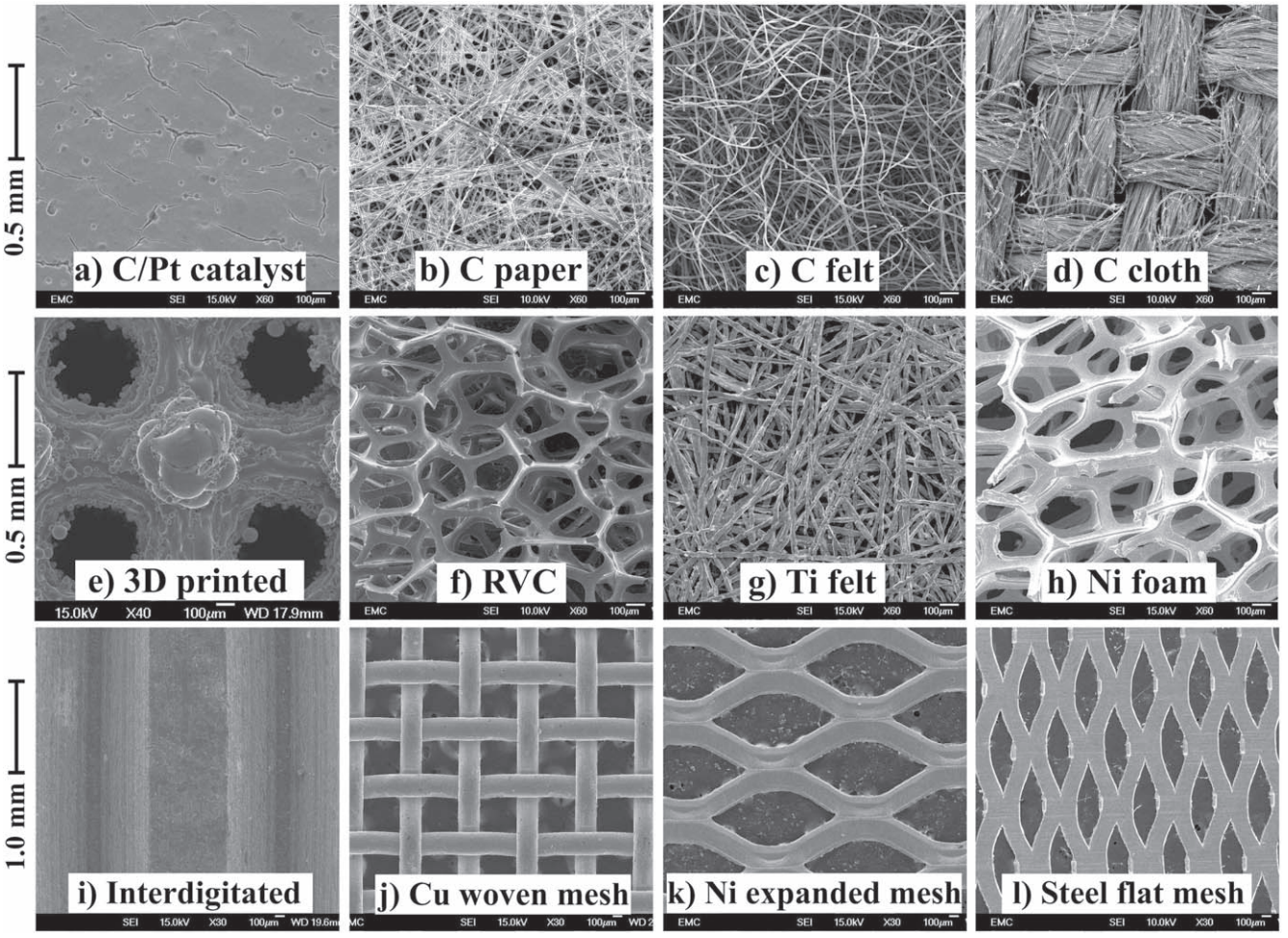


**Figure 8.** Diverse electrode materials employed in plane parallel flow cells and examples of their application. (a) Pt catalyst on a activated carbon support (fuel cells), (b) activated C paper (fuel cells), (c) activated C felt (vanadium flow batteries), (d) activated C woven cloth (electrochemical water filtration), (e) 3D printed stainless steel (specialised advanced flow cells), (f) reticulated vitreous carbon, RVC (metal ion recovery), (g) Ti felt (water electrolysers), (h) Ni foam (organic electrosynthesis), (i) machined graphite forming interdigitated channels (some flow batteries), (j) Cu woven mesh (organic electrosynthesis), (k) Ni expanded mesh (organic electrosynthesis), (l) stainless steel flat mesh (catalyst support).

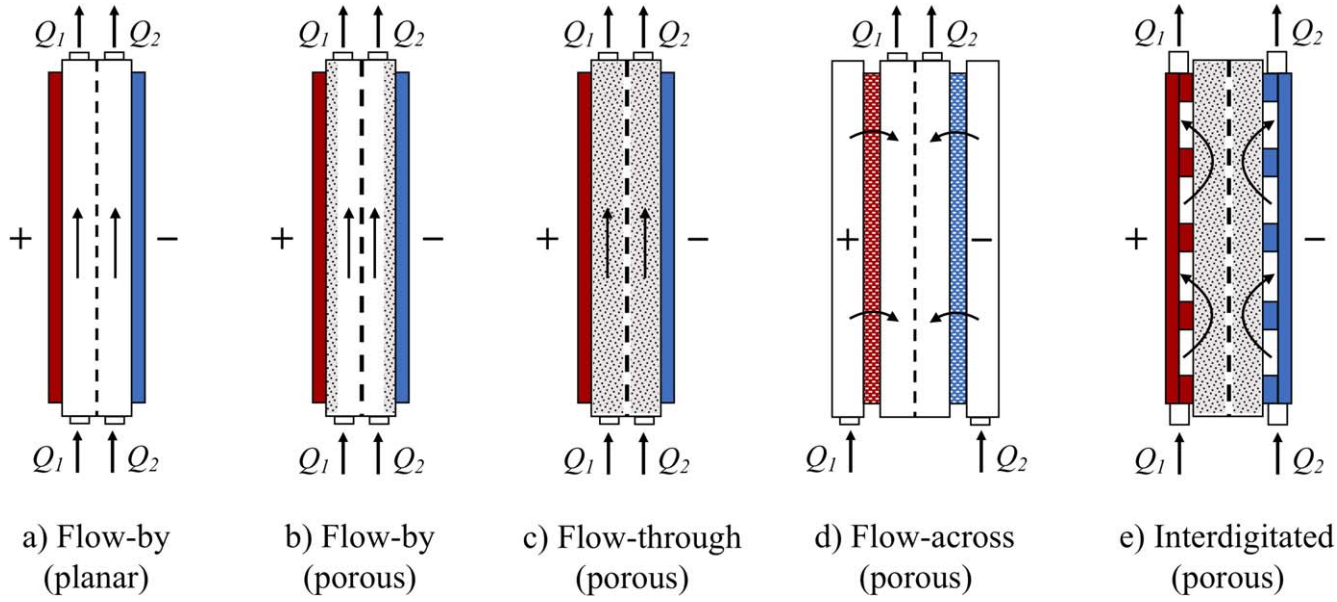


**Figure 9.** Types of electrolyte flow in plane parallel electrode cells. (a) flow-by, (b) flow-through, (c) flow-across and (c) interdigitated.

tubular cells with parallel plane electrodes.[287] In view of the potential drop through a porous electrode connected in its periphery/side, the electrode can be supported on a relative thick highly conductive expanded metal mesh. The flow-across mode is seldom reported in filter press cells, e.g.,[288] since it is more difficult to scale-up,[289] but it is understood that it has been advantageous when coupling electrosynthesis and electrodialysis in the same reactor in pharmaceutical applications. Flow-across electrodes have also been used in the simultaneous oxidation and reduction of reactants in membrane-free cells,[290] and in consecutive electrochemical reactions for organic electrosynthesis.[291] Interdigitated flow fields, shown in Fig. 9d), constitute an alternative flow configuration, which is similar to the flow-across mode but more compact. Periodically spaced channels within the electrode material, or in the bipolar plate, increase flow to the porous material, enhancing mass transfer while reducing the electrolyte path through the porous electrodes, e.g., carbon felt,[146,159,292] albeit with increasing complexity and cost. The interdigitated mode results in significantly lower pressure drop in comparison to the flow-through configuration and, by allowing the use of thinner carbon cloth electrodes, can deliver reduced ohmic losses.[147] In all of these modes, the flow can be laminar, turbulent, or transitional and the mass transfer can be modified by the electrode surface texture, gas evolution, or provision of inert turbulence promoters in the flow channel.[121]

***Polymeric inert turbulence promoter meshes.***—Turbulence promoters are inert polymer meshes used to enhance mass transfer of the electroactive species to 2D, planar electrodes within a flow channel. Furthermore, they result in more uniform local flow and mass transfer along the electrode, which also homogenises the current distribution.[121] Several turbulence promoters can be stacked to fit into the flow channel. Turbulence promoters can also act as simple physical separators, helping to maintain a constant membrane-electrode distance in divided flow cells, while allowing electrolyte flow. The meshes are usually of the expanded type, since flat meshes could partially cover the electrode surface. They should possess a high volumetric porosity in order to avoid high pressure drop. Storck and Hutin have provided a useful survey of pre-1980 literature on various types of turbulence promoters, including plastic meshes.[102] They used localised and global limiting current measurements to demonstrate that the mass transfer and the friction factor could be correlated by mathematical expressions. In a second contribution, the authors monitored the pressure drop across the flow channel and stressed the flow energy requirements using dimensionless correlations.[103] Several examples of polymer meshes, turbulence promoters by Ralph et al.[104] are shown in Fig.10a). Their space-averaged mass transfer coefficient vs the mean linear flow velocity (between 0.5 and 21 cm $s^{-1}$) for a 100 $cm^2$ Pt/Ti plate in a divided filter press cell are shown in Fig. 10b). The use of turbulence promoters resulted in mass transfer enhancement factors up to 2.20 compared to the empty channel, although values of 3.5 have been observed in the FM01-LC cell.[150]

More recently, Dendukuri et al.[112] used CFD to perform flow visualisation of various shapes and profiles of different turbulence promoters. Similarly, Fimbres-Weihs and Gilroy[293] used a numerical methods to evaluate the mass transfer rates and correlate it with pressure drop and flow rates while Koutsou et al.[105] have used both experimental and computational approaches to quantify the effects of the geometry of the promoter and Schmidt number, obtaining a dimensionless group. These studies have achieved insufficient advance from earlier knowledge. Nava et al.[115] have reported a development by validating a model of the flow development and flow dispersion effects of turbulence promoters in the FM01-LC reactor using flow visualisation. Double helix filaments, instead of woven mesh, have been proposed.[294] Although the double helix geometry appears to be less effective and shields the electrode surface to a greater extent, it would be interesting to measure mass transfer enhancement in electrochemical flow cells. Rapid developments made in computational modelling and 3D printing (see section Emerging additive manufacture techniques) offer the opportunity of tailoring turbulence promoters to optimise them for a given flow channel and electrode geometry.

### Cell Body and Flow Channel Construction

Major design trends over the last decade have been the increasing use of fast prototyping, additive construction techniques, especially 3D printing, to complement or replace classical (manual or computer controlled) machining together with the introduction of specialized, mostly conceptual, microflow cells for electrosynthesis. Flow cells intended for research are often designed and produced by academic groups, but commercial devices are also available for laboratory, pilot and full-scale applications, besides proprietary designs developed by the industry. Some of them offer proven reliability, immediate availability, characterized reaction environment, modularity and ease of reproducibility in studies. Some of them, such as the FM01-LC reactor, have been extensively studied.[55,56] However,

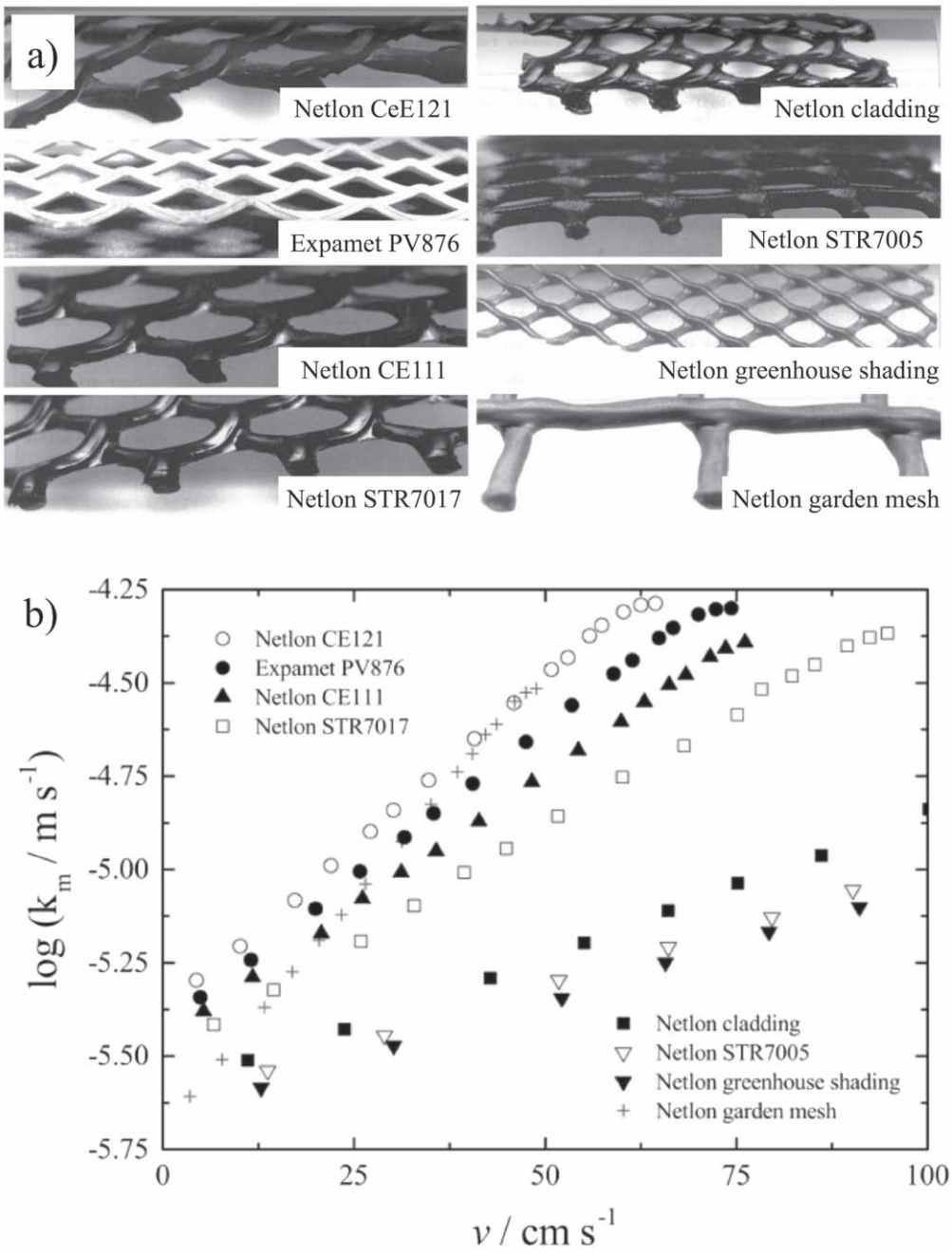


**Figure 10.** Polymer mesh, inert turbulence promoters. (a) Examples of structures and mass transfer performance of a parallel plate flow cell with the rectangular gap between electrode and membrane filled by closely stacked promoters. The photographs are taken at an angle to show their profiled shape. Reproduced with permission from T.R. Ralph, PhD Thesis.[375] (b) Mass transfer in an electrode a flow channel filled with such promoters as a function of linear electrolyte velocity. Data taken from Ralph et al.,[104] and replotted as a function of mean linear velocity.

a number of cells not designed with controlled reaction environment or with ease of use in mind are also found in the market. Regardless of their origin or intended use, manufacturing techniques should be considered against cell performance in a cost-benefit approach.

***Classical machining and moulding approaches.—***In a classical workshop approach, polymer sheet, having a typical thickness of 4–10 mm is machined to produce the required rectangular flow channel and manifolds, typically with a milling machine and possibly under CNC.[295] The removal material tends to be slow, costly and tedious, making injection moulding a more suitable method for the mass production of complex pilot and large size cells.[296,297] Inert cell components, such as electrode frames, gaskets, pipes and valves must be truly non-conductive to avoid potential corrosion and issues with electrical systems due to unintentional electrical grounding.[298] Large stacks, such as those employed in chlor-alkali processing[58] or large water electrolysers,[53] rely heavily on welded metal frames holding the flow channels and robust ancillary structures to position and compress the individual cells between massive compression plates, as seen in Fig. 6.

An example of a flow reactor manufactured by machining of materials and injection moulding for ease of production is the ElectroSyn Cell,[95] shown in Fig. 11a). This reactor was developed as a commercial, general purpose flow cell for electrochemical processing, synthesis and electrodialysis. Its components are displayed in a cut version in Fig. 11b). This cell has been used in divided and undivided modes either in monopolar or bipolar configuration, with inert polymeric mesh turbulence promoters (poly(methyl

methacrylate) and polypropylene) to promote mixing and mass transfer, as characterised by Carlsson et al.[95] The cell also permits the use of packed bed electrodes.[268] A pilot study and modelling of the electrosynthesis of an amino-alcohol was also considered for this device.[299] Flow visualisation studies were later reported,[111] followed by pressure drop,[151] and mass transfer coefficients[300] for a cell employing nickel foam electrodes.

Injection moulding of bipolar electrodes is well suited to mass production and is widely seen in fuel cells and redox flow batteries. However, this manufacturing technique is only cost effective after the reliability of the design has been exhaustively tested,[301] since semicontinuous changes in electrode material composition and shape may be made during the development phase. Injection moulding of carbon-polymer composites is has been applied to the production of bipolar plates for fuel cells.[302–305] Some of these composites contain nanomaterials that improve conductivity, as proposed for all-vanadium flow batteries.[306,307]

***Emerging additive manufacturing techniques.—***Additive manufacturing (especially 3D printing) technologies are now influencing electrochemical technology. Recent progress in CAD design, computer processing power and lower costs have stimulated an explosion of 3D printing devices and applications.[308–310] These automated manufacturing techniques can be employed for fast prototyping, fast manufacture of unique or tailored components, replication and reconstruction of objects and to produce complex, three-dimensional geometrical shapes impossible to manufacture by traditional methods, including CNC machinery. 3D printing is now routinely employed to produce rigid or elastomeric polymers,[309] metals and alloys,[311] intelligent foams,[312] composites,[313] and biological materials.[314]

Most 3D printers are based on layer-by-layer construction of objects by extrusion of molten filaments, selective polymerisation of resins or polymer powder precursors by UV light, laser, or selective fusing of metal powder by a laser.[315] Coaxial extrusion[316] can be employed to produce readily coated fibres. Further, 4D-printing involves smart materials in which their properties change over time or as a result of a stimuli or change in their environment.[317] A disadvantage of these techniques is their limited accuracy and the elevated capital cost of reliable, high precision devices. Control of process parameters are critical to avoid residual porosity and thermally induced stresses, as they can result in deformation of produced objects and detrimental changes in their mechanical properties or hydraulic permeability.

Recently, 3D printed electrodes have been introduced to plane parallel laboratory flow cells having a size capable of producing scale-up data. As shown in Fig. 12a), 3D printed porous electrodes have been used in mass transfer studies of various nickel-coated stainless steel structures[243] and multi-purpose flow cells for laboratory-scale tests of redox flow batteries, metal ion removal, electrosynthesis and electrodeposition.[318] Non-active polymer components of electrochemical flow cells, such as flow frames and endplates have been demonstrated,[319] for instance, in organic electrosynthesis.[266] 3D printing has also been applied to demonstrate the construction of several design concepts on a small scale, such as metallised polymer flow plates with integrated flow fields have in a water electrolyser,[320] or static mixers coated with a graphite to form a type of porous electrode for a mini-flow battery.[321] Other 3D printed electrodes include metal thermal sprayed PEMFC bipolar plates,[322] a miniature PEM stack with honeycomb electrodes[323,324] and micro-[325] or methanol[326,327] fuel cells.

Another application of 3D printing is the prototyping, evaluation and manufacture of electrochemically inert cell components, typically polymer electrode frames and flow channels. This approach has been applied to the design of laboratory redox flow batteries,[318]

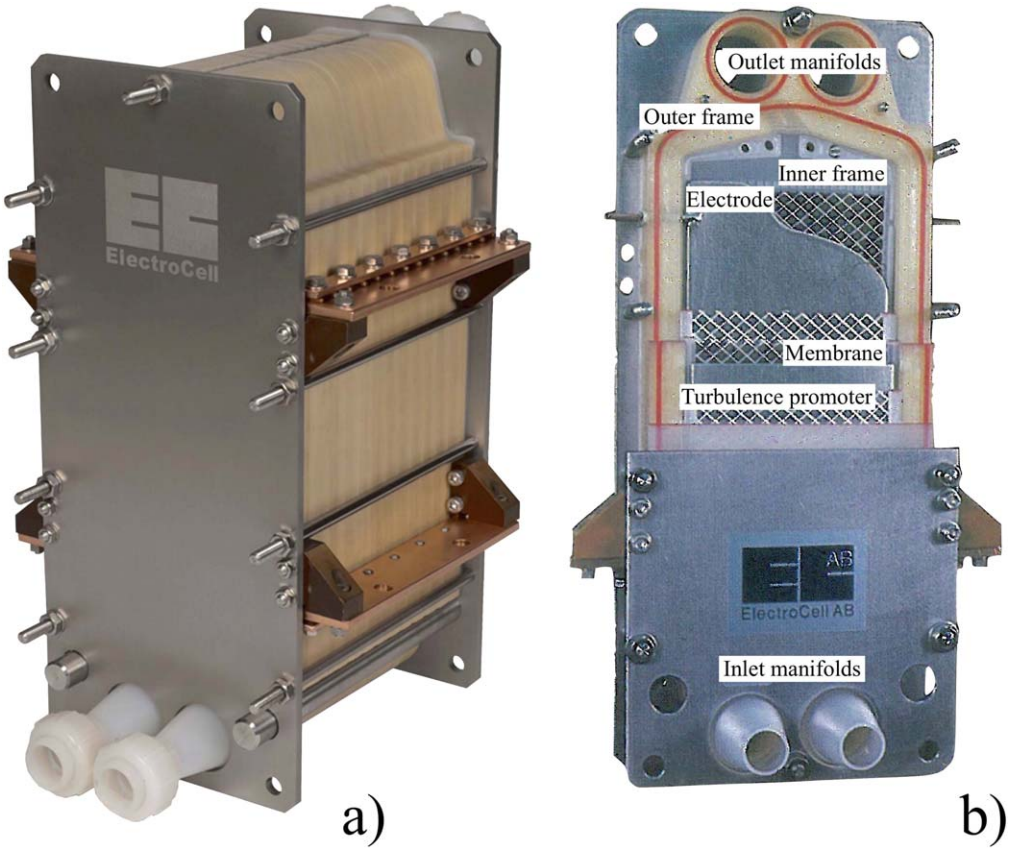


**Figure 11.** An example of an industrial, multipurpose plane parallel filter-press stack in monopolar configuration. (a) The ElectroSyn reactor for pilot and medium scale electrochemical operations. (b) A cutaway view of a unit cell showing its different components, including electrodes, turbulence promoters and polymer electrode frames. Courtesy of ElectroCell A/S, Denmark.

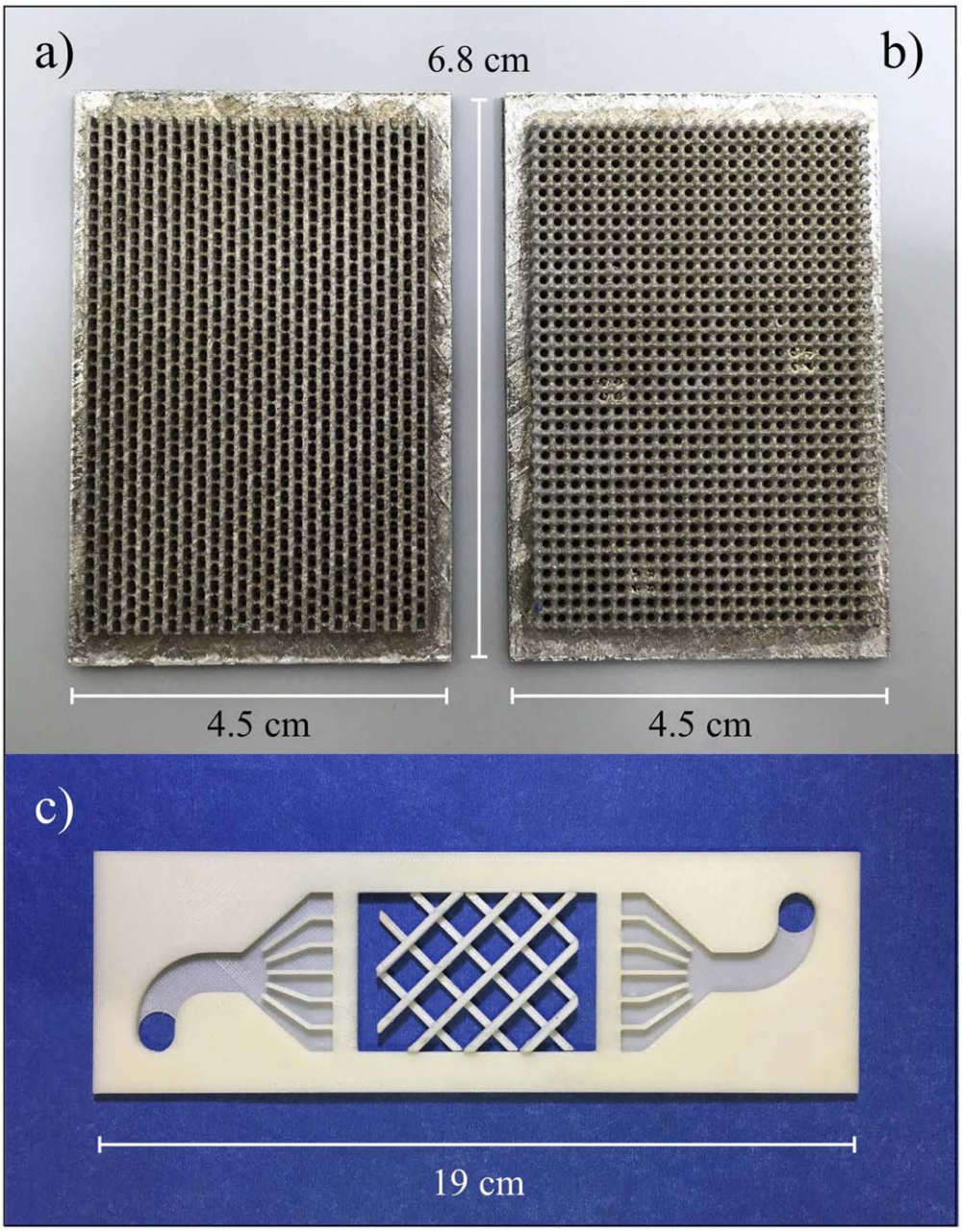


**Figure 12.** 3D printed components of a laboratory parallel plane electrochemical flow cell. (a) 3D printed electrode structure type "A" (porosity 0.64, void sphere diameter 1.8 mm, hexagonal packing); (b) 3D printed electrode structure type "B" (porosity 0.41, void sphere diameter 1.8 mm, square packing). Each stainless steel 316L electrode is nickel-coated and has an integrated current collector/feeder. (c) A 3D printed half-cell flow channel with flow distributors showing a 3D printed turbulence promoter mesh in the electrode compartment (typically used with planar electrodes). These particular pieces were made in acrylonitrile butadiene styrene (ABS) by the molten filament method and intended for use with 24 $cm^2$ electrodes.

permitting the evaluation of the impact of manifolds flow fields and turbulence promoters on electrochemical and hydraulic performance.[318,319] An example of a 3D printed cell frame is shown in Fig. 12b). Suitable 3D printing techniques can be used to produce different parts, e.g. gaskets, frames and electrodes. Thus, adding the printing of membranes, it is now possible to 3D print all the components of electrochemical cells. Given the advances in multi material 3D printing,[313] specialised flow cells could be integrally built in a single operation.

Figure 13 presents the procedure for advanced design of electrochemical flow cells and reactors. It is an iterative procedure in which computed assisted design is followed by modelling of the system and either fast prototyping or conventional manufacturing of the electrochemical cells.[328] The reaction environment is characterised and the experimental evaluation of performance for a specific application. In turn, the model comprises fluid flow, mass transfer, primary, secondary and tertiary current distributions as well as flux through the membrane, if present. Models can also consider structural properties, pressure drop, heat balance and reactant conversion over time. Based on model optimisation and experimental testing of a fast manufacture prototype, the design can be modified, as desired. Once it has been optimised, the device can be mass produced via conventional manufacture techniques, for instance by injection moulding. It can be expected that increasing computer power will result in fast, interactive and integrated "multiphysics" models. In combination with advanced manufacturing techniques, such as 3D printing of composites or

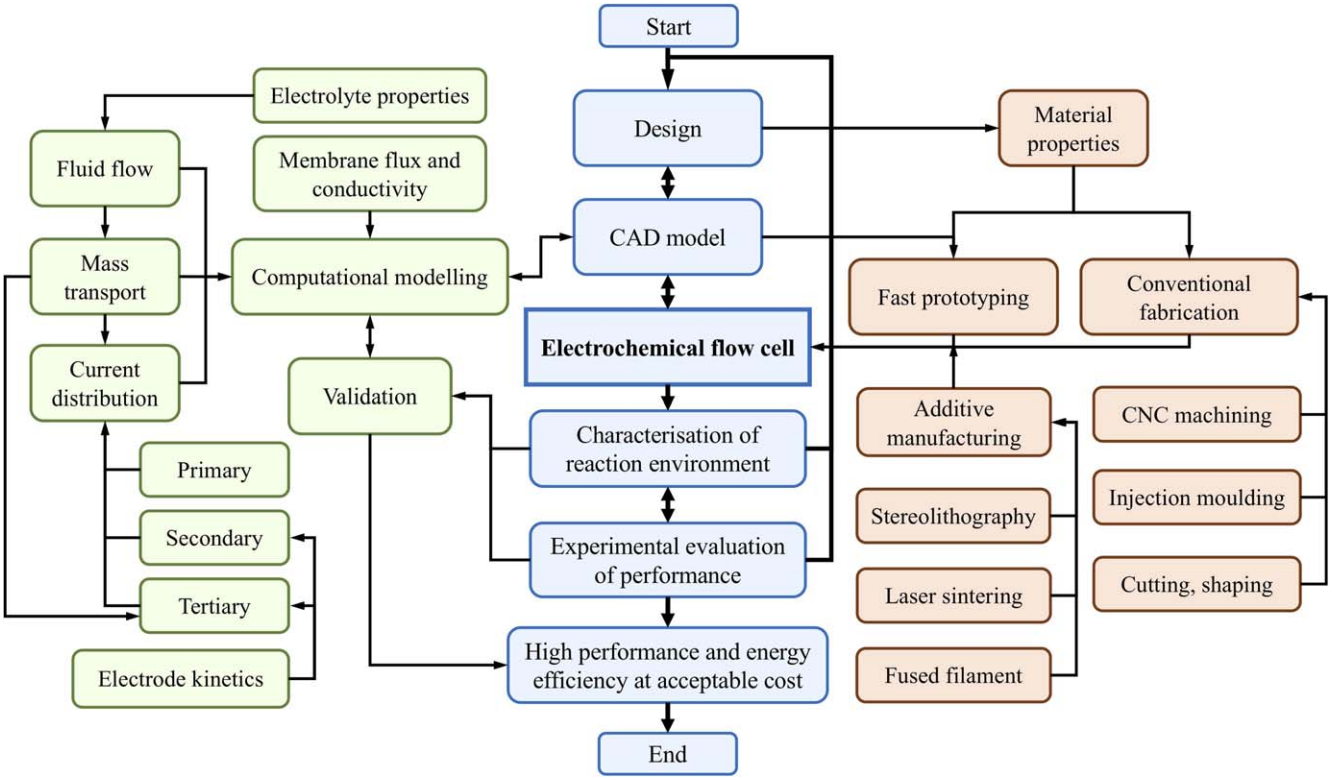


**Figure 13.** An integrated design, simulation and manufacture procedure of electrochemical plane parallel flow cells. The final aim is the production and commercialization of high performance, energy efficient devices at acceptable costs. Design is aided by CAD, which is used both as input in computational models and manufacturing equipment. An iterative process can improve the design and performance by validating the model against experimental evaluation of performance in a well-characterised reaction environment. Aspects usually considered in computation modelling of electrochemical systems and available manufacturing techniques are also outlined.

polymer welding, efficient and long-lasting electrochemical reactors could be produced with minimal waste of materials.

***Miniaturised flow ("microflow") cells.***—Laboratory microflow cells for electrochemical synthesis,[329] particularly of fine organics[17,330,331] have been increasingly introduced over the last decade (Fig. 14). Typical laboratory microflow cell sizes can vary from channels having a volume of 0.1 to 10 $cm^3$, with projected electrode areas of 1–15 $cm^2$ operating at currents $<10$ A to synthesise up to several grams of product. There is a large variation in the interelectrode gap used in microflow cells, values from 50–1000 $\mu$m being found, with volumetric flow rates from 0.01 to 10 $cm^3\ min^{-1}$. Mean linear flow velocities in the wide range of 0.001 to 100 cm $s^{-1}$ can be estimated. As in any flow cell, a flow velocity can be calculated by dividing the volumetric flow rate by the cross-sectional area of the channel or pipe,[332] with the option to consider the porosity of the channel.[145]

Obvious driving forces for the development of such cells include:

a) reasonable manufacture and running costs,
b) small space requirements and ease of handling,
c) the possibility of achieving a high yield and faster conversion,
d) the low electrolyte volume required,
e) the ability to evaluate newer electrode/membrane materials,
f) the possibility of operating in batch recirculation mode,
g) a relatively low cell voltage, hence modest power consumption (when a small interelectrode gap is used) and
h) the ease of manufacturing (and modifying) such cells using fast prototype approaches.

Classically, two parallel foil electrodes separated by thin gaskets make up the flow channel.[333] Ion exchange membrane or microporous separator are optional, depending on the application. Foil electrodes have been augmented by micromesh, foam, felt and sintered materials in metals, carbon, carbon-polymer composites and ceramics; more complex, printed films have become available. Cell bodies have typically been machined from thermoplastic polymers or thermoset resins.[295] Increasingly, photolithography then 3D printing of cells[318] and electrodes,[243] have become attractive in their low cost, versatility of design and convenience, often for the fast manufacture of prototypes.

While many studies have made no attempt to distribute flow across the electrode surface, there are clear examples of serpentine,[334] interdigitated[144] and spiral[335] flow fields. Extended electrode paths have been used with the aim of increasing the single pass convention,[280] but also cells connected in series or in the "cascade" mode.[336] Although flow-by microflow cells are the most common,[20] flow-through configurations,[287] see Fig. 9), can be advantageous when pressure drop has to be minimised for a single electrolyte at high flow rates.

Regardless of their small dimensions, the reaction environment and performance of miniaturised flow cells can be described and modelled according to well established electrochemical engineering principles,[1,4,5,7–11] although authors have not always appreciated this. For instance, individual electrode potentials are routinely overlooked, in spite of its direct impact on product selectivity. It is also rare for the mean linear velocity of electrolyte past the electrode surface, $v$ to be clearly stated; see Eq. 8 and remarks in section Flow velocity and pressure drop. Most authors state only the volumetric flow rate, which gives no indication of the flow conditions at the electrode surface and complicates comparisons among different cell designs and cell sizes. A microflow cell is characterised, in addition to its electrode area, by its mass transfer coefficient, $k_m$, even if it intended for use in a charge transfer regime. Although it can be

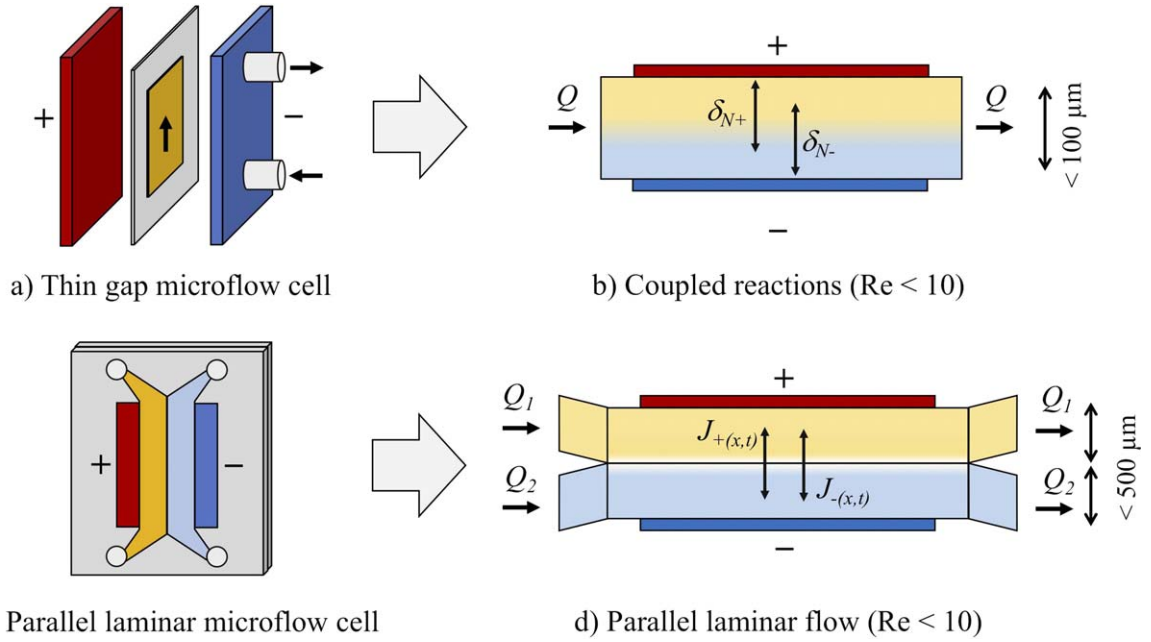


**Figure 14.** Special cases of reaction environment in microflow channel cells. (a) Thin gap (undivided) microflow cell. (b) Schematic cross-section of its flow channel, where "coupled" reactions take place by means of overlapping Nernst diffusion layers, $\delta_N$. (c) Parallel laminar flow (undivided) cell having a quasi-parallel plate configuration. (d) Schematic cross-section of the flow channel in such cell. The two electrolyte streams are only mixed by the diffusion, $J_{(x,t)}$, across the liquid-liquid interphase.

easily determined via limiting current experiments,[337] this critical value is seldom reported. The value of $k_m$ is related to the limiting current, $I_L$ by the expression:

$$I_L = k_m A z F c \quad [21]$$

For the laminar flow of electrolyte through most channels, the fractional conversion of reactant is well described by the single pass PFR design expression[178] which features the volumetric flow rate, $Q$, electrode area, $A$, and the mean mass transfer coefficient, $k_m$. See Eq. 20. Although a high conversion is possible in a single pass in microflow cells,[335] the increase of electrolyte inventory using a tank of volume $V_T$ can be achieved by batch recirculation, as described by:

$$\ln\left[\frac{c_{in(t)}}{c_{in(0)}}\right] = -\frac{Qt}{V_T}\left[1 - \exp\left(-\frac{k_m A}{Q}\right)\right] \quad [22]$$

where $c_{in(0)}$ and $c_{in(t)}$ are the reactant concentration at the inlet of a PFR at times 0 and $t$, respectively, $V_T$ is the electrolyte volume and $Q$ its volumetric flow rate; see Eq. 8. The fractional conversion in batch recirculation mode, $X_{A,t}$, is given by:

$$X_{A,t} = 1 - \frac{c_{in(t)}}{c_{in(0)}} \quad [23]$$

The majority of studies in a microflow cell have used the single pass mode, which implies either a restricted conversion rate or the need for long electrodes prone to depletion of reactant, pH gradients and parasitic reactions.

Notably, microflow cells with thin electrode channels permit to work in reaction environments which are not possible in usual "macro" flow cells. For instance, flow with Reynolds number $< 10$[338] enables "parallel laminar flow" cells where membranes or separators are not needed since the liquid-liquid interphase between two electrolytes (anodic and cathodic) depends only on diffusion. Some examples are the production of carbocations for nucleophilic reactions,[339] the regeneration of nicotinamide cofactors[340] and power delivery devices for microelectronics.[338] Similarly, channels heights below 0.01 mm have allowed to couple reactions by overlapping the diffusion layers at the electrodes.[341] These cells have sometimes been inaccurately called "electrolyte-free," meaning that the reactant itself can be used as the electrolyte (since ohmic resistance is minimised across the thin gap, no additional support electrolyte is needed). However, of course, an electrolyte is always present in an electrochemical cell. Such cells have been used, for instance, for the reduction of olefins,[341] anodic methoxylation of p-methoxy-toluene,[342] methoxylation and acetoxylation of furan,[343] a whole range of benzyl bromide derivatives,[333] synthesis of phenyl-2-propanone,[344] and paired electrosynthesis of toluene and acetophenone.[345] Thin gap microflow channels have restricted prospects for scale up, in view of the low volumetric flow rate, limited electrode area high pressure drop over the cell, which necessitates a specialised pump, secure cell flow connections and adequate closure to achieve leak-free operation.

Going back to conventional organic reactions, longer flow channels have often been used to increase the conversion in a single pass. For example, in thin gap cells, the oxidation of 4-methylanisole to 4-methoxy-benzaldehyde-dimethylacetal[346] and the methoxylation of 4-methoxytoluene[347] have been carried out at a 10 cm long segmented electrode, made by 10 pieces of glassy carbon with a separation of 100 $\mu$m. Meanwhile, tortuous flow paths[280] and spiral electrodes have been applied to the methoxylation of N-formylpyrrolidine.[335] Having an interelectrode gap of 0.5 mm, the spiral cell displayed a single pass fractional conversion of nearly 100% and a selectivity over 95% for a production rate of 20 g $h^{-1}$. Other applications consider the degradation of organic pollutants, such as Acid Orange 7 using an electro-Fenton reaction,[336] or the degradation of formic acid[348] and the pesticide clopyralid (3,6-dichloro-2-pyridinecarboxylic acid)[287] at BDD electrodes.

There are few studies on pressure drop in the channel of microflow cells as a function of flow rate together with synthesis performance, with few exceptions.[349] Gas evolved at electrode surfaces presents a particular problem in microflow cells, due to their small volume and narrow channel gap since a high gas voidage can lead to flow disturbance and greatly increased ohmic drop hence a high cell potential difference. On the other hand, numerous, identical microflow cells fed by a single-phase electrolyte, under gravity, by a common header reservoir and carefully designed fluid manifolds could realise industrial processing requirements.

### Selected Examples of Cell Designs and Their Performance

In order to illustrate the versatility of electrochemical flow reactors with parallel plane configuration, six selected representative examples are described, mainly from the author's experience. They encompass cells with geometrical electrode surface areas between 0.001 $m^2$ and 0.2 $m^2$, 2D and 3D electrode types, currents from mA to kA levels as well as anodic and cathodic reactions of interest. Applications include large-scale and specialized inorganic electrosynthesis, oxidative removal of organic pollutants, fuel cells and redox flow batteries for energy conversion and electrodeposition of metals in both laminar and turbulent flow regimes. The examples, enlisted in Table I, showcase studies based on reactant conversion vs time, quantification of mass transfer, mathematical modelling, power density considerations and measurement of pressure drop. The overall principle consists in the various possible approaches to research in this field and in the important aspects to be consider during the characterization and analysis of both reaction environment and operational performance.

***2D and 3D electrodes in a utility-scale stack (for chlor-alkali).***—Large scale electrolysis plays a critical role in industry.[64] The chlor-alkali industry and the electrowinning of metals produce hundreds of Mtonnes of essential commodity chemicals each year. However, available data on the characteristics, performance and efficiency of the electrochemical cells used in these applications is scarce, especially in view of the urgent need to cut the carbon dioxide footprint of the electrochemical industry.[352]

A notable exception has been the FM21-SP reactor,[353] a utility scale plane parallel reactor, having origins in chlor-alkali production, which was characterised and designed on the basis of mass transfer studies.[350] The monopolar stack with internal manifolds, shown in Fig. 6b) and Fig. 15a), incorporated up to 60 cells made by double sided electrodes, each with a geometrical area of $2.0 \times 0.21$ $m^2$, providing a total electrode area of 25 $m^2$. The reactor was designed for reliability, ease of manufacture and scale-up, high mass transfer and low power consumption. Electrodes were of "lantern blade" type for chlor-alkali, but could also be planar in some applications. (Other cases of documented large scale electrochemical reactors are the ElectroSynCell[95] and an XL bromine-polysulfide flow battery.[100,101]

The mass transfer characteristics of the FM21-SP reactor were studied by determining the global mass transfer coefficient, $k_m$, and the product $k_mA$ from limiting current measurements at a unit electrode using Eq. 21.[350] As explained below, these values were then applied to accurately describe reactant conversion as a function of time. This means that the productivity of the reactor is understood and can be predicted during scale up. The reduction of 0.01 mol $dm^{-3}$ ferricyanide ions in 50 $dm^3$ of deaerated 1.0 mol $dm^{-3}$ KOH solution was used as a model reaction. The oxidation of ferrocyanide ions was carried out at the anode. Flow rate was varied with a pump of 1 $m^3$ $h^{-1}$ maximum capacity.

As shown in Fig. 15b), the limiting current, $I_L$, for reduction of ferricyanide ion at a planar nickel electrode has been determined from polarisation curves obtained at increasing flow rates. As expected, even at this scale, the fast, single electrode transfer reaction displays the typical rate control regions: charge transfer, mixed and mass transfer control and gas evolution. The effect of the type of electrode (planar or lantern blade) and the presence of a polymer turbulence promoters on the limiting current was also studied. Limiting current values for different configurations are presented in Fig. 15c) as a function of flow rate. The lantern blade electrode in combination with a turbulence promoter yielded the highest limiting current density, over 25 A $m^{-2}$ at 1 $m^3$ $h^{-1}$, six times the value at the planar electrode. In the absence of a turbulence promoter, the 3D lantern blade produced only 12.5 A $m^{-2}$ at the same flow rate.

The resulting values are given in Fig. 15d) as a function of the mean linear electrolyte velocity in the electrode compartments. In log-log form, the relationship between $k_m$ and the flow rate $v$, is linear and can be described through a simple exponential expression. The mass transfer coefficient for the lantern blade/turbulence promoter combination is approximately an order of magnitude superior to a planar electrode in an empty channel. The mass transfer coefficients were then applied to the prediction of the nominal reactant conversion vs time for a two-electron reaction of interest in batch recalculation mode to an electrolyte tank. For this, the FM21-SP cell was reasonably approximated to a PFR in batch recirculation model,[179] according to Eqs. 22 and 23.

Figure 15e) presents the time taken for 90% reactant conversion of a 50 $dm^3$ batch by using different types of 0.45 $m^2$ monopolar electrode. As expected, the lantern blade/turbulence promoter configuration needs less than 5 h to reach the target fractional conversion. In contrast, an unpromoted planar electrode would require nearly 30 h for the same conversion. It is obvious that a competitive productivity is better achieved by employing practical electrodes with a large area and a moderately high rate of mass transfer. Since these characteristics are known for each electrode, the nominal scale up to 60 electrode pairs becomes facile.

Mass transfer studies on the FM21-SP reactor demonstrate the process of design, characterisation and prediction of productivity for a utility scale stack up to a combined electrode area of 25 $m^2$ operating at 37.5 kA. Reactor design was made on the basis of electrochemical mass transfer-controlled reactions and an approximation to the plug-flow reactor model in batch recirculation. It would be expected that current chemical corporations have optimised the energy efficiency of their reactor designs based on a more advanced combination of experimental characterisation and computational simulation.

***Anodic synthesis of $N_2O_5$ in anhydrous nitric acid (in a divided flow cell).***—$N_2O_5$ has specialised applications in the nitration of organics at low temperature.[354] Although its production via electrochemical dehydration of $HNO_3$ has been known for more than a century,[355] it was only in the early 80's when Harrar and Pearson demonstrated the feasibility of $N_2O_5$ synthesis by the oxidation of $N_2O_4$ in anhydrous nitric acid at platinum or $IrO_x$-coated titanium anodes.[356] The process was later improved and scaled-up by implementing the simultaneous regeneration of $N_2O_4$ in the cathode compartment,[354] and demonstrated in a plane parallel flow cell of 200 $cm^2$ electrode area. It should be highlighted that this process is one of the few instances where the anodic reactant is produced at the cathode, as seen in Fig. 16a). Harrar et al. later patented[357] and reported[358] the electrosynthesis of $N_2O_5$ in parallel plate cells with electrodes up to 2,500 $cm^2$ and current densities up to 0.2 A $cm^{-2}$ employing a porous PTFE-ethylene separator, a Pt-Ir coated niobium anode and a Hastelloy cathode. Niobium was required since titanium can catalyse the fast decomposition of unstable nitrogen compounds.

Following a multi-stage approach to the production of $N_2O_5$/$HNO_3$ solutions,[351] a method was developed at the University of Southampton for the synthesis of $N_2O_5$ in anhydrous nitric acid in the anolyte compartment of a unit filter-press cell divided by a very stable cation exchange membrane, utilising anhydrous $HNO_3$ as both anolyte and catholyte solvent (traces of $H_2O$ are readily removed from the anolyte) and generating $N_2O_4$ at the cathode, offering the possibility to return it to the anolyte as a reactant by distillation or other suitable method.[351] The reactants are managed by cooling the system below 10 °C. Apart from the advantageous reduction of species shuttle of between the two compartments and the exclusion of $NO_3^-$ transfer, the cation exchange implies electroosmotic transfer of $HNO_3$. This diminishes the anolyte volume over time. The main overall reactions are given below; $N_2O_4$ can be formally considered as a mixture of $NO^+$ and $NO_3^-$ ions, which makes the anodic reaction more complex.[351]

$$\text{Anode} \quad N_2O_4 + 2HNO_3 - 2e^- \rightarrow 2N_2O_5 + 2H^+ \qquad [24]$$

**Table I. Selected examples of the electrochemical flow reactors with plane parallel geometry used in the academy and industry for diverse applications.**

| Electrode reaction | Working electrode characteristics | Geometrical area | Channel breadth | Channel length | Channel height | Electrolyte rate | Max. mass transfer | References |
|---|---|---|---|---|---|---|---|---|
| Chlor-alkali process | Double sided nickel electrodes (planar and lantern blade) | $2 \times 0.21$ m$^2$ | 24 cm$^2$ | 93 cm$^2$ | 5.2–12.5 mm | 0 to 5.8 cm s$^{-1}$ (0 to 270 cm$^3$ s$^{-1}$) | $k_mA = 1.57$ cm$^3$ s$^{-1}$ | 350 |
| Production of $N_2O_5$ | Pt-Ir coated niobium anode and a Hastelloy cathode (plus a TP and lantern blade) | 64 cm$^2$ | 4 cm$^2$ | 16 cm$^2$ | 1–5 mm | 0 to 66 cm s$^{-1}$ (0 to 132 cm$^3$ s$^{-1}$) | $k_m = 2.8 \times 10^{-3}$ cm s$^{-1}$ | 130, 351 |
| Oxidation of Methyl Orange | $IrO_2$-$SnO_2$-$Sb_2O_5$/Ti anode and stainless steel cathode | 30 cm$^2$ | 4 cm$^2$ | 9 cm$^2$ | 6.6 mm | 0 to 10.5 cm s$^{-1}$ (0 to 27.8 cm$^3$ s$^{-1}$) | $k_m = 3.8 \times 10^{-3}$ cm s$^{-1}$ | 138, 224 |
| Oxidation of boro-hydride ions | Pt-Ir/Ti (plate, mesh, fine mesh, micromesh, felt) | 9 cm$^2$ | 2 cm$^2$ | 4.5 cm$^2$ | 2–4.3 mm | 0 to 16 cm s$^{-1}$ (0 to 9.1 cm$^3$ s$^{-1}$) | $k_mA_e = 0.804$ s$^{-1}$ | 99 |
| Reduction of Ce (IV) ions | Pt/Ti (plate, mesh, micromesh, felt) | 24 cm$^2$ | 4 cm$^2$ | 6 cm$^2$ | 2.5–7.4 mm | 0.25 to 17 cm s$^{-1}$ (0 to 16.0 cm$^3$ s$^{-1}$) | $k_mA_e = 0.103$ s$^{-1}$ | 98 |
| Electroforming of Ni and Cu foils | Stainless steel cathode Ni cathode | 15 cm$^2$ | 3 cm$^2$ | 5 cm$^2$ | 5 mm | 0 to 200 cm s$^{-1}$ | $k_m = 0.035$ cm s$^{-1}$ | 83 |

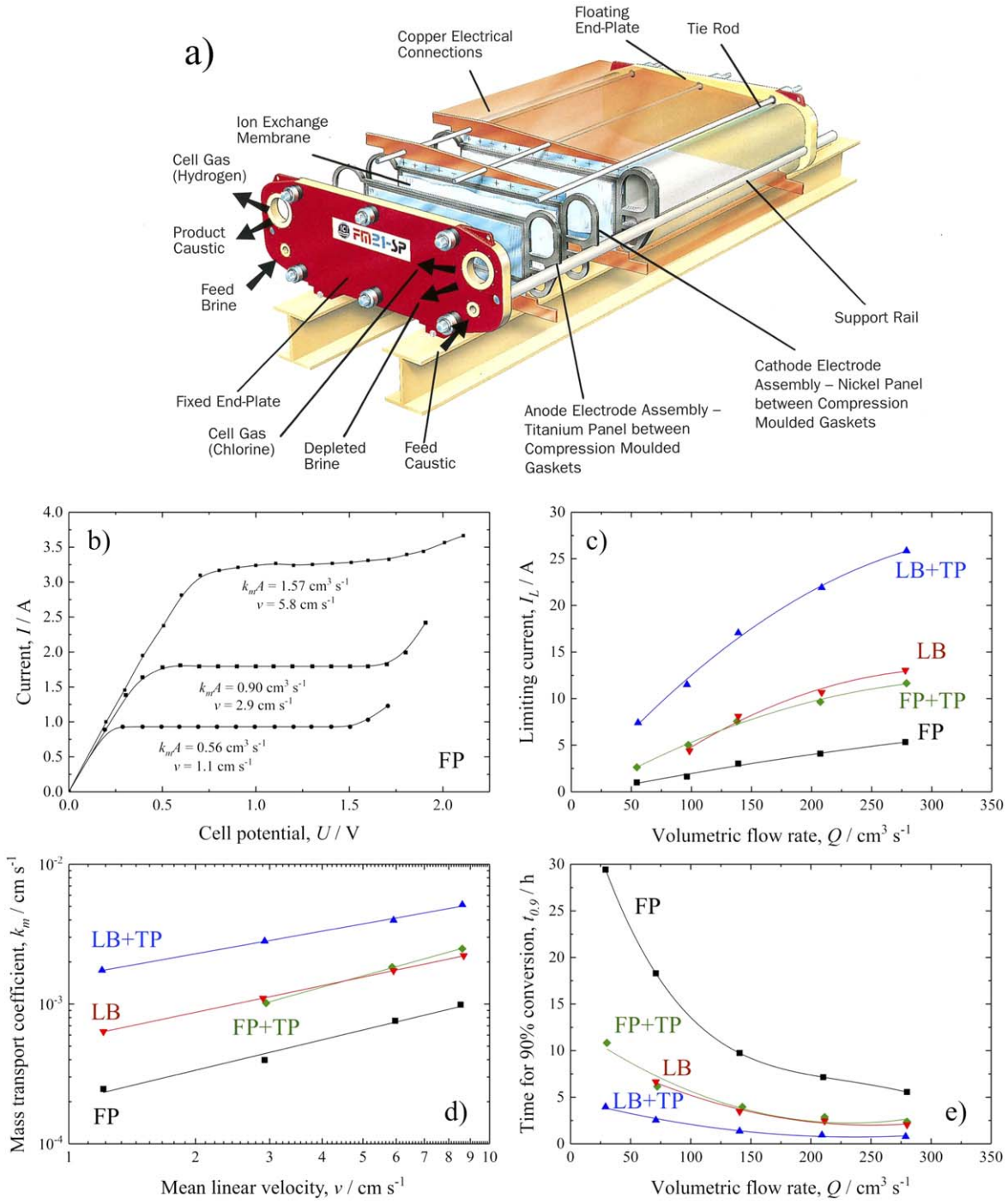


**Figure 15.** The 25 m$^2$ FM21-SP monopolar electrochemical filter-press reactor and mass transfer studies at a unit electrode. Courtesy of ICI Chemicals and Polymers Ltd (now INEOS Chlor Chemicals). (a) The parallel plane FM21-SP stack. (b) Polarisation curve for the reduction of 0.01 mol dm$^{-3}$ ferricyanide at different electrolyte flow rates for a flat planar (FP) electrode. (c) Limiting currents achieved by diverse electrodes as a function of volumetric flow rate, including flat planar plus turbulence promoter (FP + TP), "lantern blade" (LB) and "lantern blade" plus turbulence promoter (LB + TP). (d) Mass transfer coefficient as a function of mean linear flow rate for the same electrodes. (c) Time to achieve 90% of reactant conversion in a two-electron electrosynthesis reaction for different flow rates, assuming a plug flow reactor model. Data taken from Hammond et al.[350]

$$\text{Cathode} \quad 2HNO_3 + 2H^+ + 2e^- \rightarrow N_2O_4 + 2H_2O \qquad [25]$$

$$\text{Overall} \quad 2HNO_3 - H_2O \rightarrow N_2O_5 \qquad [26]$$

$N_2O_5$ electrosynthesis was performed in the divided 200 cm$^2$ laboratory flow cell shown in Fig. 16b), from 10% $N_2O_4$ in $HNO_3$ solutions, at a maximum current density of 125 mA cm$^{-2}$ and 10 °C. The typical specific energy consumption was between 1.0 and 1.5 kW h kg$^{-1}$. The components were chosen to withstand the highly corrosive, oxidising conditions. These components were held together by tie rods between 10 mm thick rigid plates, allowing for the insertion of two Luggin capillaries for electrode potential monitoring. Hydraulic sealing was guaranteed by applying a PTFE emulsion between the cell components. Nafion 425 was used as the cation exchange membrane. The charge needed to oxidise the total amount of $N_2O_4$ is shown in Fig. 16c). This relationship was consistent for a one electron reaction and a charge per mol of oxidised $N_2O_4$ of approximately 98,000 C mol$^{-1}$. The expected

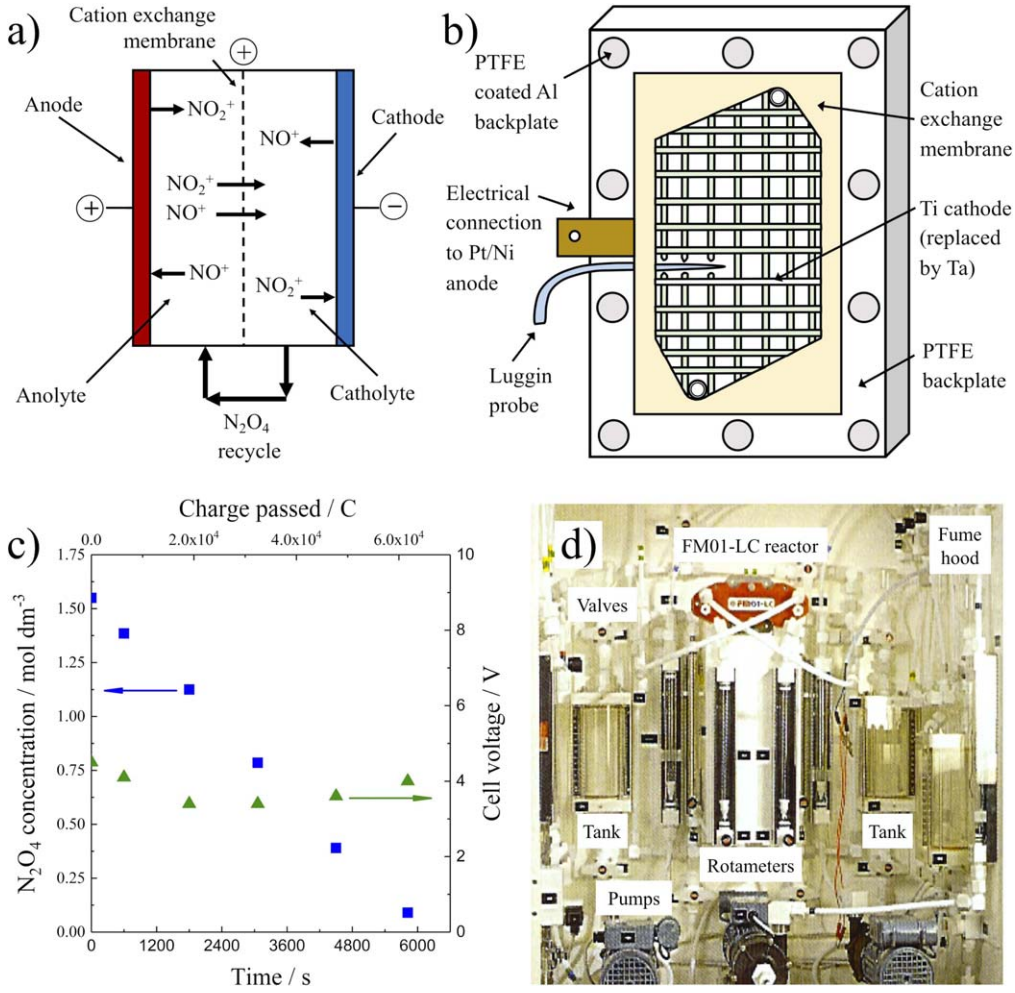


**Figure 16.** Electrosynthesis of $N_2O_5$ in anhydrous nitric acid. (a) Cell schematic, showing the production of $N_2O_5$ in the anode compartment of a unit cell divided by a cation exchange membrane and the possibility of recycling distilled $N_2O_4$ product from the cathode compartment back into the anode one. (b) PTFE coated aluminium backplate holding a platinum/nickel anode and a PTFE turbulence promoter. After Marshall et al.[351] (c) The linear relationship between the electrical charge for $N_2O_4$ oxidation and the amount originally present in the anolyte along the cell potential during the experiment. Temperature below 10 °C, electrolyte volume 250 cm$^3$. Data taken from Marshall et al.[351] (d) Pilot-plant experimental arrangement made primarily in PTFE, showing a FM01-LC flow reactor, pumps, flowmeters and reservoirs inside a fume hood.[130]

electron stoichiometry is two and the apparent one-electron stoichiometry was found to be the result of a decrease $N_2O_4$ concentration due to membrane transfer; under these conditions, the membrane showed a solvent transfer rate of approximately 68 cm$^3$ F$^{-1}$. As shown in Fig. 16d), the system was later scaled up to a pilot plant using the FM01-LC reactor. Frames, backplates, turbulence promoters, the flow system and the pump heads were made of PTFE.

***Treatment of textile effluents for environmental remediation (in a modelled cell).***—Numerous electrochemical treatments of toxic or persistent organics can be performed by their oxidation in parallel plane electrochemical flow reactors. For instance, a versatile 30 cm$^2$ cell has been used for the oxidation of Methyl Orange[138] and Reactive Black 5[71] textile dyes, which are recalcitrant pollutants present in industrial wastewaters. The oxidation of Methyl Orange was carried out using an undivided cell and anodes based on iridium dioxide, antimony-doped tin dioxide catalysts ($IrO_2$-$SnO_2$-$Sb_2O_5$/Ti),[138] which were prepared using the Pechini thermal sol-gel method on titanium substrates. It was found that a volumetric flow rate of 100 dm$^3$ h$^{-1}$ (27.8 cm$^3$ s$^{-1}$), representing a mean linear flow rate of 10.5 cm s$^{-1}$ improved the mineralization rate of the dye at the optimal conditions of pH 5 and 60 °C in a NaCl solution. On the other hand, the degradation of Reactive Black 5 was done in the same cell using Nafion 112 as separator through several methods:[71] direct oxidation by planar BDD anodes, indirect oxidation by the electro-Fenton reaction via hydrogen peroxide generation on RVC and the combination of both. As shown in Fig. 17a), more than 97% removal was reached when the current density was over 20 mA cm$^{-2}$ at BDD or when the concentration of $Fe^{2+}$ ions was over 0.04 mol dm$^{-3}$ for the RVC or combined electrodes. However, when considering the efficiency for total organics content (TOC) removal, BDD anodes were advantageous, yielding 82% TOC in 30 min at a current density of 41.1 mA cm$^{-2}$ in 0.5 mol dm$^{-3}$ $Na_2SO_4$.

The same 30 cm$^2$ undivided cell was later subject of a numerical simulation study of fluid flow velocity under turbulent flow conditions and the current distribution along planar electrodes.[224] The hydrodynamics were solved by using the RANS equations, while the primary and secondary current distributions were calculated by applying Ohm's law and the Laplace equation. For the secondary distribution, the Tafel slope of a model reduction reaction was also considered. Limiting currents were obtained from the mass transfer estimated by the $k_mA_e$ factor, whose value is available from empirical correlations for this type of cells.[163] The calculated local electrolyte velocities showed the existence of jet flow between the inlet and outlet manifold. As shown in Fig. 17b), the primary current and potential distributions were not uniform, displaying edge effects near the manifolds. The secondary distribution was close to be homogeneous, having a Wagner number of 174. The jet flow

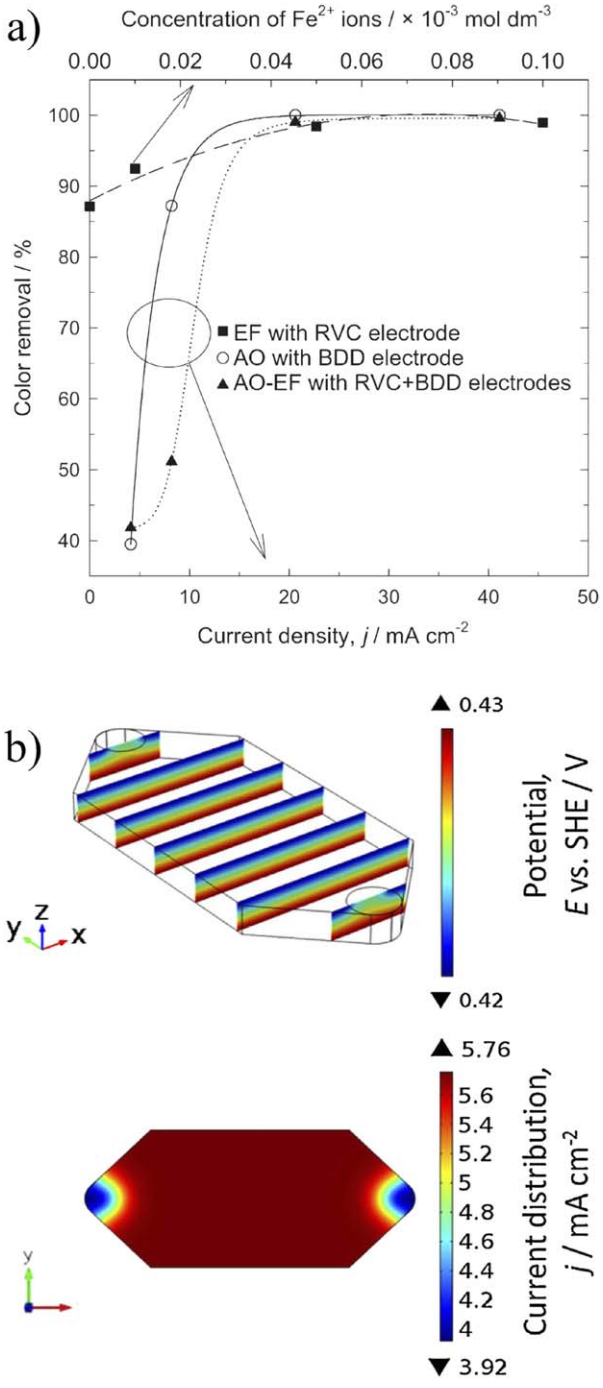


**Figure 17.** Electrochemical degradation of textile dye in a 30 $cm^2$ cell and the simulation of its reaction environment at 23 °C and a volumetric electrolyte flow rate of 27.8 $cm^3\ s^{-1}$. a) Removal of Reactive Dye 5 after 90 min of electrolysis employing different methods: (■) Electro-Fenton with RVC electrodes at −0.4 V vs Ag/AgCl as a function of $Fe^{2+}$ ion concentration. (○) Anodic oxidation at BDD electrodes and (▲) combined electro-Fenton plus BDD for different current densities. The initial concentration of the dye was $2 \times 10^{-5}$ mol $dm^{-3}$. Adapted with permission from Vasconcelos et al.,[71] Electrochemical degradation of RB-5 dye by anodic oxidation, electro-Fenton and by combining anodic oxidation and electro-Fenton in a filter-press flow cell, *J. Electroanal. Chem.* 765 (2015) 179. Copyright 2017, Elsevier. b) Calculated cross-sectional view of the primary potential distribution within the flow channel and primary current density distribution at electrode surface for the same 30 $cm^2$ cell. Adapted with permission from Pérez et al.,[224] Simulation of current distribution along a planar electrode under turbulent flow conditions in a laboratory filter-press flow cell, Electrochim. Acta 154 (2015) 352, Copyright 2015, Elsevier.

produced uneven local limiting current values at the electrode but the reaction environment could be rendered more uniform by adding turbulence promoters to the cell, as indicated in the section on Polymeric inert turbulence promoter meshes

***3D electrodes in a (borohydride-peroxide) fuel cell.—***The direct borohydride fuel cell (DBFC) has received continuous interest during the last decade due to its high specific energy.[359,360] As discussed below, it has recently been subject to mass transfer studies employing Pt-Ir 3D electrodes on titanium substrates,[99] which paves the way for achieving high performance at full scale devices. The main reactions at the anode and cathode are, respectively:

$$BH_4^- + 4H_2O \rightarrow B(OH)_4^- + 8H^+ + 8e^- \quad E^\theta = -1.24\ \text{V vs SHE} \quad [27]$$

$$4H_2O_2 + 8e^- + 8H^+ \rightarrow 8H_2O \quad E^\theta = +0.87\ \text{V vs SHE} \quad [28]$$

In alkaline media, the resulting standard cell potential of the device is 2.11 V, involving a transfer of 8 electrons in average, depending on the catalyst.[361]

The scalability of DBFC technology was first demonstrated in the FM01-LC reactor[125] in a single, two- and four-cell stack for a direct borohydride-acid peroxide fuel cell. The electrodes in the flow cell had projected areas of 64 $cm^2$ with an electrode-membrane gap of 0.55 cm. A carbon cloth anode was coated with 10 wt% gold on a Vulcan XC-72 carbon support (catalyst loading of 0.5 $mg_{Au}\ cm^{-2}$) on niobium plates. The cathode was an off-the-shelf, 0.3 mm thick carbon paper infused with a platinum catalyst on carbon black within a cationic Nafion base ink (catalyst loading of 4.0 $mg_{Pt}\ cm^{-2}$). A volumetric flow rate of 95 ± 5 $dm^3\ h^{-1}$ was used, which is equivalent to a mean linear flow velocity of 12.0 $cm\ s^{-1}$ for the single cell. The system in four-stack configuration achieved a maximum power density of 58 mW $cm^{-2}$ at 60 °C.

Further developments were made by implementing a high-surface area Pd/Ir coated microfibrous carbon electrode fabricated in-house by a direct electrostatic flocking technique.[359] A potential of 30–100 kV was applied between a titanium plate with a conductive carbon adhesive layer and a carbon plate, which contained carbon fibres of 11 $\mu$m diameter and 500 $\mu$m length). The electrostatic action caused the carbon fibres to accelerate towards the titanium plate and adhered to the carbon film in a closely-packed, vertical orientation with approximately 125,000 fibres per $cm^2$. After curing the adhesive for 1 h at 100 °C in air, the electrode was coated with a Pt/Ir catalyst by cycling voltammetry in an aqueous solution of $2 \times 10^{-3}$ mol $dm^{-3}$ $PdCl_2$ and $2 \times 10^{-3}$ mol $dm^{-3}$ $Na_2IrCl_6$ at 70 °C which resulted in a catalyst load of 12.3 mg $cm^{-2}$. The four-cell stack operating at 42 °C provided a power density of 78 mW $cm^{-2}$, an increment of 34 % over the Pt-impregnated carbon paper. Given the advantages of flow-through porous electrodes, DBFC was later evaluated at cells employing RVC decorated with gold and silver sponge.[361] RVC porosity grades between 10 and 100 ppi were sputtered with gold and studied in a three-electrode cell by linear sweep voltammetry in in 0.02 mol $dm^{-3}$ $NaBH_4$ in 3 mol $dm^{-3}$ NaOH. The maximum heterogeneous reaction rate was obtained at Au/RVC 60 ppi, which was produced by sputtering Au on the foam substrate for 3 min. The $k_m$ value was $180 \times 10^{-5}$ cm $s^{-1}$, in contrast to the silver sponge, which gave a value of $9 \times 10^{-5}$ cm $s^{-1}$.

Abahussain et al. have taken the use of off-the-shelf porous electrodes further, obtaining the volumetric mass transfer coefficient, $k_mA_e$, for the oxidation of borohydride ions at Pt-Ir coatings on titanium substrates in a 9 $cm^2$ laboratory flow cell.[99] The cell employed for this study is shown in Fig. 18a). Several anode geometries having volumetric porosities between 0.53 and 0.82 were evaluated, including mesh, micromesh, fine mesh and felt. The limiting current was measured by chronoamperometry at 0.2 V vs Hg/HgO and used to estimate an enhancement factor vs a Pt-Ir/Ti plate and $k_mA_e$ values. Linear flow velocities between 2 and

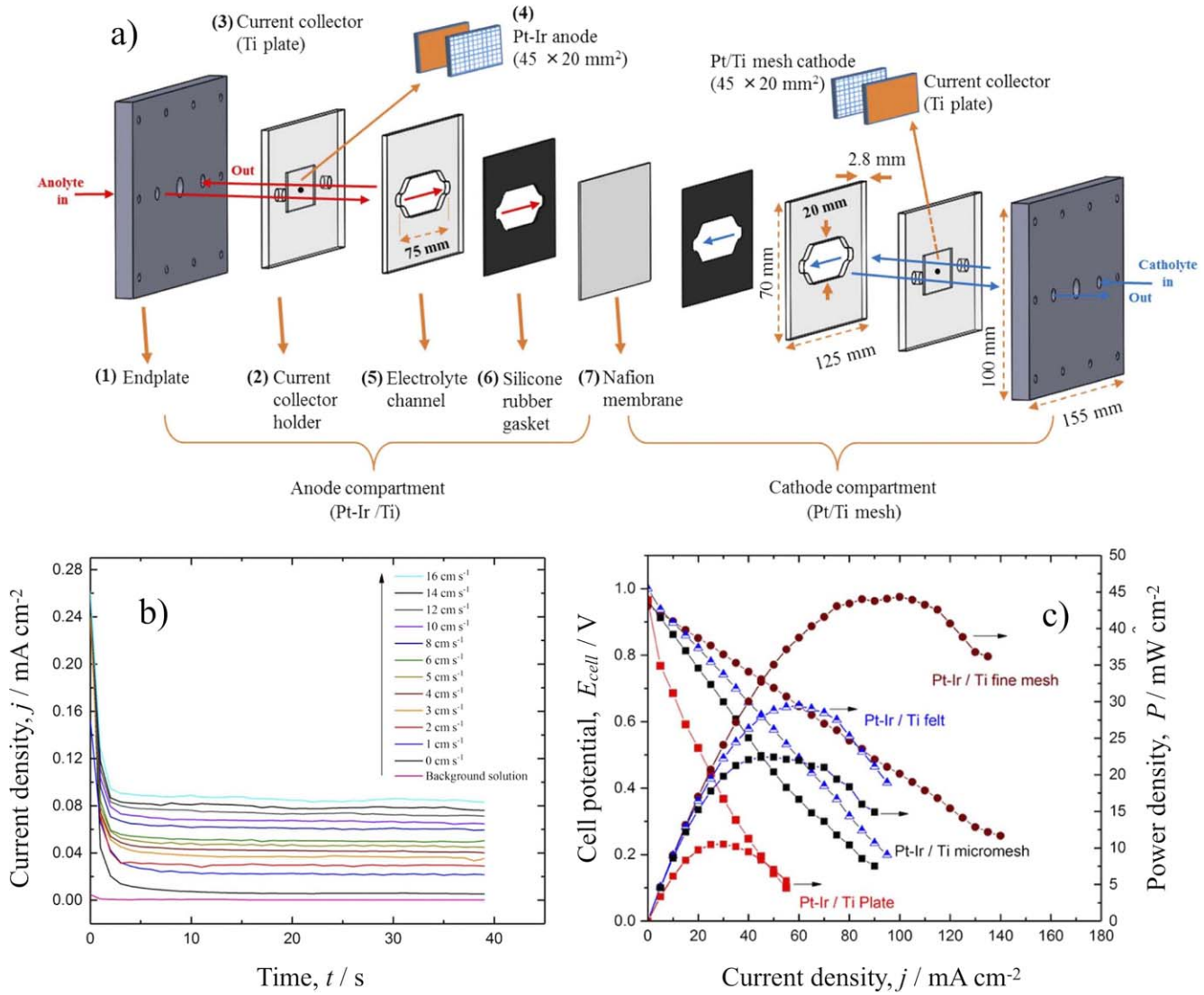


**Figure 18.** Characterization of direct borohydride membrane-divided fuel cell for mass transfer studies. (a) Exploded view of the 9 $cm^2$ anodic half-cell. (b) Current density for the oxidation of $BH_4^-$ ions as a function of mean linear flow velocities in a half-cell with a Pt-Ir/Ti mesh anode at 23 °C measured by chronoamperometry at +0.2 V vs Hg/HgO. Anolyte composition: 0.01 mol $dm^{-3}$ $NaBH_4$ in 2 mol $dm^{-3}$ NaOH. (c) Effect of electrode structure on the cell potential and power curves for a single fuel cell employing a Pt-Ir/Ti anodes at a mean linear velocity of 4 cm $s^{-1}$ and 23 °C. Anolyte composition: 2.5 mol $dm^{-3}$ $NaBH_4$ + 2 mol $dm^{-3}$ NaOH. Adapted with permission from Abahussain et al.,[99] Mass-transfer measurements at porous 3D Pt-Ir/Ti electrodes in a direct borohydride fuel cell, *J. Electrochem. Soc.* 165 (2018) F198. Copyright 2018, The Electrochemical Society.

16 cm $s^{-1}$ were evaluated for a relatively diluted 0.01 mol $dm^{-3}$ $NaBH_4$ in 2 mol $dm^{-3}$ NaOH electrolyte for all electrodes. An example of a chronoamperometry in the presence of an increasing linear flow rate is presented in Fig. 18b). The Pt-Ir/Ti felt increased the limiting current for a factor of 100 compared to the flat plate electrode, however, it was the Pt-Ir/Ti fine mesh which achieved the highest $k_mA_e$ value, 0.71 $s^{-1}$ at 16 cm $s^{-1}$, compared to the value of 0.01 $s^{-1}$ at the planar anode under the same flow rate. As shown in Fig. 18c), the maximum power density of 44.5 mW $cm^{-2}$ was achieved at a Pt-Ir/Ti fine mesh for a cell potential of 0.44 V and a current density of 100 mA $cm^{-2}$ at 23°C.

***3D platinised titanium electrodes in a flow channel (of a zinc-cerium RFB).***—The zinc-cerium redox flow battery was introduced as a logical development of well-proven industrial electrochemical operations involving continuous generation of Ce(IV) ions for mediated electrosynthesis and nuclear decontamination.[68] The battery has a thermodynamic cell potential of 2.4 V and a volumetric energy density of approximately 11 W h $dm^{-3}$ for Ce.[362] At the positive electrode, redox of cerium ions between the 3 and 4 oxidation state in the electrolyte occurs, on charge:

$$Ce(III) - e^- \rightleftarrows Ce(IV) \quad E^\theta = +1.61 \text{ V vs SHE} \qquad [29]$$

This is complemented by the deposition and dissolution of zinc at an inert negative electrode, on charge:

$$Zn^{2+} + 2e^- \rightleftarrows Zn \quad E^\theta = -0.76 \text{ V vs SHE} \qquad [30]$$

Both half-cell electrolytes are based on methanesulphonic acid and a proton membrane facilitates ion transfer between half-cells. The positive electrolyte contains between 0.6 and 0.8 mol $dm^{-3}$ $Ce(CH_3SO_3)_3$ in 4.0 mol $dm^{-3}$ $CH_3SO_3H$[126] and the negative electrolyte between 1.5 and 2.5 mol $dm^{-3}$ $Zn(CH_3SO_3)_2$ in 1.5 mol $dm^{-3}$ $CH_3SO_3H$.[363] In operation, the system develops a cell potential of 1.8 V at a discharge current density of 50 mA $cm^{-2}$, with a maximum current efficiency of 75% and a voltage efficiency of 60%.[126] Moderately high temperatures between 40–50 °C improve the cycling performance of the battery. The main limitations of the cell are parasitic oxygen evolution at the positive electrode and the slow self-discharge or the zinc side via hydrogen evolution.

Variants of the zinc-cerium flow battery such as the V-Ce,[364–367] Pb-Ce,[368] and $H_2$-Ce,[369,370] have been proposed to avoid phase changes at the negative electrode. These devices have in common the need for platinised titanium (Pt/Ti) electrodes to drive the redox reaction of cerium ions in the oxidising, acid electrolyte. For decades, it has been known that the electrode geometry, i.e., the resulting active surface area and mass transfer enhancement, affected the electrolytic cell potential difference and current efficiency during anodic oxidation of Ce(III).[68] However, cerium-based cells continued to employ traditional planar and coarse mesh electrodes while no quantitative mass transfer data was available to compare porous electrode geometries.

As a result, a laboratory zinc-cerium flow cell was developed in order to characterise the performance of such electrode materials.[98] The rectangular channel flow cell had electrodes of 24 $cm^2$ projected area. Figure 19 shows the plate, expanded mesh, micromesh and felt

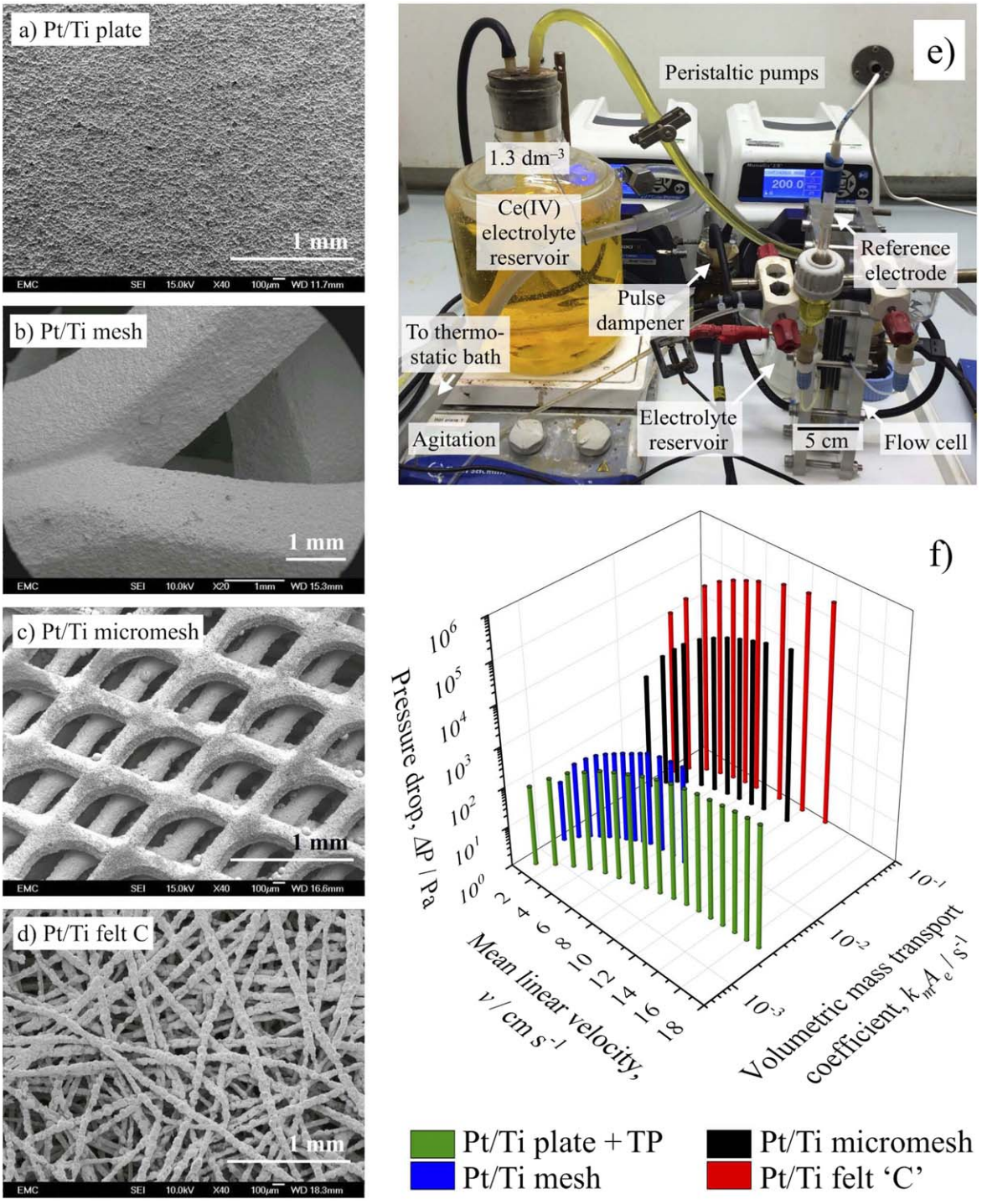


**Figure 19.** Pt/Ti electrodes for the conversion of cerium ions and their performance in a laboratory redox flow battery. Platinised porous titanium electrode structures, 24 $cm^2$ projected area: (a) plate, (b) expanded mesh, (c) micromesh and (d) felt type "C". (e) Experimental arrangement for half-cell mass transfer studies of cerium conversion. (d) Electrode performance factor $k_m A_e$ for Ce(IV) reduction and electrolyte pressure drop as a function of mean linear flow velocity for the different electrode materials. Data taken from[155]. Limiting current data for $k_m A_e$ was obtained by chronoamperometry at 0.2 V vs $Hg|Hg_2SO_{4(satd)}$ in 0.1 mol dm$^{-3}$ Ce(IV) + 0.7 mol dm$^{-3}$ Ce(III) in 4 mol dm$^{-3}$ MSA at 25 °C. Pressure drop through the Pt/Ti electrodes was measured in a solution containing 0.8 mol dm$^{-3}$ Ce(III) in 4 mol dm$^{-3}$ MSA at 25 °C.

Pt/Ti electrodes, which were platinised by electrodeposition.[136,137] The cell potential difference at current densities up to 100 mA $cm^{-2}$ was related to the electrolyte flow rate, which was varied from 0.25 to 17 cm $s^{-1}$ using the experimental arrangement shown in Fig. 19e). For instance, at 100 mA $cm^{-2}$ the cell potential was 1.80 V using a Pt/Ti felt and 1.20 V using a Pt/Ti micromesh stack. The limiting current for the reduction of Ce(IV) ions was measured by chronoamperometry in half-cell studies as a function of flow rate. Progressively higher limiting currents were achieved using porous electrodes for cerium conversion.[98] The current enhancement factor for the Pt/Ti felt and micromesh electrodes was as high as 160 and 63, respectively, compared to a planar electrode in an open channel.

The limiting current was used to calculate the volumetric mass transfer coefficient, $k_mA_e$, of the electrodes. As shown in Fig. 19f), $k_mA_e$ values for the Pt/Ti felt electrode were over 2 orders of magnitude higher than those at a planar electrode. In the case of the Pt/Ti plate + TP, $k_mA_e$ is low enough to result in a degree of mass transfer control of Ce(III) ion oxidation and significant oxygen evolution.[98] Current efficiency and cell potential difference at previously reported planar,[67,371] mesh[126] and fine mesh[370] electrodes for cerium conversion were rationalised using these results. Later, the performance factor was used to predict the reactant conversion over time and cell potential difference given suitable electrode dimensions.[372]

The electrode performance factor $k_mA_e$ was also related to their electrolyte pressure drop, $\Delta p$, to give a description of the energetic costs associated with the pump requirements and as an indication of scalability. The pressure drop for each electrode material was measured as a function of current mean linear flow rate. As shown in Fig. 19f), this data can then be used to relate the factor $k_mA_e$ as a function of pressure drop, $\Delta p$, over the material in a rectangular flow channel. Electrodes such as Pt/Ti mesh, Pt/Ti plate and a Pt/Ti plate with a turbulence promoter, TP, experienced a low pressure drop, although the relatively low $k_mA_e$ results in high cell overpotentials and low conversion per pass.[98] The Pt/Ti felt C (highest Pt content) shows a better performance than the micromesh at a given electrolyte velocity over 2 cm $s^{-1}$ (24.1 kPa) at the cost of a higher, but manageable, pressure drop in the cell.

***Electrodeposition of metals (nickel electroforming and copper electrodeposition).***—The effect of mass transfer and flow regime on the electrodeposition of metals has been performed in parallel plane flows cells as well, were well-defined flow conditions can be obtained. This means reproducible conditions defined in a quantitative manner, such as, e.g., mean linear flow rate or channel Reynolds number. Planar surfaces can be coated or electroformed in this way, in contrast to rotating cylinders. A notable example can be found in a thesis by Wood,[83] who studied the electrodeposition of metals from aqueous solutions under laminar and turbulent flow regimes, the latter under fast mean linear flow velocities, up to 200 cm $s^{-1}$ and Reynolds numbers up to 30,500 in poly(methylmethacrylate) flow cells and volumetric flow rates up to 600 $cm^3$ $s^{-1}$. Nickel foils were electroformed from an additive-free acid sulfamate bath using an undivided cell with a hydrodynamic entrance length of 50 cm, a rectangular cross-sectional flow channel of 3 cm width and 1.0 cm separation, the equivalent diameter being 1.5 cm. The stainless steel cathode had a wet surface of 3 cm × 5 cm, facing the soluble nickel anode of 3 cm × 5 cm. A Lugging probe connected to a reference electrode was inserted into a hole in the cathode in order to measure the electrode potential. Mass transfer measurements were later performed using the limiting current of copper reduction from acid copper sulfate baths at different flow rates using a second cell design. As shown in Fig. 20a), this modified cell incorporated a diaphragm between the half-cells, having then a 0.5 cm channel height and a hydraulic diameter of 0.86 cm. The electrode dimensions were modified to 3 cm × 10 cm for the cathode, 3 cm × 25 cm

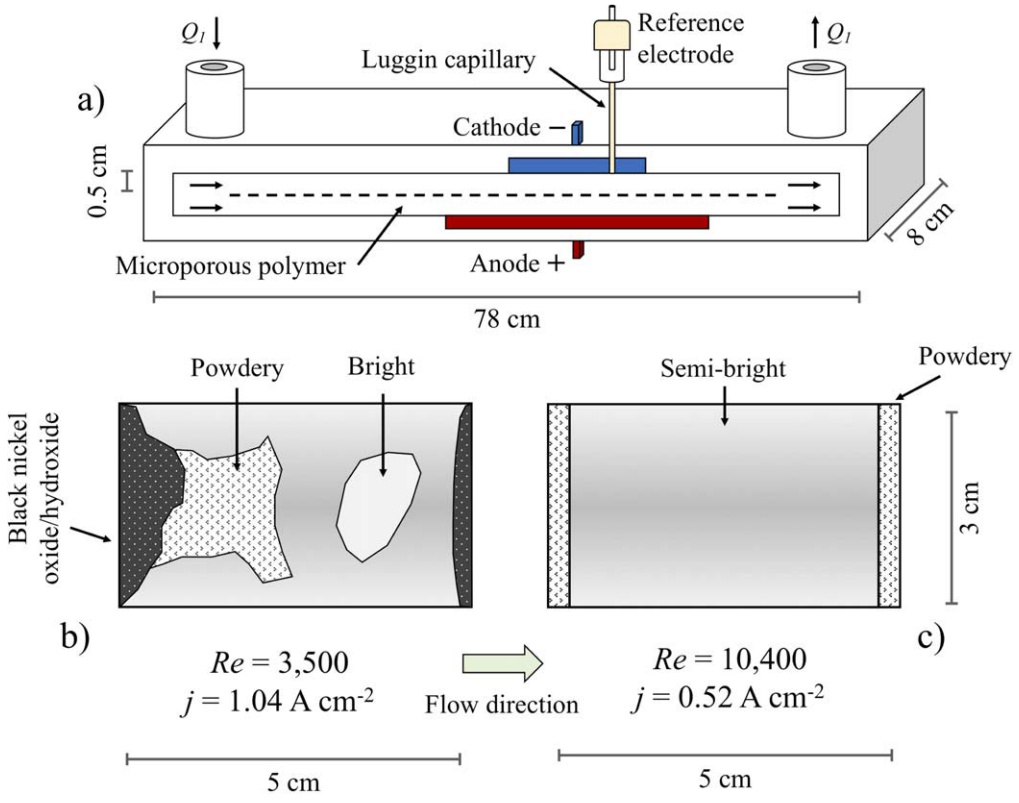


**Figure 20.** A parallel plate cell for metal deposition and electroforming at laminar and turbulent flow regimes along examples of the visual appearance of electroformed nickel sheets from an acid sulfamate bath at different Reynolds numbers and current densities. (a) Cross sectional view of a diaphragm-divided cell having a 50 cm long hydraulic inlet for producing fully developed flow and dissimilar surface area of cathode and anode in order to improve current distribution. Compression plates and bolts not shown. The cell is not to scale. (b) Deposit morphology obtained at $Re = 3{,}500$ with a current density of 1.04 A $cm^{-2}$. (c) Deposit morphology obtained at $Re = 10{,}400$ with a current density of 0.52 A $cm^{-2}$. After Wood.[83]

for the anode. In both cases, the long, unrestricted channels were intended to eliminate jet flow and create fully developed flow.

The morphology and quality of nickel deposits was assessed visually and by SEM imaging as a function of Reynolds number and current density. As shown in Fig. 20b), black nickel hydroxide and nickel powder deposits were found near the entrance and exit zones of the electrodes at $Re = 3{,}500$, while the hydrogen evolution induced pitting (21 microns). In contrast, at a high $Re$ of 10,400, Fig. 20c), the deposits were uniformly semi-bright, except for powder deposit at the edges of the electrode perpendicular to the flow direction (11 microns). Finally, fine grained deposits were achieved at $Re = 10{,}400$, which yielding maximum current densities of 1.3 A $cm^{-2}$ and >2.0 A $cm^{-2}$ at 60°C and 70°C, respectively, although the length of the anode and cathode were changed to 9 cm and 10 cm, respectively to improve current distribution. The current efficiency was over 95%.

The deposition of copper was carried out in the second cell design and produced well defined polarisation curves in both laminar and turbulent flow, permitting to establish mass transfer dimensionless group correlation for the cell. Under laminar flow the deposits were smooth and featureless and a maximum limiting current density of 4.8 mA $cm^{-2}$ was achieved at $Re = 1{,}590$ and 37°C. Copper deposits obtained in turbulent regime were rougher in comparison and developed a limiting current density up to 39.0 mA $cm^{-2}$ at $Re = 25{,}846$ and 60°C. The measurement of pressure drop over the flow channel and the current distribution determined from segmented electrodes were also reported.

Novel possibilities can be realized in similar cells for the electrodeposition of metals, such as silver,[373] palladium[69] and copper[225] in parallel plane cells. These operations have often used laminar flow regimes, implying a poor control of the deposit morphology. Furthermore, a better understanding of the relationship between mass transfer and deposit morphology can be obtained from numerical simulations studies of current density and electrolyte flow velocity. Similar studies could be applied to the electrodeposition of numerous alloys and composites, such as nickel molybdenum disulphide coatings.[374]

## Summary and Trends

Electrochemical cells and flow reactors based on parallel plane electrodes continue to be the work-horse in many important electrochemical operations. Given advances in material science, numerical simulation and manufacture techniques,continued development and increasing efficiency can be expected. Several relevant points can be drawn from this review:

1. Beaker cells have been used for convenient, preliminary batch studies of electrolysis, although they offer a poorly defined reaction environment. Plate-in-tank cells on an industrial scale have been steadily advantageous in electrowinning operations, while vertical plates and boxes in stirred tanks can be useful in the electrosynthesis of inorganics, such as dissolved metal salts and particulate metal oxides.
2. Rectangular section flow channel, filter-press cells are appropriate for parametric and scalable studies of operational conditions, being employed in continuous or batch recirculation industrial electrochemical operations, including numerous inorganic and organic electrosynthesis reactions, environmental remediation, degradation of toxic organics and energy storage applications.
3. The reaction environment in parallel plane electrochemical flow cells is defined by the following essential parameters: flow mixing, mean linear flow velocity of electrolyte past the electrode surface, average mass transfer coefficient, current and potential distribution, residence time distribution, reactant concentration distribution, fractional conversion per pass and pressure drop.
4. A wide variety of 2D and 3D electrode materials can be used in a plane parallel configuration under different electrolyte flow modes. Such diversity provides a range of properties and cost, which can be tailored for specific electrochemical operations. 3D electrodes are generally more productive in view of their extended surface area and enhanced mass transfer, yet 2D electrodes continue to be cost robust and cost effective for some applications. The benefits of polymer turbulence promoters in improving flow past 2D electrodes in rectangular flow channels should not be overlooked.
5. Components for parallel plane flow cells should be durable and cost effective. Classical techniques involve machining, CNC and injection moulding, the latter being more common in mass production. Additive manufacturing techniques offer the possibility of coupled, fast prototyping and testing of cell components. New developments and cost reductions should lead to integrated additive manufacturing of entire electrochemical reactors.
6. Numerical modelling of reaction environment can provide additional information to experimental data. Simulations can be a powerful design and optimization tool to probe charge transfer, mass transfer and hydrodynamics in electrochemical flow reactors. Advances in this field can enable interactive or automatic cell design processes. Before carrying out such tasks, it is essential that adequate experimental validation of models takes place.

## Needs For Further Research and Development

The continued development of plane parallel electrode geometry cells will demand research on:

1. Electrode materials, including better electrode coatings, enhanced three-dimensional structures[277] and hybrids such as foam/fibre or micromesh/nanoparticles.[235]
2. Characterization of the reaction environment in recent flow cells incorporating interdigitated flow channels via computational modelling and practical experimental techniques, emphasizing their suitability for scale up, e.g., mass transfer coefficient as a function of pressure drop.
3. Consideration of readily available and versatile, off-the-shelf cell designs from commercial sources, but only when their reaction environment has been characterised and reported.
4. Increased use and improvement of digital imaging of 3D electrodes, for instance by micro x-ray computed tomography, for the study of electrode structure and surface area[273] and prediction of performance by simulation.[285]
5. The development of efficient and cost effective miniaturised flow cells, which could be useful in bench organic synthesis.[17] Attention should be payed to achieve manageable pressure drop and reasonable single pass fractional conversion (due to a controlled reaction environment at the electrodes). Cells operating in batch recirculation should be considered, rather that long flow channels which may introduce mass transfer limitations and parasitic reactions.
6. Use of fast design process involving digital modelling and simulation coupled to fast prototyping techniques. Additive manufacturing techniques could be diversified into metal, alloy, metal oxide, carbon, conductive ceramic, conductive polymer, composite, tailored architectures for advanced electrodes.[246,288]
7. Accelerated ageing tests of electrode, membrane and polymer materials used in cells, cell stacks and ancillary equipment, such as pumps and pipes. Analysis of failure mechanisms of equipment due to premature degradation and corrosion protection and, when possible, remediation.
8. Improvements of simulation software focusing on user-friendly interfaces coupled to rigorous mathematical models of the reaction environment, operation and control of electrochemical

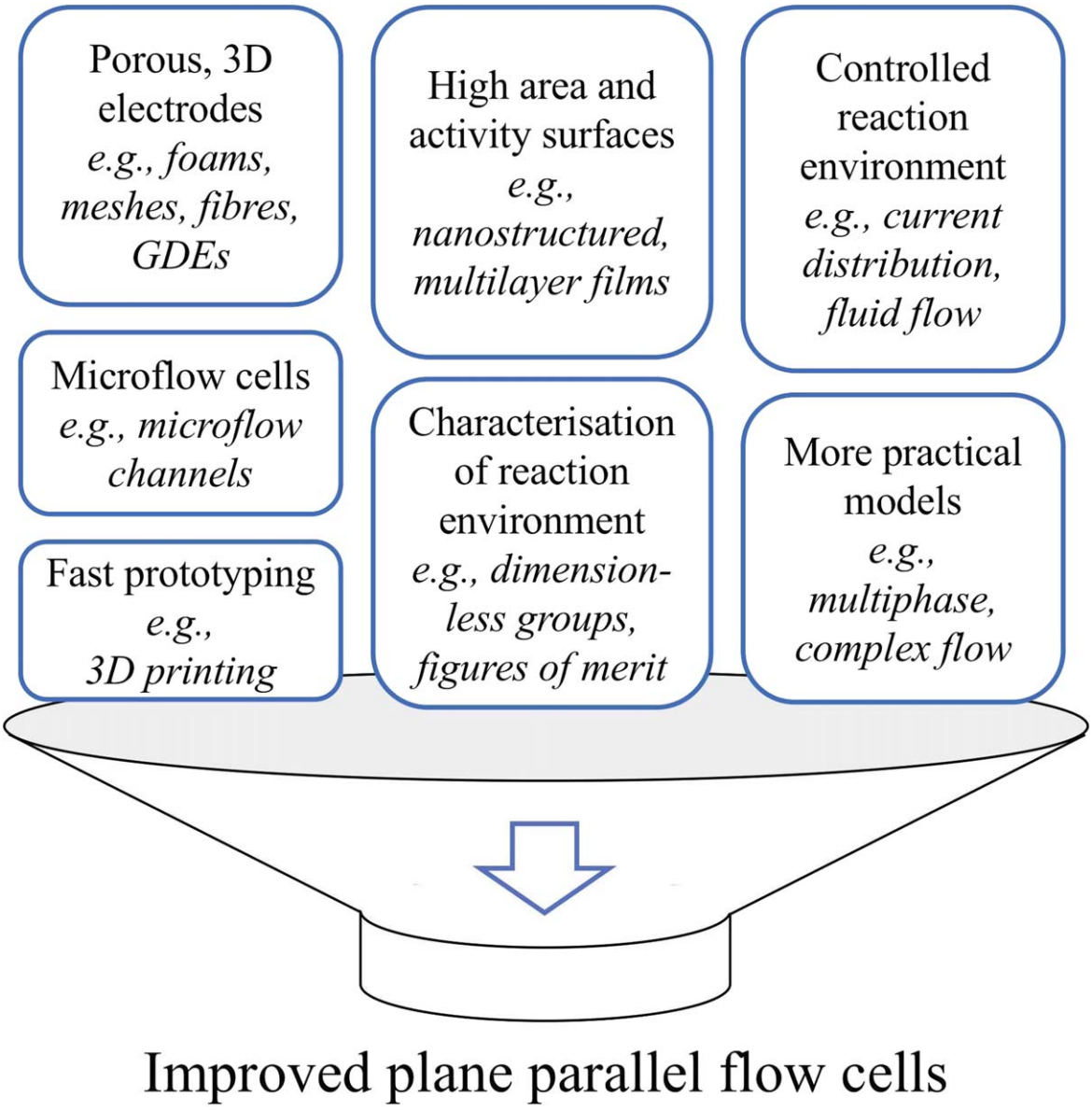


**Figure 21.** Some typical improvement strategies for plane parallel electrochemical cells resulting in enhanced reactant conversion rate as well as higher efficiency and selectivity.

flow reactors. Consideration of advanced models for two-phase flow (involving gas evolution), electrodeposition of metals and tertiary current distribution at 3D porous electrodes.

9. More work on the study of reactant conversion over time from the perspective of plug flow reactor models, in single pass, batch recirculation and cascade modes, along with their integration into modern numerical simulations.
10. Increased productivity and efficiency of electrochemical processes through their integration and combination with green technologies and sustainable energy sources.[328]

Based on the above discussions and selected examples, a summary of basic improvement strategies is offered in Fig. 21. It is suggested that further research should include rigorous reports of reaction environment in both laboratory and industrially important cells at various scales. Similarly, techniques for surface preparation, modification and coating of electrode and membrane structures should be well documented. Developments in flow cell designs other than the rectangular channel and alternatives to the plane parallel electrode geometry have been considered in a recent review.[54]

**Acknowldgements**

The authors acknowledge the colleagueship of Professor Derek Pletcher and the enthusiastic endeavours of their research students, postdoctoral workers and university colleagues. Thanks are also due to many industrial colleagues who improved our experience of plane parallel cells through funded projects, joint developments and consultancy assignments. No new data were created during the preparation of this review.

**Conflict of Interest Statement**

The authors declare that there are no conflicts of interest.

**References**

1. D. J. Pickett, *Electrochemical Reactor Design* (Elsevier, Amsterdam) 2nd ed. (1979).
2. T. Z. Fahidy, *Principles of Electrochemical Reactor Analysis* (Elsevier, Amsterdam) (1985).
3. F. Hine, *Electrode Processes and Electrochemical Engineering* (Springer, US, Boston, MA) (1985).

4. E. Heitz and G. Kreysa, *Principles of Electrochemical Engineering* (VHC, Weinheim) (1986).
5. D. Pletcher and F. C. Walsh, *Industrial Electrochemistry* (Chapman and Hall, London) 2nd ed. (1990).
6. F. Coeuret, *Introducción a la Ingeniería Electroquímica* (Editorial Reverté, Barcelona) (1992).
7. F. Coeuret and A. Storck, *Eléments de Génie Électrochimique* (Éditions TEC et DOC/Lavoisier, Paris) 2nd ed. (1993).
8. F. C. Walsh, *A First Course in Electrochemical Engineering* (The Electrochemical Consultancy, Romsey) (1993).
9. F. Goodridge and K. Scott, *Electrochemical Process Engineering* (Springer Science & Business Media, New York) (1995).
10. H. Wendt and G. Kreysa, *Electrochemical Engineering* (Springer, Berlin) (1999).
11. V. M. Schmidt, *Elektrochemische Verfahrenstechnik* (Wiley-VCH Verlag, Weinheim) (2003).
12. K. Scott, *Sustainable and Green Electrochemical Science and Technology* (John Wiley & Sons, New York) (2017).
13. T. F. Fuller and J. N. Harb, *Electrochemical Engineering* (John Wiley & Sons, Hoboken) (2018).
14. P. Hayfield, *Platinum Metals Rev.*, **42**, 116 (1998).
15. C. A. C. Sequeira and D. M. F. Santos, *J. Braz. Chem. Soc.*, **20**, 387 (2009).
16. B. A. Frontana-Uribe, R. D. Little, J. G. Ibanez, A. Palma, and R. Vasquez-Medrano, *Green Chemistry*, **12**, 2099 (2010).
17. D. Pletcher, R. A. Green, and R. C. D. Brown, *Chem. Rev.*, **118**, 4573 (2017).
18. C. L. Mantell, *Industrial Electrochemistry* (McGraw-Hill, New York) 2nd ed. (1940).
19. L. F. Arenas, C. Ponce de León, and F. C. Walsh, *J. Energy Storage*, **11**, 119 (2017).
20. C. Gütz, A. Stenglein, and S. R. Waldvogel, *Org. Process Res. Dev.*, **21**, 771 (2017).
21. M. A. Rahman, X. Wang, and C. Wen, *J. Electrochem. Soc.*, **160**, A1759 (2013).
22. M. Schlesinger and M. Paunovic (ed.), *Modern Electroplating* (John Wiley & Sons, Hoboken) 5th ed. (2010).
23. I. Rousar, V. Mejta, and V. Cezner, *Chem. Eng. Sci.*, **35**, 717 (1980).
24. N. S. Qu, W. H. Qian, W. Z. Cai, Z. H. Xing, Z. W. Zhu, and Y. B. Zeng, *Trans. Inst. Met. Finish.*, **91**, 221 (2013).
25. H. Strathmann, *Desalination*, **264**, 268 (2010).
26. K. Jüttner, U. Galla, and H. Schmieder, *Electrochim. Acta*, **45**, 2575 (2000).
27. F. C. Walsh, *Pure Appl. Chem.*, **73**, 1819 (2001).
28. A. J. Hale, *The Manufacture of Chemicals by Electrolysis* (D. Van Nostrand Co, New York) (1919).
29. G. Sandstede, E. J. Cairns, V. S. Bagotsky, and K. Wiesener, "History of low temperature fuel cells." in *Handbook of Fuel Cells*, ed. W. Vielstich, A. Lamm, H. A. Gasteiger, and H. Yokokawa (Wiley-VCH Verlag, Chichester)1 (2010).
30. F. Coeuret, *J. Appl. Electrochem.*, **23**, 853 (1993).
31. C. J. Brown, M. R. Nurmohammed, D. A. Szánto, T. G. Nevell, and F. C. Walsh, The Batch Electrochemical Reactor: Monitoring of Batch Kinetics For Ceric Ion Reduction in the Laboratory, Unpublished work. (2004).
32. T. Raju and C. A. Basha, *Ind. Eng. Chem. Res.*, **47**, 8947 (2008).
33. T. Vijayabarathi, R. K. Srinivasan, and M. Noel, *Bull. Electrochem.*, **15**, 293 (1999).
34. R. W. Houghton and A. T. Kuhn, *J. Appl. Electrochem.*, **4**, 173 (1974).
35. F. C. Walsh and C. Low, *Surf. Coat. Technol.*, 79 (2016).
36. F. C. Walsh and C. Ponce de León, *Surf. Coat. Technol.*, **259**, 676 (2014).
37. A. M. Alfantazi and R. R. Moskalyk, *Miner. Eng.*, **16**, 687 (2003).
38. G. Velasco, S. Gutiérrez-Granados, C. Ponce de León, A. Alatorre, and F. C. Walsh, *J. Environ. Chem. Eng.*, **4**, 3610 (2016).
39. H. Yang, J. Ouyang, A. Tang, Y. Xiao, X. Li, X. Dong, and Y. Yu, *Mater. Res. Bull.*, **41**, 1310 (2006).
40. S. J. Bugarinović, V. J. Grekulović, M. M. Rajčić-Vujasinović, Z. M. Stević, and Z. D. Stanković, *Hemijska industrija*, **63**, 201 (2009).
41. M. D. Gernon, M. Wu, T. Buszta, and P. Janney, *Green Chem.*, **1**, 127 (1999).
42. K. B. Keating and J. M. Williams, *Resour. Conserv. Recycl.*, **2**, 39 (1976).
43. S. Fogarasi, F. Imre-Lucaci, Á. Imre-Lucaci, and P. Ilea, *J. Hazard. Mater.*, **273**, 215 (2014).
44. M. Holm and T. J. O'Keefe, *Miner. Eng.*, **13**, 193 (2000).
45. M. K. Jha, V. Kumar, and R. J. Singh, *Resources, Conservation and Recycling*, **33**, 1 (2001).
46. N. Pradhan, P. Singh, B. C. Tripathy, and S. C. Das, *Miner. Eng.*, **14**, 775 (2001).
47. I. Ivanov, *Hydrometallurgy*, **72**, 73 (2004).
48. P. Claessens and J. L. Cromwell, *US Pat.*, 5,620,586 (1997).
49. T. E. Lister, P. Wang, and A. Anderko, *Hydrometallurgy*, **149**, 228 (2014).
50. O. Herreros, R. Quiroz, and J. Viñals, *Hydrometallurgy*, **51**, 345 (1999).
51. K. Scott, X. Chen, J. W. Atkinson, M. Todd, and R. D. Armstrong, *Resour. Conserv. Recy.*, **20**, 43 (1997).
52. P. Trinidad, F. C. Walsh, and D. Gilroy, *Int. J. Engng. Ed.*, **14**, 431 (1998).
53. M. D. Birkett, R. L. Clarke, and A. T. Kuhn, *J. Chem. Technol. Biotechnol.*, **30**, 711 (1980).
54. F. C. Walsh and C. Ponce de León, *Electrochim. Acta*, **280**, 121 (2018).
55. F. F. Rivera, C. Ponce de León, J. L. Nava, and F. C. Walsh, *Electrochim. Acta*, **163**, 338 (2015).
56. F. F. Rivera, C. Ponce de León, F. C. Walsh, and J. L. Nava, *Electrochim. Acta*, **161**, 436 (2015).
57. R. J. Marshall and F. C. Walsh, *Surface Technology*, **24**, 45 (1985).
58. T. Brinkmann, G. Giner Santonja, F. Schorcht, S. Roudier, and L. Delgado Sancho, *Best Available Techniques (BAT) Reference Document for the Production of Chlor-alkali* (European Commission , Luxembourg) (2014).
59. Euro Chlor, *Chlorine Industry Review 2015–2016*, http://eurochlor.org/media/106905/euro_chlor_review_web.pdf (2016).
60. R. Chen, V. Trieu, B. Schley, H. Natter, J. R. Kintrup, A. Bulan, R. Webber, and R. Hempelmann, *Z. Phys. Chem.*, **227**, 651 (2013).
61. I. Moussallem, J. Jörissen, U. Kunz, S. Pinnow, and T. Turek, *J. Appl. Electrochem.*, **38**, 1177 (2008).
62. Uhde Chlorine Engineers, *Solutions provided by NaCl-ODC electrolysis technology*, https://thyssenkrupp-uhde-chlorine-engineers.com/en/products/chlor-alkali-electrolysis/odc-technology/benefits-of-the-odc-technology/ (2019).
63. R. K. B. Karlsson and A. Cornell, *Chem. Rev.*, **116**, 2982 (2016).
64. G. G. Botte, *Electrochem. Soc. Interface*, **23**, 49 (2014).
65. D. E. Danly and C. R. Campbell, "Experience in the scale-up of the Monsanto adiponitrile process." in *Techniques of Electroorganic Synthesis, Part III. Scale-Up and Engineering*, ed. N. L. Weinberg and B. V. Tilak (John Wiley & Sons, New York) p. 284 (1982).
66. C. Z. Smith, J. H. P. Utley, and J. K. Hammond, *J. Appl. Electrochem.*, **41**, 363 (2010).
67. S. Harrison and A. Théorêt, *J. New Mat. Electrochem. Systems*, **2**, 1 (1999).
68. L. F. Arenas, C. Ponce de León, and F. C. Walsh, *Electrochim. Acta*, **205**, 226 (2016).
69. J. E. Terrazas-Rodríguez, S. Gutiérrez-Granados, M. A. Alatorre-Ordaz, C. Ponce de León, and F. C. Walsh, *Electrochim. Acta*, **56**, 9357 (2011).
70. E. Brillas and C. A. Martínez-Huitle, *App. Catal. B: Environ.*, **166–167**, 603 (2015).
71. V. M. Vasconcelos, C. Ponce de León, J. L. Nava, and M. R. V. Lanza, *J. Electroanal. Chem.*, **765**, 179 (2015).
72. A. Kraft, M. Stadelmann, M. Blaschke, D. Kreysig, B. Sandt, F. Schröder, and J. Rennau, *J. Appl. Electrochem.*, **29**, 859 (1999).
73. C. Y. Cheng and G. H. Kelsall, *J. Appl. Electrochem.*, **37**, 1203 (2007).
74. L. Bazinet, F. Lamarche, and D. Ippersiel, *Trends. Food Sci. Technol.*, **9**, 107 (1998).
75. M. Carmo, D. L. Fritz, J. Mergel, and D. Stolten, *Int. J. Hydrogen Energy*, **38**, 4901 (2013).
76. D. Stolten and B. Emonts, *Fuel Cell Science and Engineering* (John Wiley & Sons, Wenheim) (2012).
77. L. F. Arenas, C. Ponce de León, and F. C. Walsh, *Curr. Opin. Electrochem.*, **16**, 117 (2019).
78. M. Skyllas-Kazacos, M. H. Chakrabarti, S. A. Hajimolana, F. S. Mjalli, and M. Saleem, *J. Electrochem. Soc.*, **158**, R55 (2011).
79. P. C. Butler, P. A. Eidler, P. G. Grimes, S. E. Klassen, and R. C. Miles, "Zinc/bromine batteries." in *Handbook of Batteries*, ed. D. Linden and T. B. Reddy (McGraw-Hill, New York)Chapter 39 (2001).
80. J. Noack, N. Roznyatovskaya, T. Herr, and P. Fischer, *Angew. Chem. Int. Ed.*, **54**, 2 (2015).
81. X. Wei et al., *ACS Energy Lett.*, **2**, 2187 (2017).
82. A. Frías-Ferrer, J. González-García, V. Sáez, E. Expósito, C. M. Sánchez-Sánchez, V. Montiel, and A. Aldaz, *J. Chem. Educ.*, **82**, 1395 (2005).
83. D. J. D. Wood, *Some aspects of the high speed electrodeposition of metals*, Doctoral Thesis, Loughborough University, https://dspace.lboro.ac.uk/2134/25905 (1988).
84. Y. Yu, J. Chen, and J. Zhou, *J. Micromech. Microeng.*, **24**, 015020 (2014).
85. I. M. S. Pillai and A. K. Gupta, *J. Electroanal. Chem.*, **756**, 108 (2015).
86. S. Bebelis, K. Bouzek, A. Cornell, M. G. S. Ferreira, G. H. Kelsall, F. Lapicque, C. Ponce de León, M. A. Rodrigo, and F. C. Walsh, *Trans. IChemE*, **91**, 1998 (2013).
87. R. Leroy, *Int. J. Hydrogen Energy*, **8**, 401 (1983).
88. M. M. Rashid, M. K. Al Mesfer, H. Naseem, and M. Danish, *IJEAT*, **4**, 80 (2015).
89. M. Atobe, H. Tateno, and Y. Matsumura, *Chem. Rev.*, **118**, 4541 (2017).
90. I. Sirés, E. Brillas, M. A. Oturan, M. A. Rodrigo, and M. Panizza, *Environ Sci Pollut Res*, **21**, 8336 (2014).
91. F. C. Moreira, R. A. R. Boaventura, E. Brillas, and V. J. P. Vilar, *App. Catal. B: Environ.*, **202**, 217 (2017).
92. A. Z. Weber, M. M. Mench, J. P. Meyers, P. N. Ross, J. T. Gostick, and Q. Liu, *J. Appl. Electrochem.*, **41**, 1137 (2011).
93. J. González-García, A. Frías, E. Exposito, V. Montiel, and A. Aldaz, *Ind. Eng. Chem. Res.*, **39**, 1132 (2000).
94. M. Guarnieri, A. Trovò, A. D'Anzi, and P. Alotto, *Appl. Energy*, **230**, 1425 (2018).
95. L. Carlsson, B. Sandegren, D. Simonsson, and M. Rihovsky, *J. Electrochem. Soc.*, **130**, 342 (1983).
96. F. DiMascio, Halox Technologies Inc, *US Patent*, 7,476,307 B2 (2009).
97. D. Patel and M. Ghadia, *WO Pat. Application* 2011/086579 A1 (2011).
98. L. F. Arenas, C. Ponce de León, and F. C. Walsh, *Electrochim. Acta*, **221**, 154 (2016).
99. A. A. Abahussain, C. Ponce de León, and F. C. Walsh, *J. Electrochem. Soc.*, **165**, F198 (2018).
100. C. Ponce de León, G. W. Reade, I. Whyte, S. E. Male, and F. C. Walsh, *Electrochim. Acta*, **52**, 5815 (2007).
101. C. Ponce de León, I. Whyte, G. W. Reade, S. E. Male, and F. C. Walsh, *Aust. J. Chem.*, **61**, 797 (2008).
102. A. Storck and D. Hutin, *Can. J. Chem. Eng.*, **58**, 92 (1980).
103. A. Storck and D. Hutin, *Electrochim. Acta*, **26**, 127 (1981).
104. T. R. Ralph, M. L. Hitchman, J. P. Millington, and F. C. Walsh, *Electrochim. Acta*, **41**, 591 (1996).

105. C. P. Koutsou, S. G. Yiantsios, and A. J. Karabelas, *J. Membrane Sci.*, **326**, 234 (2009).
106. A. N. Colli and J. M. Bisang, *Electrochim. Acta*, **56**, 7312 (2011).
107. A. Frías-Ferrer, J. González-García, V. Sáez, C. Ponce de León, and F. C. Walsh, *AIChE J.*, **54**, 811 (2008).
108. R. E. W. Jansson and R. J. Marshall, *Electrochim. Acta*, **27**, 823 (1982).
109. P. Trinidad, C. Ponce de León, and F. C. Walsh, *Electrochim. Acta*, **52**, 604 (2006).
110. M. Cruz-Díaz, F. F. Rivera, E. P. Rivero, and I. González, *Electrochim. Acta*, **63**, 47 (2012).
111. C. Bengoa, A. Montillet, P. Legentilhomme, and J. Legrand, *J. Appl. Electrochem.*, **27**, 1313 (1997).
112. D. Dendukuri, S. K. Karode, and A. Kumar, *J. Membrane Sci.*, **249**, 41 (2005).
113. G. Velasco-Martínez, S. Gutierrez-Granados, A. Alatorre-Ordaz, and I. Rodríguez-Torres, *ECS Trans.*, **3**, 1 (2007).
114. U. M. López-García, P. E. Hidalgo, J. C. Olvera, F. Castañeda, H. Ruiz, and G. Orozco, *Fuel*, **110**, 162 (2013).
115. L. Castañeda, R. Antaño, F. F. Rivera, and J. L. Nava, *Int. J. Electrochem. Sci.*, **12**, 7351 (2017).
116. K. Aldas, N. Pehlivanoglu, and M. Mat, *Int. J. Hydrogen Energy*, **33**, 3668 (2008).
117. G. Rodríguez, F. Z. Sierra-Espinosa, and J. Teloxa, *Desalin. Water Treat.*, **57**, 22968 (2015).
118. J. Newman and W. Tiedemann, *J. Electrochem. Soc.*, **140**, 1961 (1993).
119. F. Leroux and F. Coeuret, *Electrochim. Acta*, **30**, 167 (1985).
120. Y. A. Gandomi, D. S. Aaron, T. A. Zawodzinski, and M. M. Mench, *J. Electrochem. Soc.*, **163**, A5188 (2016).
121. C. J. Brown, D. Pletcher, F. C. Walsh, J. K. Hammond, and D. Robinson, *J. Appl. Electrochem.*, **22**, 613 (1992).
122. R. Suzuki, W. H. Li, M. Schwartz, and K. Nobe, *Plat. Surf. Finish.*, **82**, 58 (1995).
123. D. Aaron, Z. Tang, A. B. Papandrew, and T. A. Zawodzinski, *J. Appl. Electrochem.*, **41**, 1175 (2011).
124. T. R. Ralph, M. L. Hitchman, J. P. Millington, and F. C. Walsh, *J. Electroanal. Chem.*, **375**, 17 (1994).
125. C. Ponce de León, G. W. Reade, I. Whyte, S. E. Male, and F. C. Walsh, *J. Power Sources*, **164**, 441 (2007).
126. P. K. Leung, C. Ponce de León, C. T. J. Low, A. A. Shah, and F. C. Walsh, *J. Power Sources*, **196**, 5174 (2011).
127. T. R. Ralph, M. L. Hitchman, J. P. Millington, and F. C. Walsh, *J. Electroanal. Chem.*, **462**, 97 (1999).
128. T. R. Ralph, M. L. Hitchman, J. P. Millington, and F. C. Walsh, *J. Electrochem. Soc.*, **152**, D54 (2005).
129. R. Chetty, P. A. Christensen, B. T. Golding, and K. Scott, *App. Catal. A: Gen.*, **271**, 185 (2004).
130. C. Ponce de León and R. W. Field, *J. Membrane Sci.*, **171**, 67 (2000).
131. J. P. Fornés and J. M. Bisang, *Electrochim. Acta*, **173**, 743 (2015).
132. H. K. Khattar, S. W. R. Al-Hasnawi, and F. A. A. Al-Saady, *IJECS*, **15**, 6 (2015).
133. C. Ponce de León and D. Pletcher, *Electrochim. Acta*, **41**, 533 (1996).
134. P. A. Christensen, W. F. Lin, H. Christensen, A. Imkum, J. M. Jin, G. Li, and C. M. Dyson, *Ozone Sci. Eng.*, **31**, 287 (2009).
135. A. Estejab, D. A. Daramola, and G. G. Botte, *Water Res.*, **77**, 133 (2015).
136. L. F. Arenas, C. Ponce de León, R. P. Boardman, and F. C. Walsh, *J. Electrochem. Soc.*, **164**, D57 (2017).
137. L. F. Arenas, C. Ponce de León, R. P. Boardman, and F. C. Walsh, *Electrochim. Acta*, **247**, 994 (2017).
138. R. Chaiyont, C. Badoe, C. Ponce de León, J. L. Nava, F. J. Recio, I. Sirés, P. Herrasti, and F. C. Walsh, *Chem. Eng. Technol.*, **36**, 123 (2013).
139. C. E. Schaefer, C. Andaya, A. Urtiaga, E. R. McKenzie, and C. P. Higgins, *J. Hazard. Mater.*, **295**, 170 (2015).
140. J. O. Bockris and J. Kim, *J. Appl. Electrochem.*, **27**, 623 (1997).
141. *Electrochemical Treatment of Alkaline Nuclear Wastes. Innovative Technology Summary Report. DOE/EM-0560*, Innovative Technology (2001).
142. N. Aust and A. Kirste, "Paired Electrosynthesis." in *Encyclopedia of Applied Electrochemistry* (Springer, New York)1505 (2014).
143. K. Scott, *Electrochim. Acta*, **36**, 1447 (1991).
144. C. A. Paddon, M. Atobe, T. Fuchigami, P. He, P. Watts, S. J. Haswell, G. J. Pritchard, S. D. Bull, and F. Marken, *J. Appl. Electrochem.*, **36**, 617 (2006).
145. D. Pletcher and F. C. Walsh, *Electrochemistry for a Cleaner Environment*, ed. D. Genders and N. Weinberg (The Electrosynthesis Company, New York) (1992).
146. R. J. Kee and H. Zhu, *J. Power Sources*, **299**, 509 (2015).
147. R. M. Darling and M. L. Perry, *J. Electrochem. Soc.*, **161**, A1381 (2014).
148. V. Müller and I. Rousar, *Dechema Monographs* (VCH, Weinhein) Vol. 123, p. 331 (1991).
149. M. Griffiths, C. Ponce de León, and F. C. Walsh, *AIChE J.*, **51**, 682 (2005).
150. C. J. Brown, F. C. Walsh, and D. Pletcher, *Trans. IChemE*, **73**, 196 (1995).
151. A. Montillet, J. Comiti, and J. Legrand, *J. Appl. Electrochem.*, **23**, 1045 (1993).
152. J. González-García, V. Montiel, A. Aldaz, J. A. Conesa, J. R. Pérez, and G. Codina, *Ind. Eng. Chem. Res.*, **37**, 4501 (1998).
153. M. Averbukh, A. Pozin, and S. Sukoriansky, *J. Energy Eng.*, **143**(2), 04016050 (2017).
154. A. N. Colli, R. Toelzer, M. E. H. Bergmann, and J. M. Bisang, *Electrochim. Acta*, **100**, 78 (2013).
155. L. F. Arenas, C. Ponce de León, and F. C. Walsh, *AIChE J.*, **64**, 1135 (2018).
156. J. González-García, P. Bonete, E. Expósito, V. Montiel, A. Aldaz, and R. Torregrosa-Maciá, *J. Mater. Chem.*, **9**, 419 (1999).
157. F. Moro, A. Trovò, S. Bortolin, D. Del Col, and M. Guarnieri, *J. Power Sources*, **340**, 229 (2017).
158. S. Kumar and S. Jayanti, *J. Power Sources*, **307**, 782 (2016).
159. D. Reed, E. Thomsen, B. Li, W. Wang, Z. Nie, B. Koeppel, and V. Sprenkle, *J. Power Sources*, **306**, 24 (2016).
160. T. Jyothi Latha and S. Jayanti, *J. Appl. Electrochem.*, **44**, 995 (2014).
161. Q. Ye, J. Hu, P. Cheng, and Z. Ma, *J. Power Sources*, **296**, 352 (2015).
162. A. Tang, J. Bao, and M. Skyllas-Kazacos, *J. Power Sources*, **248**, 154 (2014).
163. L. Vázquez, A. Alvarez-Gallegos, F. Z. Sierra, C. P. León, and F. C. Walsh, *J. Appl. Electrochem.*, **43**, 453 (2013).
164. A. Alexiadis, M. P. Dudukovic, P. Ramachandran, A. Cornell, J. Wanngård, and A. Bokkers, *Int. J. Chem. Eng.*, **2012**, 1 (2012).
165. A. Alexiadis, M. P. Dudukovic, P. Ramachandran, and A. Cornell, *J. Appl. Electrochem.*, **42**, 679 (2012).
166. H. Vogt, *J. Appl. Electrochem.*, **12**, 261 (1982).
167. H. Vogt, *J. Appl. Electrochem.*, **13**, 705 (1983).
168. H. C. Brinkman, *Appl. Sci. Res.*, **1**, 27 (1949).
169. K. Bromberger, J. Kaunert, and T. Smolinka, *Energy Technology*, **2**, 64 (2014).
170. X. Ke, J. I. D. Alexander, J. M. Prahl, and R. F. Savinell, *J. Power Sources*, **270**, 646 (2014).
171. J. Houser, J. Clement, A. Pezeshki, and M. M. Mench, *J. Power Sources*, **302**, 369 (2016).
172. M. L. Hitchman, J. P. Millington, F. C. Walsh, and T. R. Ralph, *Inst. Chem. Eng. Symp. Ser.* (IChemE, London) Vol. 127, p. 23 (1992).
173. J. Eigeldinger and H. Vogt, *Electrochim. Acta*, **45**, 4449 (2000).
174. D. Deconinck, W. Hoogsteen, and J. Deconinck, *Electrochim. Acta*, **103**, 161 (2013).
175. D. Landolt, *Rev. Sci. Instrum.*, **43**, 592 (1972).
176. A. Gyr and H. W. Bewersdorff, *Drag Reduction of Turbulent Flows by Additives* (Springer Science & Bussiness Media, Dordrecht) (1995).
177. N. Ibl, *Electrochim. Acta*, **1**, 117 (1959).
178. A. Walker and A. A. Wragg, *Electrochim. Acta*, **22**, 1129 (1977).
179. F. C. Walsh, P. Trinidad, and D. Gilroy, *Int. J. Engng. Ed.*, **21**, 981 (2005).
180. M. Panizza and G. Cerisola, *Chemosphere*, **77**, 1060 (2009).
181. R. E. Sioda, *J. Appl. Electrochem.*, **5**, 221 (1975).
182. T. Doherty, J. G. Sunderland, E. P. L. Roberts, and D. J. Pickett, *Fuel Process. Technol.*, **41**, 519 (1996).
183. R. Alkire and B. Cracon, *J. Electrochem. Soc.*, **122**, 1594 (1975).
184. J. R. Selman and C. W. Tobias, "Mass-transfer measurements by the limiting current technique." in *Advances in Chemical Engineering*, ed. T. B. Drew, G. R. Cokelet, J. W. Hoopes, and T. Vermeulen (Academic Press, New York) 211 (1978).
185. G. Coria, T. Pérez, I. Sirés, and J. L. Nava, *J. Electroanal. Chem.*, **757**, 225 (2015).
186. J. R. Selman and C. W. Tobias, *J. Electroanal. Chem.*, **65**, 67 (1975).
187. A. I. Masliy, N. P. Poddubny, A. Z. Medvedev, and V. O. Lukyanov, *J. Electroanal. Chem.*, **757**, 128 (2015).
188. A. I. Maslii, N. P. Poddubnyi, and A. Z. Medvedev, *Russ. J. Electrochem.*, **52**, 576 (2016).
189. J. S. Newman and C. W. Tobias, *J. Electrochem. Soc.*, **109**, 1183 (1962).
190. A. Storck, M. A. Enriquez-Granados, M. Roger, and F. Coeuret, *Electrochim. Acta*, **27**, 293 (1982).
191. M. Fleischmann and R. E. W. Jansson, *Electrochim. Acta*, **27**, 1029 (1982).
192. S. Langlois and F. Coeuret, *J. Appl. Electrochem.*, **20**, 740 (1990).
193. P. S. Fedkiw, *J. Electrochem. Soc.*, **128**, 831 (1981).
194. Y. P. Sun, W. L. Xu, and Scott, *J. Appl. Electrochem.*, **25**, 755 (1995).
195. J. Newman and K. E. Thomas-Alyea, *Electrochemical Systems* (John Wiley & Sons, Hoboken) 3rd ed. (2004).
196. N. Ibl, "Current Distribution." in *Comprehensive Teatrise of Electrochemistry: Electrochemical Processing*, ed. J. O. M. Bockris, B. E. Conway, E. Yeager, and R. E. White (Plenum Press, New York) p. 239 (1981).
197. K. I. Popov, S. S. Djokić, and B. N. Grgur, "The Current Distribution in Electrochemical Cells." in *Fundamental Aspects of Electrometallurgy* (Kluwer Academic Publishers, Boston) p. 101 (2002).
198. J. W. Haverkort, *Electrochim. Acta*, **295**, 846 (2019).
199. V. Boovaragavan and C. A. Basha, *J. Appl. Electrochem.*, **36**, 745 (2006).
200. S. J. C. Cleghorn, C. R. Derouin, M. S. Wilson, and S. Gottesfeld, *J. Appl. Electrochem.*, **28**, 663 (1998).
201. F. Leroux and F. Coeuret, *Electrochim. Acta*, **30**, 159 (1985).
202. M. Matlosz, *J. Electrochem. Soc.*, **142**, 1915 (1995).
203. C. Wieser, A. Helmbold, and E. Gülzow, *J. Appl. Electrochem.*, **30**, 803 (2000).
204. L. R. Czarnetzki and L. J. J. Janssen, *J. Appl. Electrochem.*, **19**, 630 (1989).
205. K. Scott, W. Taama, and B. R. Williams, *J. Appl. Electrochem.*, **28**, 259 (1998).
206. H. F. M. Gijsbers and L. J. J. Janssen, *J. Appl. Electrochem.*, **19**, 637 (1989).
207. J. M. Bisang, *J. Appl. Electrochem.*, **21**, 760 (1991).
208. J. M. Bisang, *J. Appl. Electrochem.*, **23**, 966 (1993).
209. E. R. Henquín and J. M. Bisang, *Electrochim. Acta*, **56**, 5926 (2011).
210. A. N. Colli and J. M. Bisang, *J. Electrochem. Soc.*, **160**, E5 (2013).
211. A. N. Colli and J. M. Bisang, *Electrochim. Acta*, **113**, 575 (2013).
212. A. N. Colli and J. M. Bisang, *J. Electrochem. Soc.*, **164**, E42 (2017).
213. A. N. Colli and J. M. Bisang, *J. Electrochem. Soc.*, **165**, E81 (2018).
214. M. Paulin, D. Hutin, and F. Coeuret, *J. Electrochem. Soc.*, **124**, 180 (1977).
215. C. Wagner, *J. Electrochem. Soc.*, **98**, 116 (1951).
216. W. R. Parrish and J. Newman, *J. Electrochem. Soc.*, **117**, 43 (1970).
217. R. E. White, M. Bain, and M. Raible, *J. Electrochem. Soc.*, **130**, 1037 (1983).

218. T. V. Nguyen, C. W. Walton, R. E. White, and J. Van Zee, *J. Electrochem. Soc.*, **133**, 81 (1986).
219. J. Divisek, R. Jung, and D. Britz, *J. Appl. Electrochem.*, **20**, 186 (1990).
220. M. Georgiadou, *Electrochim. Acta*, **48**, 4089 (2003).
221. G. Nelissen, A. Van Theemsche, C. Dan, B. Van den Bossche, and J. Deconinck, *J. Electroanal. Chem.*, **563**, 213 (2004).
222. K. I. Popov, P. M. Zivkovic, and N. D. Nikolic, *J. Serb. Chem. Soc.*, **76**, 805 (2011).
223. T. Pérez, M. I. León, and J. L. Nava, *J. Electroanal. Chem.*, **707**, 1 (2013).
224. T. Pérez, C. Ponce de León, F. C. Walsh, and J. L. Nava, *Electrochim. Acta*, **154**, 352 (2015).
225. E. P. Rivero, M. R. Cruz-Díaz, F. J. Almazán-Ruiz, and I. González, *Trans. IChemE*, **100**, 422 (2015).
226. E. P. Rivero, F. A. Rodríguez, M. R. Cruz-Díaz, and I. González, *Trans. IChemE*, **138**, 533 (2018).
227. M. N. Nandanwar and S. Kumar, *J. Electrochem. Soc.*, **161**, A1602 (2014).
228. P. Trinidad and F. C. Walsh, *Electrochim. Acta*, **41**, 493 (1996).
229. F. Lapicque and A. Storck, *J. Appl. Electrochem.*, **15**, 925 (1985).
230. A. Galia, *Ind. Eng. Chem. Res.*, **46**, 2360 (2007).
231. F. E. Durán, D. Medeiros de Araújo, C. do Nascimento Brito, E. Vieira Santos, S. O. Ganiyu, and C. A. Martínez-Huitle, *J. Electroanal. Chem.*, **818**, 216 (2018).
232. C. Díaz-Flores, M. L. Alvarez, S. Silva-Martinez, and A. Alvarez-Gallegos, *Int. J. Green Technol.*, **1**, 13 (2015).
233. P. Trinidad, C. Ponce de León, and F. C. Walsh, *J. Environ. Manage.*, **88**, 1417 (2008).
234. A. Thiam, R. Salazar, E. Brillas, and I. Sirés, *Chem. Eng. J.*, **335**, 133 (2018).
235. F. C. Walsh, L. F. Arenas, and C. Ponce de León, *J. Chem. Technol. Biotechnol.*, **93**, 3073 (2018).
236. A. M. Couper, D. Pletcher, and F. C. Walsh, *Chem. Rev.*, **90**, 837 (1990).
237. G. K. Chandler, J. D. Genders, and D. Pletcher, *Platinum Metals Rev.*, **41**, 54 (1997).
238. P. Hayfield, *Platinum Metals Rev.*, **42**, 27 (1998).
239. S. Trasatti, *Electrochim. Acta*, **45**, 2377 (2000).
240. F. Cardarelli, "Electrode materials for electrolytic cells." in *Materials Handbook: A Concise Desktop Reference* (Springer-Verlag, London) 2nd ed., 8, 323 (2008).
241. *Final Report Summary—MEMLAB (Melt Spun and Sintered Metal Fibre Networks for Lead-Acid Battery Advancement) 315261* , Fibre Technology Ltd., European Commission https://cordis.europa.eu/result/rcn/193490_en.html (2017).
242. M. F. Ashby, A. Evans, N. A. Fleck, L. J. Gibson, J. W. Hutchinson, and H. N. G. Wadley, *Metal Foams: A Design Guide* (Butterworth-Heinemann, Boston) (2000).
243. L. F. Arenas, C. Ponce de León, and F. C. Walsh, *Electrochem. Commun.*, **77**, 133 (2017).
244. J. Lölsberg, O. Starck, S. Stiefel, J. Hereijgers, T. Breugelmans, and M. Wessling, *ChemElectroChem*, **4**, 3309 (2017).
245. X. Li, D. Pletcher, and F. C. Walsh, *Chem. Soc. Rev.*, **40**, 3879 (2011).
246. J. R. Smith, F. C. Walsh, and R. L. Clarke, *J. Appl. Electrochem.*, **28**, 1021 (1998).
247. F. C. Walsh and R. G. A. Wills, *Electrochim. Acta*, **55**, 6342 (2010).
248. E. Brillas and C. A. Martínez-Huitle, *Synthetic Diamond Films: Preparation, Electrochemistry, Characterization and Applications* (John Wiley & Sons, Hoboken) (2011).
249. F. C. Walsh, C. Ponce de León, D. V. Bavykin, C. T. J. Low, S. C. Wang, and C. Larson, *Trans. Inst. Met. Finish.*, **93**, 209 (2015).
250. F. C. Walsh, C. Ponce de León, D. V. Bavykin, C. T. J. Low, S. C. Wang, and C. Larson, *Trans. Inst. Met. Finish.*, **93**, 241 (2015).
251. F. J. Recio, P. Herrasti, L. Vázquez, C. Ponce de León, and F. C. Walsh, *Electrochim. Acta*, **90**, 507 (2013).
252. M. J. Kim, M. A. Cruz, F. Yang, and B. J. Wiley, *Curr. Opin. Electrochem.*, **16**, 19 (2019).
253. M. H. Chakrabarti, N. P. Brandon, S. A. Hajimolana, F. Tariq, V. Yufit, M. A. Hashim, M. A. Hussain, C. T. J. Low, and P. V. Aravind, *J. Power Sources*, **253**, 150 (2014).
254. R. Schweiss, C. Meiser, T. Damjanovic, I. Galbati, and N. Haak, *Sigracet® gas Diffusion Layers for PEM Fuel Cells, Electrolyzers and Batteries*, https://sglcarbon.com (2016).
255. F. C. Walsh, L. F. Arenas, C. Ponce de León, G. W. Reade, I. Whyte, and B. G. Mellor, *Electrochim. Acta*, **215**, 566 (2016).
256. W. M. Haynes, *CRC Handbook of Chemistry and Physics* (CRC Press, Boca Raton) 95th ed. (2014).
257. C. Y. Ho and T. K. Chu, "Electrical resistivity and thermal conductivity of nine selected AISI stainless steels." *CINDAS Report 45*, Center for Information and Numerical Data Analysis and Synthesis, Purdue University West Lafayette, https://apps.dtic.mil/dtic/tr/fulltext/u2/a129160.pdf (1977).
258. J. Wang, *Electrochim. Acta*, **26**, 1721 (1981).
259. S. Langlois and F. Coeuret, *J. Appl. Electrochem.*, **19**, 43 (1989).
260. Entegris Fuel Cells, *Entegris Cell Stack Plates*, *Resource 6002-2153-0312*, www.entegris.com/resources/assets/6002-2153-0312.pdf (2012).
261. SGL Carbon, *Sigracell® Bipolar Plates*, https://sglcarbon.com/pdf/SGL-Datasheet-SIGRACELL-Bipolar-Plates-EN.pdf (2019).
262. Y. B. Xie and X. Z. Li, *Materials Chemistry and Physics*, **95**, 39 (2006).
263. G. Harikrishnan, T. Umasankar Patro, and D. V. Khakhar, *Carbon*, **45**, 531 (2007).
264. H. Zhou, H. Zhang, P. Zhao, and B. Yi, *Electrochim. Acta*, **51**, 6304 (2006).
265. C. F. Oduoza and A. A. Wragg, *J. Appl. Electrochem.*, **30**, 1439 (2000).
266. A. A. Folgueiras-Amador, K. Philipps, S. Guilbaud, J. Poelakker, and T. Wirth, *Angew. Chem. Int. Ed.*, **56**, 15446 (2017).
267. C. F. Oduoza, A. A. Wragg, and M. A. Patrick, *Chem. Eng. J.*, **68**, 145 (1997).
268. D. Simonsson, *J. Appl. Electrochem.*, **14**, 595 (1984).
269. A. Storck, P. M. Robertson, and N. Ibl, *Electrochim. Acta*, **24**, 373 (1979).
270. L. Lipp and D. Pletcher, *Electrochim. Acta*, **42**, 1101 (1997).
271. L. F. Castañeda, F. C. Walsh, J. L. Nava, and C. Ponce de León, *Electrochim. Acta*, **258**, 1115 (2017).
272. F. Coeuret, E. O. Vilar, and E. B. Cavalcanti, *J. Appl. Electrochem.*, **32**, 1175 (2002).
273. L. F. Arenas, R. P. Boardman, C. Ponce de León, and F. C. Walsh, *Carbon*, **135**, 85 (2018).
274. A. Tentorio and U. Casolo-Ginelli, *J. Appl. Electrochem.*, **8**, 195 (1978).
275. E. Fockedey and A. V. Lierde, *Water Res.*, **36**, 4169 (2002).
276. N. Aguiló-Aguayo and T. Bechtold, *J. Power Sources*, **254**, 224 (2014).
277. L. F. Arenas, C. Ponce de León, and F. C. Walsh, *Curr. Opin. Electrochem.*, **16**, 1 (2019).
278. W. M. Taama, R. E. Plimley, and K. Scott, *Electrochim. Acta*, **41**, 543 (1996).
279. C. A. Martínez-Huitle, S. Ferro, and A. de Battisti, *J. Appl. Electrochem.*, **35**, 1087 (2005).
280. R. A. Green, R. C. D. Brown, and D. Pletcher, *J. Flow Chem.*, **6**, 191 (2016).
281. B. Tjaden, D. J. L. Brett, and P. R. Shearing, *Int. Mater. Rev.*, **63**, 47 (2016).
282. C. Liu, M. Carmo, G. Bender, A. Everwand, T. Lickert, J. L. Young, T. Smolinka, D. Stolten, and W. Lehnert, *Electrochem. Commun.*, **97**, 96 (2018).
283. X. Ou et al., *Mater. Charact.*, **123**, 20 (2017).
284. D. Maggiolo, F. Zanini, F. Picano, A. Trovò, and M. Guarnieri, *Energy Storage Mater.*, **16**, 91 (2018).
285. M. D. R. Kok, R. Jervis, T. G. Tranter, M. A. Sadeghi, D. J. L. Brett, P. R. Shearing, and J. T. Gostick, *Chem. Eng. Sci.*, **196**, 104 (2019).
286. X. Ke, J. M. Prahl, J. I. D. Alexander, J. S. Wainright, T. A. Zawodzinski, and R. F. Savinell, *Chem. Soc. Rev.*, **41**, 54 (2018).
287. J. F. Pérez, J. Llanos, C. Sáez, C. López, P. Cañizares, and M. A. Rodrigo, *Electrochem. Commun.*, **82**, 85 (2017).
288. H. Xu, W. Huang, Y. Xing, H. Lin, H. Ji, M. Jiang, X. Liu, and S. Gan, *Chin. J. Chem. Eng.*, **16**, 198 (2008).
289. J. A. Trainham and J. Newman, *Electrochim. Acta*, **26**, 455 (1981).
290. C. Bae, H. Chakrabarti, and E. Roberts, *J. Appl. Electrochem.*, **38**, 637 (2008).
291. C. Lamoureux, C. Moinet, and A. Tallec, *J. Appl. Electrochem.*, **16**, 819 (1986).
292. X. You, Q. Ye, and P. Cheng, *Int. Commun. Heat. Mass.*, **75**, 7 (2016).
293. G. A. Fimbres-Weihs and D. E. Wiley, *J. Membrane Sci.*, **306**, 228 (2007).
294. C. Fritzmann, M. Hausmann, M. Wiese, M. Wessling, and T. Melin, *J. Membrane Sci.*, **446**, 189 (2013).
295. J. D. Fisk and J. D. Boyle, *Trans. Inst. Met. Finish.*, **78**, 113 (2000).
296. D. G. Clark, S. H. Joseph, and S. E. Male, Regenesys Technologies Ltd, *European Patent*, 0,870,342 B1 (2002).
297. H. Nakaishi, T. Kanno, S. Ogino, T. Ito, T. Shigematsu, and N. Tokuda, *US Pat. application* 2004/0202915 (2004).
298. E. Kizhnerman, "Voltage propagation within flow battery system and its implications on safety, DC topology, PCS type and material selection." *The International Flow Battery Forum 2018* Laussanne 10th to 12th July (2018).
299. A. Savall, J. Quesado, M. Rignon, and J. Malafosse, *J. Appl. Electrochem.*, **21**, 805 (1991).
300. A. Montillet, J. Comiti, and J. Legrand, *J. Appl. Electrochem.*, **24**, 384 (1994).
301. S. Clarke, "Some lessons learned from 20 years in redox flow battery R&D." *DOE Workshop*Washington DC(US Department of Energy) (2012).
302. E. Middelman, W. Kout, B. Vogelaar, J. Lenssen, and E. de Waal, *J. Power Sources*, **118**, 44 (2003).
303. F. Mighri, M. A. Huneault, and M. F. Champagne, *Polymer Eng. Sci.*, **44**, 1755 (2004).
304. A. Heinzel, F. Mahlendorf, O. Niemzig, and C. Kreuz, *J. Power Sources*, **131**, 35 (2004).
305. A. Müller, P. Kauranen, A. Von Ganski, and B. Hell, *J. Power Sources*, **154**, 467 (2006).
306. B. Caglar, P. Fischer, P. Kauranen, M. Karttunen, and P. Elsner, *J. Power Sources*, **256**, 88 (2014).
307. B. Caglar, J. Richards, P. Fischer, and J. Tuebke, *Adv. Mat. Lett.*, **5**, 299 (2014).
308. D. T. Pham and R. S. Gault, *Int. J. Mach. Tool. Manufact.*, **38**, 1257 (1998).
309. H. Lipson and M. Kurman, *Fabricated: The New World of 3D Printing* (Wiley, Indianapolis) (2013).
310. J.-Y. Choi, S. Das, N. D. Theodore, I. Kim, C. Honsberg, H. W. Choi, and T. L. Alford, *ECS J. Solid State Sci. Technol.*, **4**, P3001 (2015).
311. D. D. Gu, W. Meiners, K. Wissenbach, and R. Poprawe, *Int. Mater. Rev.*, **57**, 133 (2012).
312. R. Critchley, I. Corni, J. A. Wharton, F. C. Walsh, R. J. K. Wood, and K. R. Stokes, *Phys. Status Solidi B*, **250**, 1963 (2013).
313. M. Vaezi, S. Chianrabutra, B. Mellor, and S. Yang, *Virtual Phys. Prototyp.*, **8**, 19 (2013).
314. H. N. Chia and B. M. Wu, *J Biol Eng*, **9**, 4 (2015).
315. A. Ambrosi and M. Pumera, *Chem. Soc. Rev.*, **45**, 2740 (2016).
316. R. Cornock, S. Beirne, B. Thompson, and G. G. Wallace, *Biofabrication*, **6**, 025002 (2014).
317. J. Choi, O.-C. Kwon, W. Jo, H. J. Lee, and M.-W. Moon, *3D Print. Addit. Manuf.*, **2**, 159 (2015).
318. L. F. Arenas, F. C. Walsh, and C. Ponce de León, *ECS J. Solid State Sci. Technol.*, **4**, P3080 (2015).
319. C. Ponce de León, W. Hussey, F. Frazao, D. Jones, E. Ruggeri, S. Tzortzatos, R. D. Mckerracher, and R. G. A. Wills, *Chem. Eng. Trans.*, **41**, 1 (2014).

320. G. Chisholm, P. J. Kitson, N. D. Kirkaldy, L. G. Bloor, and L. Cronin, *Energy Environ. Sci.*, **7**, 3026 (2014).
321. K. Percin, A. Rommerskirchen, R. Sengpiel, Y. Gendel, and M. Wessling, *J. Power Sources*, **379**, 228 (2018).
322. B. Lyons, M. Batalov, P. Mohanty, and S. Das, "Rapid prototyping of PEM fuel cell bi-polar plates using 3D printing and thermal spray deposition." *Proc. SFF Symposium*Austin446 (2005).
323. C.-Y. Chen, W.-H. Lai, B.-J. Weng, H.-J. Chuang, C.-Y. Hsieh, and C.-C. Kung, *J. Power Sources*, **179**, 147 (2008).
324. C.-Y. Chen, Y.-C. Wen, W.-H. Lai, M.-C. Chou, B.-J. Weng, C.-Y. Hsieh, and C.-C. Kung, *J. Fuel Cell Sci. Technol*, **8**, 014502 (2011).
325. G. Scotti, V. Matilainen, P. Kanninen, H. Piili, A. Salminen, T. Kallio, and S. Franssila, *J. Power Sources*, **272**, 356 (2014).
326. K. Alayavalli and D. L. Bourell, *Rapid Prototyping J.*, **16**, 268 (2010).
327. J. Weber, A. J. Wain, H. Piili, V. P. Matilainen, A. Vuorema, G. A. Attard, and F. Marken, *ChemElectroChem*, **3**, 1020 (2016).
328. F. C. Walsh, L. F. Arenas, and C. Ponce de León, *Curr. Opin. Electrochem.*, **16**, 10 (2019).
329. J. I. Yoshida and A. Nagaki, "Electrochemical Reactions in Microreactors." in *Microreactors in Preparative Chemistry: Practical Aspects in Bioprocessing, Nanotechnology, Catalysis and More* (Wiley-VCH Verlag, Weinheim)231 (2013).
330. A. Ziogas, G. Kolb, M. O'Connell, A. Attour, F. Lapicque, M. Matlosz, and S. Rode, *J. Appl. Electrochem.*, **39**, 2297 (2009).
331. M. Atobe, *Curr. Opin. Electrochem.*, **2**, 1 (2017).
332. G. Takacs, "A Review of Production Engineering Fundamentals." in *Sucker-Rod Pumping Handbook* (Gulf Professional Publishing, Amsterdam) Chap. 2, p. 13 (2015).
333. P. He, P. Watts, F. Marken, and S. J. Haswell, *Lab on a Chip*, **7**, 141 (2007).
334. M. R. Chapman, Y. M. Shafi, N. Kapur, B. N. Nguyen, and C. E. Willans, *Chem. Commun. (Camb.)*, **51**, 1282 (2014).
335. R. A. Green, R. C. D. Brown, D. Pletcher, and B. Harji, *Org. Process Res. Dev.*, **19**, 1424 (2015).
336. S. Sabatino, A. Galia, and O. Scialdone, *ChemElectroChem*, **3**, 83 (2015).
337. J. Kuleshova, J. T. Hill-Cousins, P. R. Birkin, R. C. D. Brown, D. Pletcher, and T. J. Underwood, *Electrochim. Acta*, **56**, 4322 (2011).
338. M.-A. Goulet and E. Kjeang, *J. Power Sources*, **260**, 186 (2014).
339. D. Horii, T. Fuchigami, and M. Atobe, *J. Am. Chem. Soc.*, **129**, 11692 (2007).
340. S. K. Yoon, E. R. Choban, C. Kane, T. Tzedakis, and P. J. A. Kenis, *J. Am. Chem. Soc.*, **127**, 10466 (2005).
341. C. A. Paddon, G. J. Pritchard, and T. Thiemann, *Electrochem. Commun.*, **4**, 825 (2002).
342. R. Horcajada, M. Okajima, S. Suga, and J. I. Yoshida, *Chem. Commun.*, **33**, 1303 (2005).
343. D. Horii, M. Atobe, T. Fuchigami, and F. Marken, *J. Electrochem. Soc.*, **153**, D143 (2006).
344. P. He, P. Watts, F. Marken, and S. J. Haswell, *Green Chem.*, **9**, 20 (2007).
345. F. Amemiya, D. Horii, T. Fuchigami, and M. Atobe, *J. Electrochem. Soc.*, **155**, E162 (2008).
346. A. Attour, S. Rode, A. Ziogas, M. Matlosz, and F. Lapicque, *J. Appl. Electrochem.*, **38**, 339 (2007).
347. A. Attour, S. Rode, F. Lapicque, A. Ziogas, and M. Matlosz, *J. Electrochem. Soc.*, **155**, E201 (2008).
348. O. Scialdone, C. Guarisco, and A. Galia, *Electrochim. Acta*, **58**, 463 (2011).
349. A. Attour, S. Rode, A. Ziogas, M. Matlosz, and F. Lapicque, *Chem. Eng. Sci.*, **66**, 480 (2011).
350. J. K. Hammond, D. Robinson, and F. C. Walsh, *Dechema Monographs*, ed. G. Kreysa (VCH, Weinheim) Vol. 123, p. 279 (1991).
351. R. J. Marshall, D. J. Schiffrin, F. C. Walsh, and G. E. G. Bagg, *US Pat.*, 5,120,408 A (1992).
352. I. Garcia-Herrero, M. Margallo, R. Onandía, R. Aldaco, and A. Irabien, *Sci. Total Environ.*, **580**, 147 (2017).
353. F. C. Walsh and D. Robinson, *Chem. Tech. Europe*, **May/June**, 16 (1995).
354. G. E. G. Bagg, R. J. Marshall, D. J. Schiffrin, and F. C. Walsh, *European Pat. Application* 88305440 (1988).
355. Anon., German pat. 231,546 (1910).
356. J. E. Harrar and R. K. Pearson, *J. Electrochem. Soc.*, **130**, 108 (1983).
357. J. E. Harrar, R. Quong, L. P. Rigdon, and R. R. McGuire, *US Pat.* 6,200,456 B1 (2001).
358. J. E. Harrar, R. Quong, L. P. Rigdon, and R. R. McGuire, *J. Electrochem. Soc.*, **144**, 2032 (1997).
359. C. Ponce de León, F. C. Walsh, R. R. Bessette, C. J. Patrissi, M. G. Medeiros, A. Rose, D. Browning, J. B. Lakeman, and R. W. Reeve, *ECS Trans.*, **15**, 25 (2008).
360. I. Merino-Jiménez, C. Ponce de León, A. A. Shah, and F. C. Walsh, *J. Power Sources*, **219**, 339 (2012).
361. C. Ponce de León, A. Kulak, S. Williams, I. Merino-Jiménez, and F. C. Walsh, *Catalysis Today*, **170**, 148 (2011).
362. F. C. Walsh, C. Ponce de León, L. Berlouis, G. Nikiforidis, L. F. Arenas-Martínez, D. Hodgson, and D. Hall, *ChemPlusChem*, **80**, 288 (2015).
363. G. Nikiforidis and W. A. Daoud, *Electrochim. Acta*, **168**, 394 (2015).
364. B. Fang, S. Iwasa, Y. Wei, T. Arai, and M. Kumagai, *Electrochim. Acta*, **47**, 3971 (2002).
365. Y. Liu, X. Xia, and H. Liu, *J. Power Sources*, **130**, 299 (2004).
366. P. K. Leung, M. R. Mohamed, A. A. Shah, Q. Xu, and M. B. Conde-Duran, *J. Power Sources*, **274**, 651 (2015).
367. V. Amstutz, K. E. Toghill, F. Powlesland, H. Vrubel, C. Comninellis, X. Hu, and H. H. Giraoult, *Energy Environ. Sci.*, **7**, 2350 (2014).
368. Z. Na, S. Xu, D. Yin, and L. Wang, *J. Power Sources*, **295**, 28 (2015).
369. H. M. H. Dewage, B. Wu, A. Tsoi, V. Yufit, G. J. Offer, and N. Brandon, *J. Mater. Chem. A*, **3**, 9446 (2015).
370. M. C. Tucker, A. Weiss, and A. Z. Weber, *J. Power Sources*, **327**, 591 (2016).
371. G. Nikiforidis, L. Berlouis, D. Hall, and D. Hodgson, *J. Power Sources*, **243**, 691 (2013).
372. L. F. Arenas, *An Electrochemical Engineering Approach to Improvements in the Zinc-Cerium Redox Flow Battery*, Doctoral Thesis, University of Southampton, https://eprints.soton.ac.uk/413466/ (2017).
373. P. A. Ramírez Ortega, V. E. Reyes Cruz, and M. A. Veloz Rodríguez, "Silver recovery of radiological waste in a press-type electrochemical reactor on an A304 stainless steel electrode varying the flow rate [in Spanish]." *XXIV Congress of the Mexican Society of Electrochemistry*Puerto VallartaIE-18, https://uaeh.edu.mx/investigacion/icbi/LI_RecCorr/maria_veloz/IE-18.pdf (2009).
374. N. Zhou, S. Wang, and F. C. Walsh, *Electrochim. Acta*, **283**, 568 (2018).
375. T. R. Ralph, *The electroreduction of L-cystine hydrochloride to L-cysteine hydochloride*, Doctoral Thesis, University of Strathclyde, https://ethos.bl.uk/OrderDetails.do?uin=uk.bl.ethos.760295 (1991).